UNIVERSITY BLIDA 1
FACULTY OF TECHNOLOGY
DEPARTMENT OF MECHANIC
RESEARCH LABORATORY OF STRUCTURE « L.S »

Project Graduation

For Obtaining the Master's Degree In

Mechanical Construction

Centrifugal fan aerodynamic & rotor dynamic study

Realized by:

Amrani Abderrahmane

El Aichi Mhamed Abdelbasset

Kasri Mohamed Amine

Proposed and supervised by:

Professor Mohammed OUALI

Dr. Rabah MAGRAOUI

2020/2021

Appreciation

At the end of this thesis, we would like to thank Allah for giving us the strength, patience, and courage to finish this work.

All the work that has been achieved here is done under the supervision of Professor Mohammed OUALI and Doctor Rabah MEGRAOUI. We are really glad for their help, guidance, and their thoughtful insight which led to the results desired.

We are also thankful for everyone who helped us and supported us during all those years of study especially our respected teachers from the mechanical department.

Dedication

First of all, we are grateful for Allah and his blessings over us that guided us to the right path.

We dedicate this work to our parents, families, friends, and our loved ones who believed in our abilities throughout the years.

To our great teachers Mr.Ouali and Mr.Magraoui for their time and help.

Thank you.

Amrani Abderrahmane

El Aichi Mhamed Abdelbasset

Kasri Mohamed Amine

Abstract

In this work, we propose a complete study about a centrifugal fan (FN 501). First, we conduct a theoretical and numerical aerodynamic study to evaluate the fan performance and its capacity to evacuate the required air flowrate from the flour milling machines and overcome the resistance of a complex duct system that passes by a dust collector filter (FL 301). Then we conduct a static study about the motor shaft to verify its resistance to bending and torsion, we calculate the deflection and the unbalance mass, using classical methods and FEA, after that, we perform a rotor dynamic study to estimate the vibration of the rotor due to the unbalance mass. Experimental tests are provided to validate the previous results.

Keywords: Centrifugal fan, resistance to bending, resistance to torsion, deflection, unbalance mass, vibration.

ملخص

في هذا العمل ، نقترح دراسة كاملة حول مروحة طرد مركزي (FN 501). أولاً ، نجري دراسة ديناميكية هوائية نظرية ورقمية لتقييم أداء المروحة وقدرتها على تفريغ تدفق الهواء المطلوب من آلات طحن الدقيق والتغلب على مقاومة نظام مجاري معقد يمر عبر مرشح جامع الغبار (FL 301). ثم نجري دراسة حول عمود المحرك للتحقق من مقاومته للانحناء والالتواء ، ونحسب الانحراف وكتلة عدم الاتزان باستخدام الطرق التقليدية و FEA ، وبعد ذلك نجري دراسة ديناميكية للجزء المتحرك لتقدير اهتزاز الدوار. بسبب كتلة عدم التوازن.

يتم توفير الاختبارات التجريبية للتحقق من صحة النتائج السابقة.

كلمات مفتاحية: مروحة طرد مركزي، مقاومة الانحناء، مقاومة الالتواء، كتلة عدم الاتزان، اهتزاز الدوار.

Résumé

Dans ce travail, nous proposons une étude complète sur un ventilateur centrifuge (FN 501). Dans un premier temps, nous menons une étude aérodynamique théorique et numérique pour évaluer les performances du ventilateur et sa capacité à évacuer le débit d'air requis des moulins à farine et surmonter la résistance d'un système de conduits complexe qui passe par un filtre dépoussiéreur (FL 301). Ensuite, nous effectuons une étude statique sur l'arbre du moteur pour vérifier sa résistance à la flexion et à la torsion, nous calculons la déflexion et la masse de balourd, en utilisant des méthodes classiques et FEA, après cela, nous effectuons une étude dynamique théorique et numérique pour estimer la vibration du rotor à cause du balourd.

Des tests expérimentaux sont fournis pour valider les résultats précédents.

Mots clés : Ventilateur centrifuge, résistance à la flexion, résistance à la torsion, déflexion, balourd, vibration.

Table of Contents

List of Figures

List of Tables

Nomenclature

D_1 Impeller eye diameter (m)
D_2 Impeller outer diamer (m)
b_1 Impeller inner width (m)
b_2 Impeller outer width (m)
β_1 Blade inner angle (degrees)
β_2 Blade outer angle (degrees)
Z   Number of blades
A_1 Flow area at the impeller inlet
A_2 Flow area at the impeller outlet
A_{out} Fan outlet area (m²)
N   Rotational speed (rpm)
Ω Angular velocity rad/s)
U   Peripheral (tangential) speed of blade (m/s)
C   Absolute velocity of the air (m/s)
W   The velocity of the air relative to the impeller (m/s)
C_m Radial component of the absolute velocity of the air (m/s)
C_u Tangential component of the absolute velocity of the air (m/s)
ρ Air density (kg/m^3)
Q   Air flow rate (m^3/s)
P_E Euler pressure (pa)
P_f Fan actual pressure (pa)
T   Impeller torque (N.m)
P   Motor power (kW)
P_{in} Power into the fan (kW)
P_{air} Air power (kW)
Eff_{imp} Impeller efficiency (%)
L   Shaft length (m)
L_1 Distance between the left bearing and the shaft left edge (m)
L_2 Distance between the two bearings (m)
L_3 Distance between the right bearing and the shaft right edge (m)
R_A Reaction at the left bearing (N)
R_B Reaction at the right bearing (N)
τ Shear stress (N/m^2)
I_0 Shaft Polar moment of inertia (m^4)
M_t Torsional moment (N.m)
s   Factor of safety
σ_y The yield strength of the shaft material (Mpa)
M_{max} Maximum bending moment (N.m)

I_x	Second moment of inertia of the neutral axis of the shaft (m^4)
M(x)	Bending moment (N.m)
$v(x)$	Shaft deflection (m)
$v(L)$	Shaft deflection at the right edge (m)
m_u	Unbalance mass (kg)
$M_{impeller}$	Impeller mass (kg)
M_{Shaft}	Shaft mass (kg)
e	Eccentricity (m)
V_i	Deflection at node i (m)
B_i	Rotation at node i (degrees)
M_i	Bending moment at node i (N.m)
T_D	Kinetic energy of the disk (J)
I_{D_d}	The diametral mass moment of inertia of the disk (m²)
I_{D_p}	Polar mass moment of inertia of the disk (m²)
T_s	Kinetic energy of the shaft (J)
ρ_{Shaft}	Shaft material density (kg/m^3)
S_{Shaft}	Shaft cross-sectional area (m²)
I_{S_d}	Diametric area moment of inertia of the shaft (m^4)
I_{S_p}	Polar area moment of inertia of the shaft (m^4)
U_s	Shaft strain energy (J)
E	Young modulus (N/m²)
ω_i	Natural pulsation (rad/s)
f_i	Natural frequency (Hz)
Q_i	Amplitude (m)
Ω_c	Critical speed (rad/s)

Chapter 1: General introduction

1.1 State of the art

The centrifugal fan has been in existence for over two hundred years but its perfection and rapid development occurred only in the last sixty years. The centrifugal fan is found in centrifugal pumps and compressors. Next to the electric motor, centrifugal pumps and compressors are believed to be the most widely used machines of our time. The field of application of these rotary machines has been continually widening, as they are developed for handling a wider range of liquids and gases at a higher pressure and greater temperatures, and whole industries become more and more dependent on them. The first centrifugal impeller with ten wooden double-curved blades and dating back to the fifth century was found in 1772 in an abandoned Portuguese copper mine in San Dominigos. Centrifugal fans had been used for mine ventilation as early as in the sixteenth century. The invention of the centrifugal impeller is a disputed issue whether the credit goes to Leonardo Da Vinci (1452 - 1519), who suggested the idea of using centrifugal force for lifting liquid, or to Johann Jordan about 1680. Most place the origin of the centrifugal impeller with Denis Papin in 1689. The importance of Papin's contribution lies in his understanding of the concept of creating a forced vortex within a circular, or spiral casing by means of blades. Following Papin, Kernelien Le Demour in 1732 and Daniel Gabriel Fahrenheit in 1736 described other designs for centrifugal impellers, but there is no evidence of their practical use. Euler presented in his 1754 memoir an idealized theoretical application of Newton's law to centrifugal impellers, based on a conceptualization of his tubular turbine run backwards and now universally known as the "Euler equation". His publication caused a great development of hydraulic turbines in the eighteenth century but did little to influence the development of centrifugal impellers, which had to gradually develop through tedious cut-and-try methods. The one thing Euler contributed was to initiate a true mathematical inquiry into the employment of centrifugal force as a means of raising fluid. About the same time as Euler, John Smeaton introduced in 1752 the study of turbomachinery by models. He also defined power as equivalent to the rate of the lifting of a weight, a concept that is still fundamental in thermo-fluids. Today both centrifugal fans and compressors have reached high-efficiency levels and are built in sizes from a few Watts to Megawatts. [1]

1.2 Prologue

It is a fact that fan science has been developing for a long time and high levels of efficiency have been achieved (up to 92%), therefore, every step in its development requires more and more effort. And today the development is, as a rule, at the junction of directions, when it is necessary, for example, not only to reduce the power consumption of the fan but also to reduce its noise. Or increase the pressure of the fan while increasing the temperature of the drawn medium [2].In this study we have a fully functioning system combined of a centrifugal fan (FN 301) and a filtering system (FL 301), the former was lacking in performance, therefore our goal is to keep the (FL 301) filter and replace the fan with a new one which is identic to another existing fan (FN 501) and check its capacity to lift the required air flowrate, then a rotor-dynamic study was performed on the system to avoid operation that is closed to the critical speed.

Our thesis is based on five linked chapters and it's constructed as follow:

The first chapter is an introduction about the thesis and what chapters it's constructed from, including the state of art.

The second one is an introduction to rotating machines and centrifugal fans, where we address the topic of fan types and their applications in the industry in addition to its conditional maintenance.

The third chapter is about the design of our desired fan and the science behind it, in our case the fluid mechanics and aerodynamics, where we have conducted both theoretical and numerical types of study using Solidworks to get the results wanted.

The fourth chapter focuses on the stiffness of our system where we followed in this chapter the same steps of the previous one in addition to a finite element method study to verify the theoretical results.

In the fifth chapter, we used an approximate model of the shaft-turbine system and conduct theoretical vibration analysis, and follows it with a numerical one to validate our work.

Finally, we conclude our study with a comparison between the results we got and the experimental one that we already have from the existing model.

Chapter 2: Introduction to rotating machines and centrifugal fans

2.1 Centrifugal fans principals

Centrifugal fans are one of the most versatile and widely used pieces of rotating mechanical equipment found today. The fan is an essential part of all heating, air conditioning, air handling, and ventilation systems. Fans are used in automobiles, homes, offices, industry, and many other applications. The most common use of centrifugal fans is to move air and gases for the air handling or ventilation systems.

The basic principle of operation for a centrifugal fan is that a shaft-mounted rotating wheel (impeller) inside a scroll-type housing imparts energy to the airstream or gas being moved by the fan. Centrifugal fans utilize centrifugal force (thus their name) to increase the velocity of the air as it passes between the fan wheel blades and exits at the tip of the fan wheel. This action converts mechanical energy (shaft torque) into kinetic energy by the acceleration of the air stream to a higher velocity) and potential energy Fans are velocity generators for the air being moved. The centrifugal fan is the obvious choice for a ducted air system because of its capacity to produce pressure. Even though a disc or propeller fan can move a lot of air, it would have to be a lot more complicated and sophisticated to achieve the same job as a basic centrifugal fan when flow resistance is a significant factor. Some commercial fans are designed to deliver air at extremely high pressures that they should be called compressors. [3]

2.2 Predictable behavior of centrifugal fans

A fan does a measurable amount of labor because air has mass and solidity. Fortunately, the physical laws that govern its operation are simple and easy to understand. The volume, pressure, and velocity of air movement are the most important factors to consider while designing a fan. These measurable variables, as well as the amount of power necessary to produce them, maybe predicted with fair accuracy before construction using simple formulas if a few physical and mechanical concepts are recognized. Despite the sophistication of modern fan engineering, it is still impossible to create a flawless fan using only mathematical calculations. Following the calculations, after you've calculated the approximate size and proportions, you'll need to build and test a model. If adequate design allowances are made, it is realistic to expect the first model to meet the requirements. Performance can be improved by changing the wheel speed or modifying the input or outlet. Although complicated formulas have been developed to account for practically every conceivable factor, we will simply cover the most fundamental formulas in this thesis.

2.3 Basic fan types and applications

The diameter, width, and speed of the wheel, or rotor, are unquestionably the most crucial design features. Understanding the effects of these parameters and how the formulas are used will be aided by a review of the various fan kinds. Forward curved vane, backward inclined vane, and radial vane are the three most frequent forms of fan rotors. Below is a diagrammatic representation of each type.

2.3.1 Forward curved vane type

  The familiar quiet "squirrel cage fan" common in low-pressure applications is a forward curved vane type. It is made up of several small-area vanes that are bent in the rotational direction. The wheel will usually be around the same width as its
diameter, and the intake opening will be nearly the same size. Although it can generate pressures of up to 1-1/2" water column, it is most commonly used at pressures of less than 1".Forward-curved fans are used in clean environments and operate at lower temperatures. They are well suited for low tip speed and high-airflow work - they are best suited for moving large volumes of air against relatively low pressures

2.3.2 Backward inclined vane fans

 Have fewer, larger vanes that are slanted away from the rotational direction. This results in a non-overloading property, making it perfect for commercial heating, air conditioning, and ventilation applications where load conditions in complicated duct systems change dramatically over time. To conduct the same job as forward-curved fans, these fans must run at higher speeds, resulting in a noisier operation. Despite their ability to handle higher pressures, backward inclined vane fans are rarely used over a 3" water column of pressure. Backward inclined vane fans are more efficient than fans with a forward curve. Backward-inclined fans achieve their peak power consumption, after which demand falls well within the range of their usable airflow. Because fluctuations in static pressure do not overload the motor.

2.3.3 Radial vane type

  Straight vanes of higher depth characterize the radial vane type, and the wheel is usually narrow in relation to its diameter. It can withstand pressures well above 12" water column and move at a rapid rate. Radial vane fans are typically significantly heavier and stronger than standard ventilating fans, as well as being much noisy. This type is frequently required in retail settings. Because it is ideal for exhausting, conveying dust and dirt, and forced draft applications, this is the basic design type addressed in this manual. A wheel's performance and efficiency are affected by the number of blades or vanes, it contains. Many blades will be present in low-pressure, high-volume fans. [4]

Backward inclined vane fans	Backward inclined vane fans	radial vane type

Figure 2-1 Types of Centrifugal Fans

2.4 Fan Design and Selection Criteria

   The most critical factor in choosing the right fan type and size is determining the exact airflow and required outlet pressure. The amount of air required is dictated by the process requirements, which are usually determined by heat transfer rates or the amount of combustion air or flue gas to be handled. It's frequently more difficult to calculate or forecast the system pressure demand. Pressure drop across the length of the duct system, bends, contractions and expansions in the ducting system, pressure drop via filters, drop-in branch lines, and other factors should all be considered. These pressure dips should be added to any process-specific fixed pressures. Frequently, a cautious approach is used, with huge safety margins, resulting in over-sized fans that run at flow rates far below their design values, resulting in poor efficiency. The fan and impeller types are chosen once the system flow and pressure requirements have been determined. Values for specific fans and impellers should be obtained from the manufacturer for the best results. The magnitudes of needed flow and static pressure determine which fan type is best for a given application. The selection of the optimal impeller for a given fan type is also influenced by rotational speed. The speed of operation differs depending on the application. Because of their better hydraulic efficiency and low cost, high-speed compact units are often more cost-effective. Large, low-speed units, on the other hand, are preferable at low-pressure ratios.

2.5 Conditional maintenance

2.5.1 Introduction

   Condition-based maintenance (CBM) is being acknowledged as the most efficient technique for performing maintenance in a wide range of sectors, and machine condition monitoring is an important aspect of it. Machines were originally designed to be 'run to break,' which provided maximum operational duration between shutdowns but also meant that breakdowns might be catastrophic, posing severe safety, productivity loss, and repair cost concerns. The initial answer was "preventive maintenance," which is performing maintenance at regular intervals such that there is a very low chance of failure between repairs. However, this necessitates a far higher utilization of spare parts and additional maintenance work than necessary. To base maintenance on the perceived condition of operational machines (many of which must operate continuously for 12 months or longer), means to determine their internal condition must be available while they are in use. Vibration analysis and data transmission are the two basic methods for getting information from inside working machines to the outside. Although there are a few additional procedures that can be used, lubricant analysis is the most useful.

2.5.2 Maintenance Strategies

2.5.2.1 Run-to-Break: This is the old practice, in which machines were simply run until they broke. There was a breakdown. This gives the longest period between shutdowns in theory, but failure can be catastrophic and cause significant consequences, such as damage to components other than the ones that failed, as well as to connected devices. As a result, the time it takes to repair a vehicle can be significantly extended, including the time it takes to procure replacement parts, some of which may be large items that take a long time to manufacture. In many industries, the principal cost would be output loss, which is typically far higher than the cost of

individual machines. In industries with a large number of tiny equipment, such as sewing machines, where the loss of one machine for a short period is not crucial to output and failure is unlikely to be catastrophic, run-to-break maintenance still has a role.

2.5.2.2 (Time-Based) Preventive Maintenance: Regular maintenance is performed at intervals that are less than the projected "time between breakdowns." It's customary to set the intervals so that no more than 1–2% of the machines fail in that time. This means that the great majority of them could have run two or three times longer. This strategy has the advantage of allowing most maintenance to be planned ahead of time and reducing the risk of catastrophic failure. Aside from the possibility of a small number of unforeseen failures, the downsides include excessive maintenance and the need for an excessive number of replacement components. This approach has been known to lower morale among maintenance workers (who are aware that they are replacing perfectly good parts most of the time), causing their work to suffer as a result. This can lead to increased machine "infant mortality" by introducing faults that would not have occurred otherwise. When the time to failure can be adequately predicted, such as when it is based on well-defined "lifing" processes that can forecast the fatigue life of critical components based on a certain operational regime, time-based preventative maintenance is appropriate

2.5.2.3 Condition-Based Maintenance (CBM): This is also known as 'predictive maintenance,' because a machine's potential breakdown is predicted through regular condition monitoring, and repair is performed at the most appropriate moment. It has clear advantages over either run-to-break or preventative maintenance, but it does necessitate access to reliable condition monitoring systems that can not only evaluate the current state but also provide credible projections of remaining usable life. For example, the above-mentioned paper [6] by Neale and Woodley anticipated in 1978 that maintenance costs in British industry might be lowered by around 65 percent by appropriate implementation in several industries that they identified, However, because the range of monitoring approaches was initially limited and not always effectively deployed, it was only in the last 15 years or so that it was acknowledged as the optimal maintenance plan in the vast majority of cases. Initially, the biggest accomplishments were achieved in industries such as power generation and (petro)chemicals, where machines were required to run for lengthy periods without shutting down. Because the machines in these industries normally run at a near-constant speed and with a consistent load, the technical issues related to condition monitoring were greatly minimized. As more sophisticated diagnostic tools have become accessible.

2.5.3 Condition Monitoring Methods: Condition monitoring is based on the ability to monitor and anticipate the existing and future state of machines while they are in use. As a result, information about internal effects must be obtained outside while the machines are in operation. The following are the two most common methods for acquiring information on interior conditions :

2.5.3.1 Vibration Analysis: When a machine is in good working order, it has a distinct vibration signature. The signature of a fault changes in a way that can be linked to the defect. The phrase "mechanical signature analysis" was coined as a result of this.

2.5.3.1 Lubricant analysis: In the form of wear particles, chemical impurities, and other contaminants, the lubricant also transports information from the inside to the exterior of functioning machinery. Its primary application is in circulating oil lubricating systems, while it can also be used to analyze grease lubricants.

In this thesis, we are more interested in vibration analysis so it will be discussed in more detail in the following pages.

2.5.4 The purpose of maintenance

In any firm, the primary goal of maintenance is to keep things running smoothly. The minimum amount of capacity required for manufacturing at the lowest cost it ought to be not as a repair function, but as a RELIABILITY function. The reason for an organization's existence is "production". It is clear for other organizations, such as process or batch production factories, buildings, hospitals, the military, and transportation all require their unique security procedures, production, or a track record of success Major machine replacements or upgrades, which are often capital works projects, are frequently included in "maintenance" work. A machine's reliability is determined by whether it does what it's supposed to do when it's supposed to do it. In statistics, dependability refers to the likelihood that a machine will continue to produce as needed for a specified amount of time. It is determined by the machine's design (materials used, design quality, and construction quality) as well as the maintenance philosophy.

The core aim of maintenance may alternatively be expressed as contributing to the organization's production and profit objectives by maintaining plant reliability at an optimal level while maintaining people and plant safety. Maintenance is a strategic instrument for gaining a competitive advantage for your company. Only 10-20% of machines reach their design life, therefore there is lots of room for improvement.
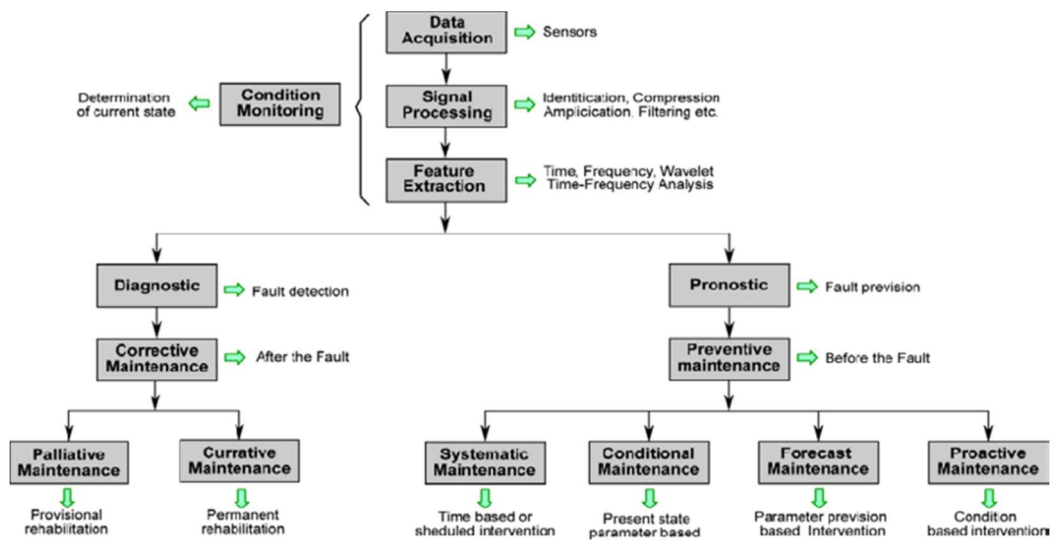

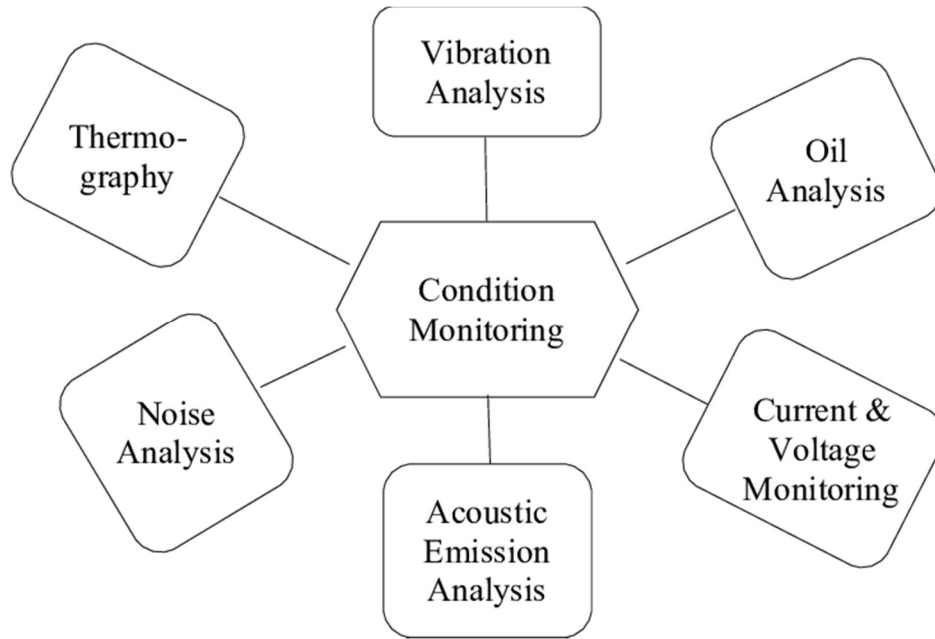*Figure 2-2* *Strategies of maintenance*

Figure 2-3 *Condition Monitoring Methods*

2.6 vibration analysis

  Vibration monitoring and analysis are probably the best known and most publicized techniques and the most powerful for rotating machines such as pumps. It seems logical that well-aligned and smoother running machines should use less energy and in general will also cost less to maintain.

Machines produce vibrations even when they are in good working order. Many of these vibrations may be traced back to regular events in the machine's operation, such as rotating shafts, meshing gear teeth, revolving electric fields, and so on. The regularity with which such events occur often provides a direct indication of the source, and so frequency analysis is used in many strong diagnostic approaches. Some vibrations are caused by events that are not phase-locked to shaft rotations, such as combustion in IC (internal combustion) engines, but which occur in a constant number each engine cycle, even if they are not completely repeatable. As will be seen, this can even be a benefit, as I will demonstrate to be separated from perfectly periodic ones. Other vibrations are linked to fluid flow, as in pumps and gas turbines, and these also have particular, quite often unique, characteristics. The term 'vibration' can be interpreted in different ways.

The absolute vibration of a machine housing and the relative vibration of a shaft and the housing, especially when the bearing separating the two is a fluid film or journal bearing, is an immediate difference. Because both forms of vibration measurements are widely utilized in machine condition monitoring, it's crucial to know what information they provide.

Another type of vibration which carries diagnostic information is torsional vibration, that is, angular velocity fluctuations of the shafts and components such as gears and rotor discs.

2.6.1 Vibration measurement

To carry out a vibration measurement chain, the following steps must be taken:

1- Transform the mechanical vibration into an electrical signal: this is the role of the sensor. The delivered signal can be expressed using the following quantities:

- The electrical voltage (in mV/g, mV/μm, ...) for voltage sensors.

- The electric charge (in pC/g) for piezoelectric accelerometers.

2- Amplify the output signal of the sensor to make it usable and transportable:

This is the role of the preamplifier. Necessary for piezoelectric accelerometers, it may or may not be incorporated into the sensor and it provides either a simple amplification of the sensor output voltage (voltage amplifier) or a transformation of the electrical charge into voltage before its amplification (charge-to-voltage converter, improperly called a preamplifier) (charge-voltage converter improperly called charge preamplifier).

3- Integrating the signal: This function allows you to transform accelerations measured with an accelerometer, if necessary, into speed or displacement, or to transform speeds measured with a velocimeter into displacement.

4- Limit the frequency range of the signal: High-pass or low-pass filters with adjustable or non-adjustable cut-off frequencies play this duty. This procedure allows you to limit the influence of unwanted high or low-frequency components and focus your research on a certain frequency range.

5- Amplify again the obtained signal to transmit it either:

- A detection and display device in global mode (peak amplitude, peak to peak, and RMS) these devices are intended for the monitoring of bearings,

- An analog/digital converter for digital data processing (computerized data collectors)

- A spectrum analyzer

- A storage unit (magnetic or digital recorder) for deferred signal processing.

One of the elements of the material used to carry out these various stages is the sensor.

 - Vibration captors**:** Sensors that measure displacement are known as proximometers, whereas those that measure speed are known as velocimeters, and those that measure acceleration are known as accelerometers. The first link in the measuring chain is the signal's sensors. A sensor's key characteristics include its range of applications, amplitude measurement range, sensitivity, temperature resistance, influence factors, weight, and size. Absolute vibration sensors, such as piezoelectric accelerometers, are becoming increasingly used for monitoring rotating machinery. Their operation is dependent on a property of piezoelectric materials called piezoelectricity. Produce an electrical charge proportional to the compressive or shear stress that the material is subjected to.

An accelerometer is made up of a piezoelectric disk that functions as a spring and rests a pre-stressed seismic mass on it. When a mass accelerates, it imposes pressures on the piezoelectric disk, causing an electric charge to form on its surface proportionate to the acceleration.

The response of a piezoelectric accelerometer shows the existence of two zones:

- An area of linearity of the sensor. It is the range of frequencies within which the response of the sensor corresponds to the amplitude of the measured signal with a relative sensitivity (precision) which is generally defined by a percentage of variation equal to 5% or 10%. This zone defines the frequency range for good use of the sensor.

- A zone encompassing the resonance of the sensor within which the amplitude measurements are amplified, in a controlled way, by this resonance. This zone will generally be avoided since the measurement is distorted. It will only be used for specific applications where the measurement of certain specific indicators including the sensor resonance is required (for example, parameters specific to bearing monitoring).

2.6.2 Finding the vibration frequency

An oscilloscope view of a vibration amplitude-time trace (i.e. in the time domain) will usually reveal the presence of one or more frequencies in addition to the basic signal, which is normally at the frequency corresponding to running speed. A better way is to use a frequency analyzer to view the vibration pattern in the frequency domain, which is referred to as the vibration spectrum or vibration signature because it is unique to that machine at that point of measurement. The vibration spectrum of a machine displays the consequences of various exciting forces inside the machine, providing a "window" into the machine, and any change in the signature signals a change in the machine. It is a matter of expertise and experience to determine whether this is significant in measuring machine health. Changes in machine condition are substantially more susceptible to signature analysis than overall measurement alone. A big shift in one vibration component may signal a significant change in the machine, yet the overall vibration level may not vary much. The simplest and oldest sort of analyzer is similar to radio in that it is manually tuned and displays the amplitude at each tuned frequency on a meter. The spectrum display is created by gently tuning the filter over the desired frequency range and drawing the greatest amplitude measurements at each frequency, either manually or with the help of a chart recorder.[5]

2-7 vibration in centrifugal fans

Vibration in a centrifugal fan can cause a host of problems that, if left unchecked, can lead to issues ranging from periodic downtime to catastrophic failure. Here are some of the more common causes of centrifugal fan vibration :

1- Resonance: On big fan assemblies, resonance issues are frequently twofold. Critical speeds are the first thing that must be addressed. Critical speed mapping is a process that is usually handled during the design of a new fan. The majority of fans are made to run at speeds below the first critical speed. The overall rotating mass, the span between bearings, and the needed operating speed to create the requisite airflow are all variables in avoiding critical speed in fan design. If a fan is operated above the first critical speed, vibration levels must be carefully

monitored while the fan accelerates to working speed and, more crucially, coasts down to a stop from operating speed. Vibrations that are too high while passing through a critical speed can cause serious damage to bearings, seals, and other related equipment. The second factor, structural resonance, is far more difficult to forecast. Every structure has a natural frequency that it will reverberate at. Component failures can occur if a fan operates at a structural resonance point that is not rectified. At 1X operating speed or at a harmonic frequency, structural resonance can arise (2X, 3X, etc.). Structural resonance varies with operating speed and can be easily determined by plotting vibration amplitude against frequency versus rotating speed on a signature plot.

2- Shaft Misalignment: The alignment of a drive motor shaft and a fan shaft is an important step that must be addressed when installing a new fan or replacing a shaft/rotor assembly. A 1X and 2X harmonic component of vibration is caused by misalignment of the driving motor shaft and the fan shaft. Excessive amounts of axial vibration are frequently caused by misalignment problems. Because most fans lack axial vibration probes, this is frequently undetected unless the 2X vibration component is present. Careless installation of new equipment can result in misalignment, although bent shafts or poorly seated bearings are the most common causes.

3- Mechanically loose Connections: Excessive vibration levels can be caused by looseness in any mechanical connection between bearing caps, bearing pedestals, or foundations, or it might increase an already existing unbalance problem. In most circumstances, a physically loose connection will produce harmonic vibration levels (2X, 3X, etc.) as well as subharmonic vibration levels (X/2, X/3, etc.). Because of the presence of sub-harmonic vibration levels, vibration induced by mechanically weak connections is frequently misdiagnosed. If the connection between the fan rotor and the fan shaft is loose, the second form of vibration induced by mechanically loose connections can occur. In many circumstances, this will result in an unusually high amount of unbalance-related vibration, which is not always at 1X running speed. This type of vibration can be difficult to detect, but once identified, it's simple to fix. In most circumstances, this issue can be avoided by using correctly engineered interference fits between the rotor hub and fan shaft.

4- Cracked Shafts or Rotors: One of the most dreaded failure modes in any sort of rotating equipment is crack propagation in the fan shaft or rotor. A break in the shaft or rotor of a fan might eventually lead to catastrophic failure if it goes undiagnosed. If vibration trending and analysis is performed on a piece of equipment, early crack identification can be achieved. The appearance and growth of a 2X vibration component, as well as a change in the phase and amplitude of the 1X vibration component, are common indicators of a crack propagating in a fan.

5-Rotor Mass Unbalance: A fan rotor generally consists of a welded, riveted, or cast fan impeller mounted on a shaft. Even if the manufacturer takes care in locating blades and weighing parts, the weight center is separated from the axis of rotation. This difference between the weight center and axis of rotation is referred to as "imbalance.".

Rotor mass unbalance is the most common cause of excessive vibration in most rotating equipment and fans. The primary symptom of rotor mass unbalance is a high 1X vibration level.

Rotor mass variation leading to an unbalanced condition is typically caused by three primary factors.[6]

- Variations in manufacturing can lead to unevenly distributed mass in the fan rotor.

- Exposure to high airstream temperatures can cause uneven growth of the fan rotor.

- Deterioration of the fan rotor caused by either high-speed particle collisions

Chapter 3: Fan Aerodynamic Study

3.1 Introduction

The purpose of using centrifugal fans in milling plants is to evacuate a certain amount of air from the working machines to the outside, where the air needs to pass through a duct system including a dust collector filter. The fan has to maintain and generate sufficient pressure to overcome the resistance which it faces during its passage.

In this chapter, we will study the performance of a centrifugal fan and its capacity for lifting the required air volume flowrate.

Fan performance is usually presented in the form of a characteristic curve of air volume flow against the pressure developed by the fan. In the first part, we will plot these curves using fan laws, then we will design the fan and simulate it using CAD software (Solidworks).

In the second part we will design the dust collector filter and the duct system, then run a CFD simulation to get the system pressure drop curve.

The fan operational point will be the intersection of the fan curve and the system curve pressure drop curve.

3.2 Background and objective

The old system consists of a centrifugal fan (FN 301) with a closed backward impeller of 800 mm diameter, connected to the factory flour milling machines through a duct system passing by a dust-collector filter (FL 301), the system shows a lack of performance since the fan can only lift an amount of 6.5 tons per hour while the factory owners want the machine to lift a minimum airflow rate of 10 tons per hour.

We proposed to replace the old fan with a new one that is identical to an existing fan (FN 501). The main characteristic of the (FN 501) are:
- The impeller diameter is 920 mm.
- It is connected to the (FL 501) filter which is bigger than the (FL 301) filter.
- The (FN 501) can lift 19 tons per hour of air when it is attached to the (FL 501) filter.

This study aims to check the capacity of the (FN 501) centrifugal fan to lift a minimum mass flow rate of 10 tons/hour when we connected to the (FL 301).

3.3 Machine description

The system consists of centrifugal fan FN 501 (Photo 3.1) with a backward closed impeller (Photo 3.2), attached directly to an electric motor with the capacity of 110 kW and a constant rotation speed of 2985 (rpm), the fan inlet is connected to the flour milling machines through a set of complex ducts system, including a dust collector filter (FL 301), while the fan outlet is connected to a simple duct leading to the outside.

Photo 3.1: *The centrifugal fan*

Photo 3.2: *The impeller*
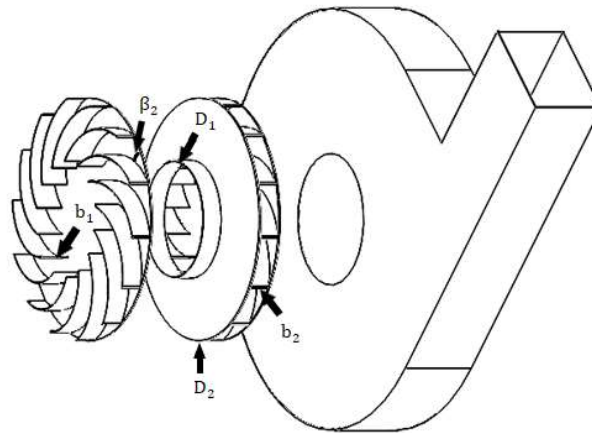
3.4 Fan dimensions

Figure 3.1: *Fan dimensions*

The (FN 501) fan dimensions are:

Impeller outer diamer: $D_2 = 920$ mm

Impeller eye diameter: $D_1 = 439$ mm

Impeller outer width: $b_2 = 80$ mm

Impeller inner width: $b_2 = 110$ mm

Blade length: 390 mm

Blade inner angle: $\beta_1 = 56°$

Blade outer angle: $\beta_2 = 20°$

Blade thickness: 3 mm

Number of blades: Z=14

Impeller hub thickness: 6 mm

Impeller shroud thickness: 6 mm

Fan case diameter 1600 mm.

Fan outlet area: $A_{out} = 404 \times 284$ mm²

3.5 Fan performance
The fan performance was evaluated using both fan laws and CFD simulation.
3.5.1 Using fan laws:
3.5.1.1 Impeller velocity triangles [7]
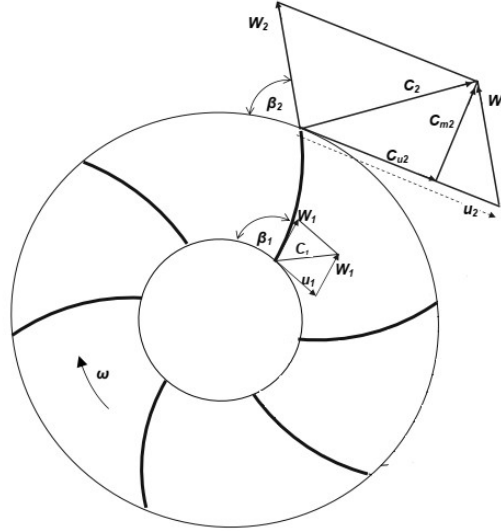
Figure 3.2: Impeller velocity triangles

ω: The Angular velocity of the impeller (rad/s).
U: The Peripheral (tangential) speed of the blade (m/s).

$$U_1 = \frac{\pi \cdot D_1 \cdot N}{60} = \frac{\pi \cdot 0.439 \cdot 2985}{60} = 68.61 \text{ m/s} \tag{3.1}$$

$$U_2 = \frac{\pi \cdot D_2 \cdot N}{60} = \frac{\pi \cdot 0.920 \cdot 2985}{60} = 143.79 \text{ m/s} \tag{3.2}$$

Where N is the impeller rotational speed (rpm).
W: The velocity of the air relative to the impeller (m/s).
C: The absolute velocity of the air (m/s).
C_m: The radial component of the absolute velocity of the air (m/s).
C_u: The tangential component of the absolute velocity of the air (m/s)
β: The Blade angle, the angle between the tangent of the blade curve and the tangent of the impeller edge (degree).
$\beta_1 = 56°$
$\beta_2 = 20°$

3.5.1.2 Euler pressure
According to Euler fundamental equation, the pressure developed by the fan impeller is given as:[8]

$$P_E = \rho(C_{u2}U_2 - C_{u1}U_1) \qquad \text{(pa)} \tag{3.3}$$

Where ρ is the air density (kg/m³).

By applying Pythagoras theorem on the velocity triangles (Figure 3.2):

$$W_2^2 = C_{m2}^2 + (U_2 - C_{u2})^2$$
$$= C_{m2}{}^2 + U_2{}^2 - 2U_2 C_{u2} + C_{u2}{}^2$$

giving:

$$2U_2 C_{u2} = U_2^2 - W_2^2 + (C_{m2}^2 + C_{u2}^2)$$
$$= U_2^2 - W_2^2 + C_2^2$$

Similarly for the inlet:

$$2U_1 C_{u1} = U_1^2 - W_1^2 + C_1^2$$ By rearranging the previous equations we get:

$$P_E = \rho \left(\frac{U_2^2 - U_1^2}{2} - \frac{W_2^2 - W_1^2}{2} + \frac{C_2^2 - C_1^2}{2} \right) \tag{3.4}$$

The first two terms represent the gain in static pressure where the first refers to the centrifugal effect and the second refers to the effect of relative velocity, while the third term refers to the change in kinetic energy and represents the gain in velocity pressure.[9]

3.5.1.3 Euler's pressure-flow rate relationship
For an ideal centrifugal impeller, the flow Q is assumed to inter the impeller radially therefore the tangential component of the absolute velocity is set to be zero, $C_{u1} = 0$.
Equation (3.1) becomes:
$$P_E = \rho U_2 C_{u2} \tag{3.5}$$
From the outlet velocity triangle in Figure 1 we have:

$$\tan \beta_2 = \frac{C_{m2}}{U_2 - C_{u2}}$$

giving $C_{u2} = U_2 - \dfrac{C_{m2}}{\tan \beta_2}$

$$P_E = \rho U_2 \left(U_2 - \frac{C_{m2}}{\tan \beta_2} \right)$$

Knowing that $C_{m2} = \dfrac{Q}{A_2} = \dfrac{\text{volume flowrate}}{\text{flow area at impeller outlet}} = \dfrac{Q}{\pi \cdot b_2 \cdot D_2}$ (Figure 3.3):[10]

Equation (3.3) becomes

$$P_E = \rho \cdot \left[U_2{}^2 - \frac{U_2}{\pi \cdot b_2 \cdot D_2} \cot \beta_2 \cdot Q \right] \tag{3.6}$$
$$P_E = \rho \cdot \left[143.79^2 - \frac{143.79}{\pi \cdot 0.080 \cdot 0.920} \cdot \cot(20) \cdot Q \right]$$
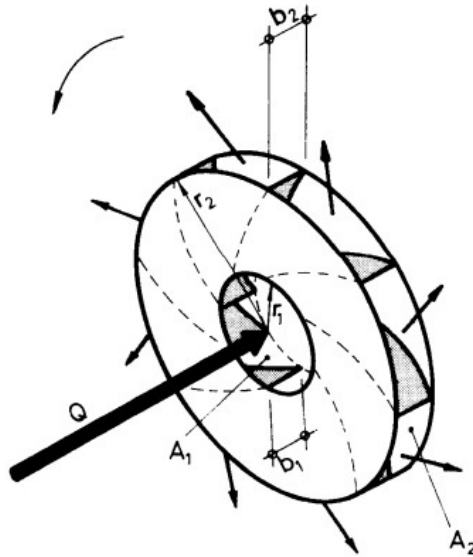$$P_E = \rho \cdot [20675.56 - 226.34 \cdot Q] \tag{3.7}$$

Figure 3.3: Flow area at impeller inlet and outlet

3.5.1.4 Pressure Losses

The actual performance of a centrifugal fan differs from the one predicted by Euler's equation due to several losses:

3.5.1.4.1 Inter-blade circulation

The Euler equation assumes the air follows the blade profiles exactly. This can only be justified if the number of blades is infinite. The cause of the deviation of flow from the ideal is known as inter-blade circulation sometimes called Slip: [11]

$$\text{Inter-blade Circulation Loss} = \rho \cdot (U_2)^2 \cdot \frac{\pi}{z} \cdot \sin \beta_2 \tag{3.8}$$

$$\text{Inter-blade Circulation Loss} = \rho \cdot (143.)^2 \cdot \frac{\pi}{14} \cdot \sin(20)$$

$$= 1586.83 \cdot \rho \tag{3.9}$$
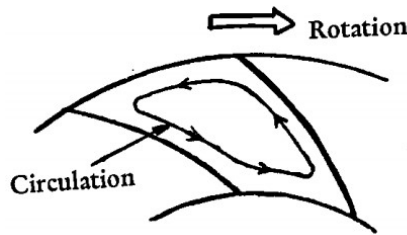
Figure 3.4: Inter-blade circulation

3.5.1.4.2 Impeller loss

Pressure loss will occur within the blade passage due to flow separation resulting from excessive decreases in relative velocity. This loss may be written in the following calculation :[11]

$$\text{Impeller pressure loss} = k_{(imp)} \cdot \frac{1}{2} \cdot \rho \cdot Q^2 \cdot \left[\frac{1}{\pi \cdot D_1 \cdot b_1 \cdot \sin \beta_1} - \frac{1}{\pi \cdot D_2 \cdot b_2 \cdot \sin \beta_2} \right]^2 \tag{3.10}$$

$$\text{Impeller pressure loss} = k_{(imp)} \cdot \frac{1}{2} \cdot \rho \cdot Q^2 \cdot \left[\frac{1}{\pi \cdot 0.439 \cdot 0.1 \cdot \sin(61)} - \frac{1}{\pi \cdot 0.920 \cdot 0.080 \cdot \sin(20)} \right]^2$$

$$= 9.48 \cdot k_{(imp)} \cdot \rho \cdot Q^2 \tag{3.11}$$

17

$k_{(imp)}$= Loss Factor (of the order of 0.2 to 0.3 for sheet metal blades).

3.5.1.4.3 Outlet loss
Loss due the eddy formation resulting from the retardation of flow velocity between the impeller and the casing and it is given as:[11]

$$\text{Outlet Pressure Loss} = k_{(out)} \cdot \frac{\rho}{2} \cdot \left(\sqrt{(U_2)^2 + \left(\frac{C_{m2}}{\sin \beta_2} \right)^2 - \left(2U_2 \cdot \frac{C_{m2}}{\tan \beta_2} \right)} - \left(\frac{Q}{A_{out}} \right) \right)^2 \qquad (3.12)$$

$$C_{m2} = \frac{Q}{A_2} = \frac{Q}{\pi \cdot b_2 \cdot D_2} = 4.32 \cdot Q \qquad (3.13)$$

$$A_{out} = 0.404 \cdot 0.284 = 0.1147 \, m^2 \qquad (3.14)$$

$$\text{Outlet Pressure Loss} = k_{(out)} \cdot \frac{\rho}{2} \cdot \left(\sqrt{159.53 \cdot Q^2 - 3413.31 \cdot Q + 20675.56} - 8.718 \cdot Q \right)^2 \qquad (3.15)$$

Were: $k_{(out)} = $ Loss Factor (of the order of 0.4).

3.5.1.4.4 Inlet loss
Loss due to the change from axial to radial flow, these inlet losses can be calculated as follows:[11]

$$\text{Inlet pressure loss} = k_{(in)} \cdot \frac{\rho}{2} \cdot \left(\frac{4 \cdot Q}{\pi \cdot D_2^2} \right)^2 \qquad (3.16)$$

$$\text{Inlet pressure loss} = 1.13 \cdot k_{(in)} \cdot \rho \cdot Q^2 \qquad (3.17)$$

$$k_{(in)} = 0.7 \text{ to } 1.1 \text{ (for sheet metal blades)}$$

3.5.1.5 Fan actual pressure
The actual pressure developed by the fan P_f is the difference between the Euler pressure and the sum of the pressure losses.

P_f = Euler pressure- $\sum$ Losses

= P_E - (Inter-blade Circulation Loss+ Impeller pressure loss+ Outlet Pressure Loss+ Inlet pressure loss)

$$P_f = \rho \, [20675.56 - 226.34 \cdot Q] - \left[(1586.83 \cdot \rho + 9.48 \cdot k_{(imp)} \cdot \rho. Q^2 + \right.$$

$$\left. k_{(out)} \cdot \frac{\rho}{2} \cdot \left(\sqrt{159.53 \cdot Q^2 - 3413.31 \cdot Q + 20675.56} - 8.718 \cdot Q \right)^2 + 1.13 \cdot k_{(in)} \cdot \rho \cdot Q^2 \right]$$

$$P_f = \rho \cdot \left[-\left(9.48 \cdot k_{(imp)} + 1.13 \cdot k_{(in)} \right) \cdot Q^2 - \right.$$

$$\left. \frac{k_{(out)}}{2} \cdot \left(\sqrt{159.53 \cdot Q^2 - 3413.31 \cdot Q + 20675.56} - 8.718 \cdot Q \right)^2 - 226.34 \cdot Q + 19088.73 \right] \qquad (3.18)$$

3.5.1.6 Impeller torque
The impeller torque is given as:[9]

$$T = Q \cdot \rho \cdot [r_2 \cdot C_{u2} - r_1 \cdot C_{u1}] \qquad \text{(Nm)} \qquad (3.19)$$

$C_{u1} = 0$; from equation (3.3) development.

$$C_{u2} = U_2 - \frac{C_{m2}}{\tan \beta_2} = 143.79 - \frac{4.32 \, Q}{\tan(20)} = 143.79 \text{ - } 11.86 \, Q \qquad (3.20)$$

Therefore:

$$T = Q \cdot \rho \cdot 0.46 \cdot [143.79 - 11.86 \cdot Q] \qquad \text{(Nm)} \qquad (3.21)$$

$$T = \rho \cdot (-5.45 \cdot Q^2 + 66.14 \cdot Q) \tag{3.22}$$

3.5.1.7 Power into the fan

The power consumed by the impeller is given as:
$$P_{in} = T \cdot \omega \qquad (W) \tag{3.23}$$
$$P_{in} = \rho \cdot \omega \cdot (-5.45 \cdot Q^2 + 66.14 \cdot Q)$$
$$P_{in} = \rho \cdot 312.588 \cdot (-5.45 \cdot Q^2 + 66.14 \cdot Q) \tag{3.24}$$

3.5.1.8 Airpower

The power transmitted by the impeller to the air is given as:
$$P_{air} = P_f \cdot Q \qquad (W) \tag{3.25}$$
$$P_{air} = \rho \cdot Q \cdot \Big[-\big(9.48 \cdot k_{(imp)} + 1.13 \cdot k_{(in)}\big) \cdot Q^2 -$$
$$\frac{k_{(out)}}{2} \cdot \Big(\sqrt{159.53 \cdot Q^2 - 3413.31 \cdot Q + 20675.56} - 8.718 \cdot Q\Big)^2 - 226.34 \cdot Q + 19088.73 \Big] \tag{3.26}$$

3.5.1.9 Fan efficiency

The impeller efficiency is defined as:
$$\text{Eff}_{imp} = \frac{\text{Airpower}}{\text{Power into the fan}} = \frac{P_{air}}{P_{in}} = \frac{Q}{312.588 \cdot (-5.45 \cdot Q + 66.14 \cdot)} \cdot \Big[-\big(9.48 \cdot k_{(imp)} + 1.13 \cdot k_{(in)}\big) \cdot$$
$$Q^2 - \frac{k_{(out)}}{2} \cdot \Big(\sqrt{159.53 \cdot Q^2 - 3413.31 \cdot Q + 20675.56} - 8.718 \cdot Q\Big)^2 - 226.34 \cdot Q +$$
$$19088.73 \Big] \tag{3.27}$$

3.5.1.10 Fan performance curves

We assume the maximum values for the loss factors:[11]
$$k_{(imp)} = 0.3$$
$$k_{(out)} = 0.4$$
$$k_{(in)} = 1.1$$
We neglect the thermal effect and we assume that the air density is constant and equal to 1.2 kg/m^3.

By substituting the values of the loss factors and the air density in equations (3.7), (3.18), (3.24), and (3.27), the fan characteristic curves can be plotted using Matlab as follows:
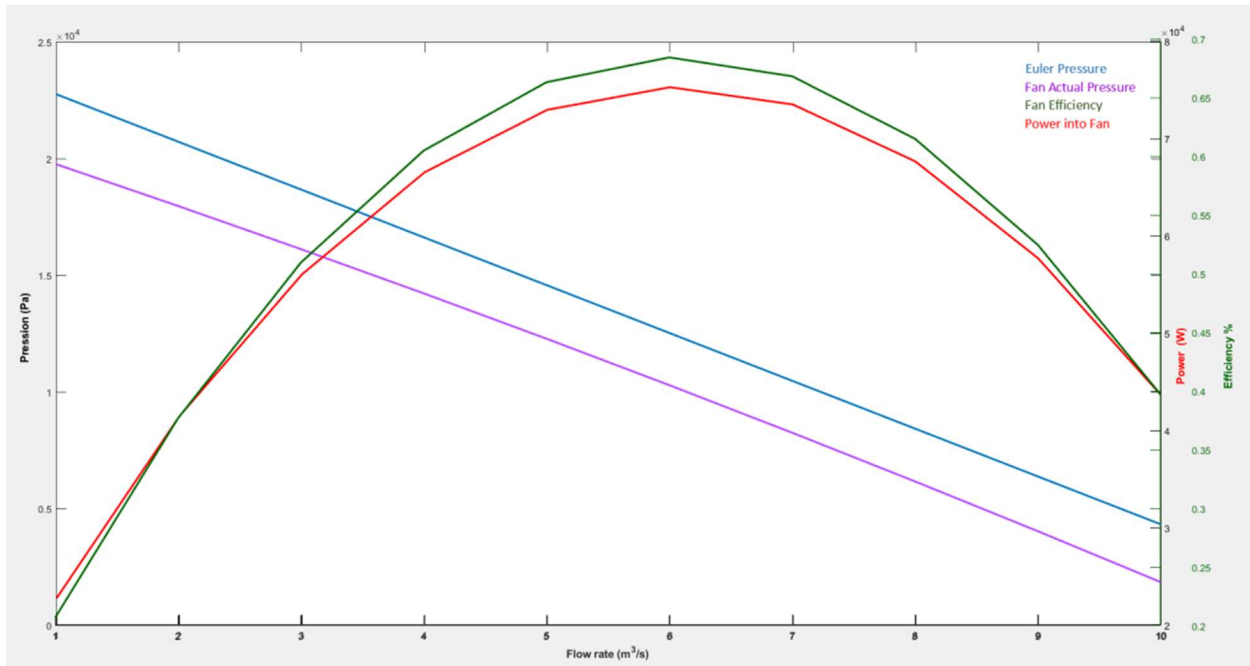
Figure 3-5: *Fan performance curves*

   The pressure curves show the relationship between the pressure capabilities of the fan compared to the fan's air volume flow rate at the given fan speed (2985 rpm).
We can see that Euler pressure is linearly dependent on the flow rate while the actual pressure curve is a parabola that opens downwards.
The area between the pressure curves is due to the losses, the distance between them is getting smaller as we getting close to the high-efficiency point.
The pressure curves flow from upper left to lower right start at the Shut-off Head point where zero flow occurred. The curves continuous to the right, with pressure reducing and flow increasing until the Run-out point, and that can be explained as the more pressure enters the fan the lower the fan can lift it.
The power curve shows the relationship between the fan's air volume flow rate and the power required from the motor to run the fan, the curve shows that more air needs more power.
The efficiency curve shows the relationship between the air volume flow rate and the fan efficiency, which is the ratio of the air power to the shaft power, the highest point refers to the best efficiency point.

3.5.2 Fan CFD simulation
3.5.2.1 Fan modeling
We start by modeling the (FN 501) fan parts using Solidworks.
We also need to design the aspiration duct system to fit the (FL 301) dust collector filter.
The discharge duct system is also needed.
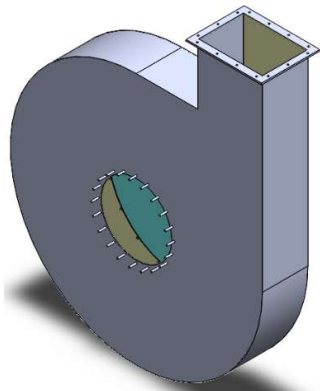
20
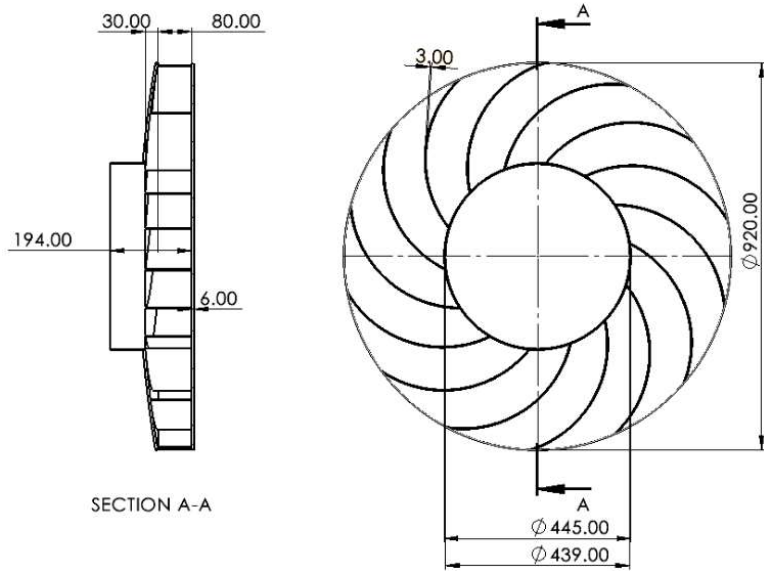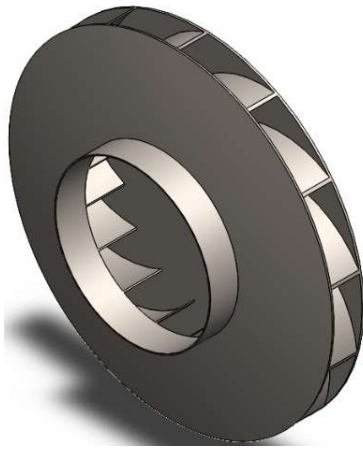
1- Impeller:

Figure 3.6: *Impeller*

2- Volute:
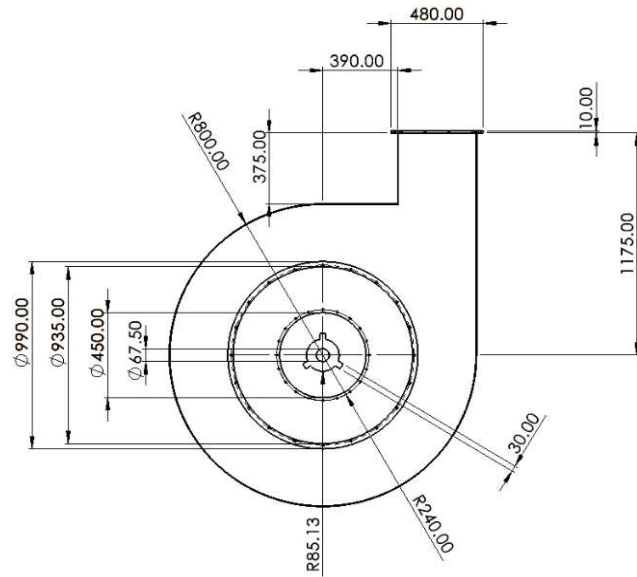
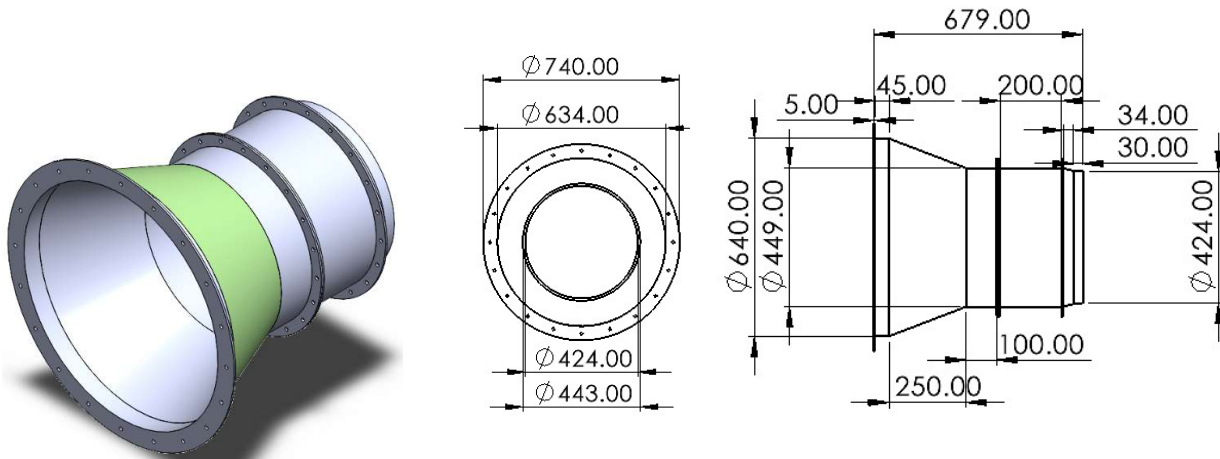**Figure 3.7:** *Volute*

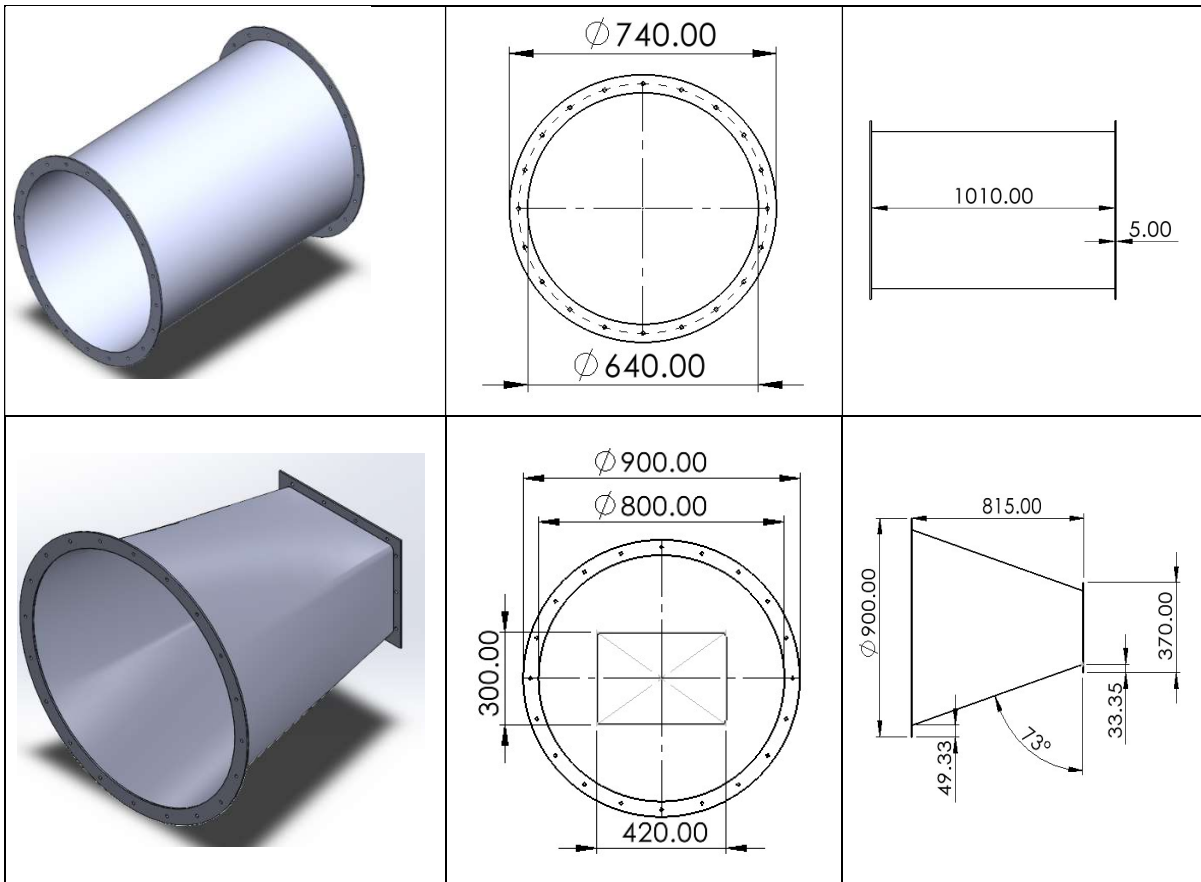3- Inlet cone:

Figure 3.8: *Inlet cone*
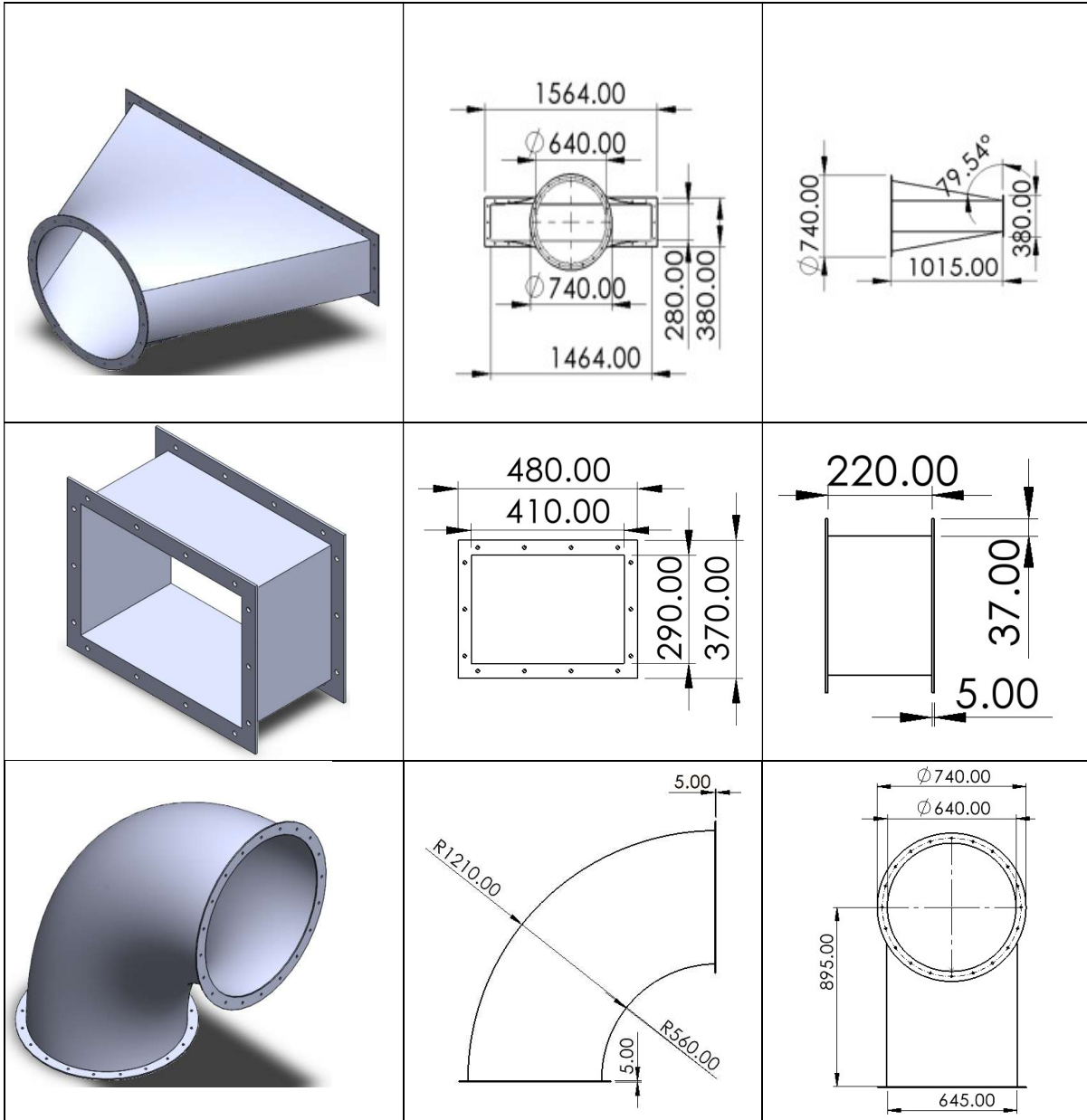
4- Duct:

Figure 3.9: *Ducts*

System assembly:

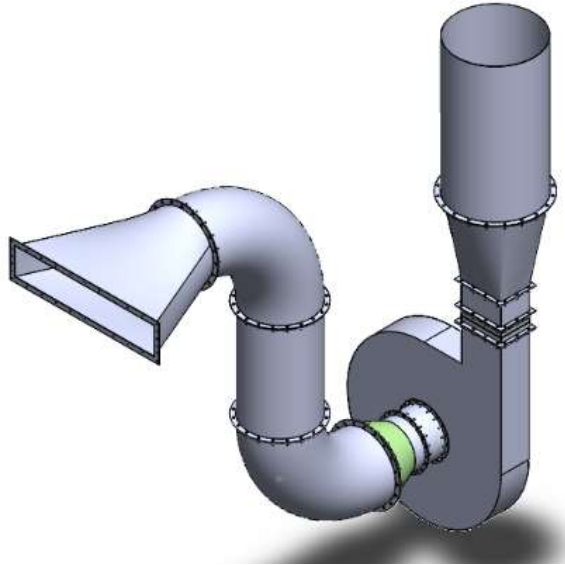This is how the fan-duct system looks like after the parts assembly.

Figure 3.10: *System assembly*

3.5.2.2 Flow simulation

First, we set up the boundary conditions:

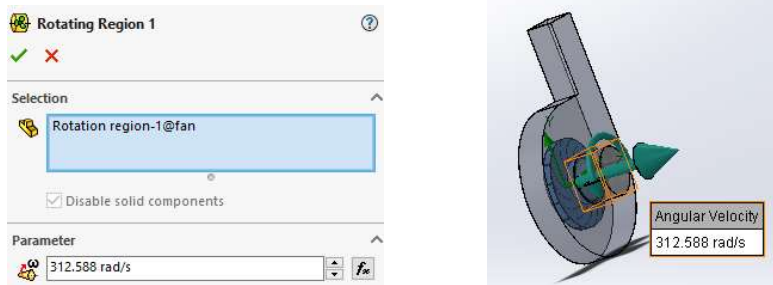We start by inserting the rotating region and setting the angular velocity to (312.588 rad/s):

Figure 3-11: *Selecting the rotating region*

Then we set the outlet to the environment pressure (101325 pa):
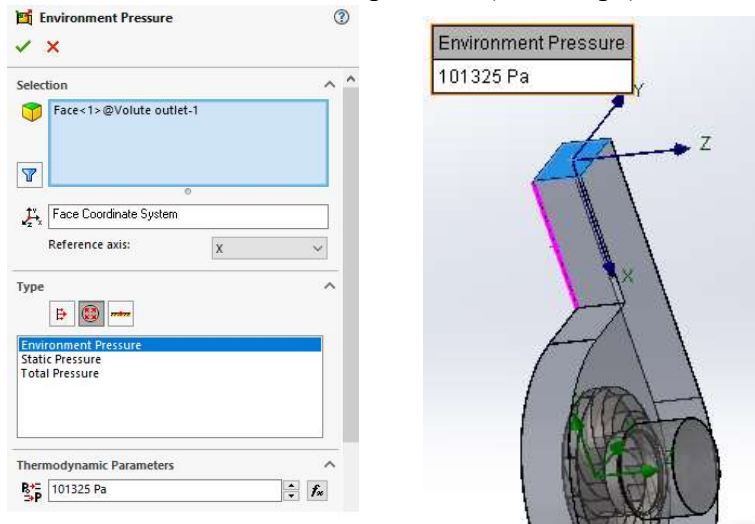
Figure 3-12: *Setting the Outlet boundary condition*

24

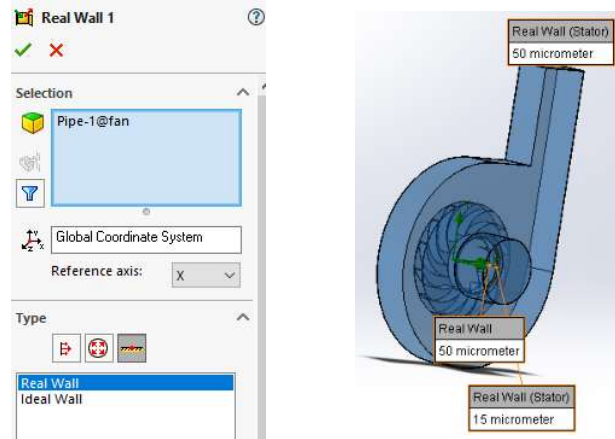After that we define the inner surfaces of the pipe, the volute, and the impeller as real walls:

Figure 3.13: *Defining real walls*

For the goals, we define the static, dynamic, and total pressure for both inlet and outlet:
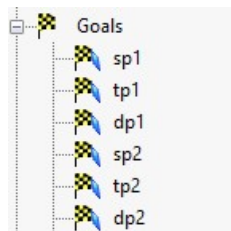

Figure 3.14: *Defining simulation goals for both inlet and outlet*

Then we set another goal for the impeller torque, we select the impeller and we choose the torque about the Z axis:
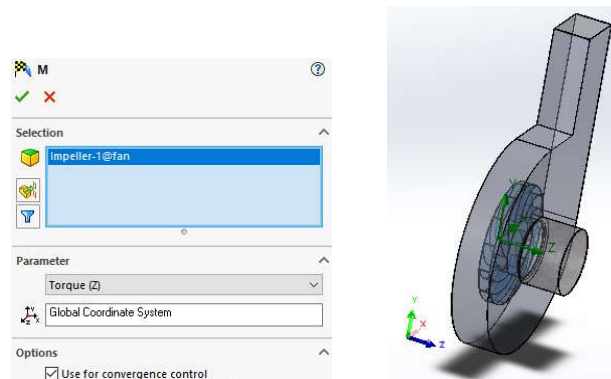

Figure 3-15: *Defining the impeller torque*

We set equation goals to calculate the total pressure difference, the static pressure difference, and the dynamic pressure difference and that can simply be done by subtracting the inlet pressure from the outlet pressure for the three parameters:

Figure 3.16: Setting equation goals

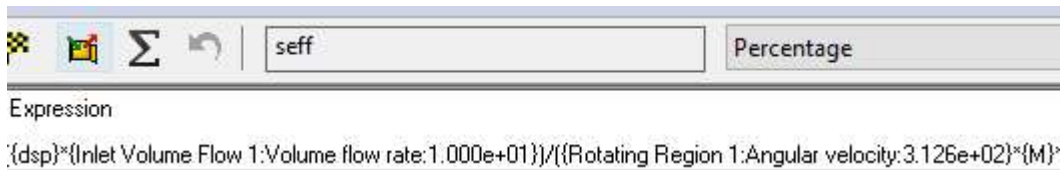We define another equation goal for static and total efficiency:

Figure 3.17: Static efficiency goal

Figure 3.18: Total efficiency goal

Again we define an equation goal for the impeller input power and airpower:
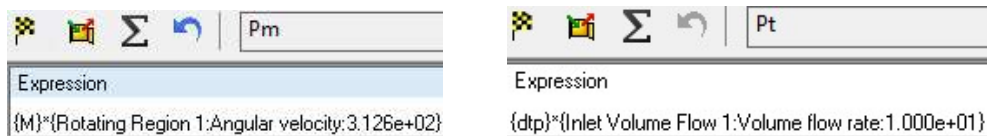

Figure 3.19: Defining equation goal for impeller

For the meshing, we apply a fine mesh for the entire fan and a finer mesh for the impeller surface and the rotating region:
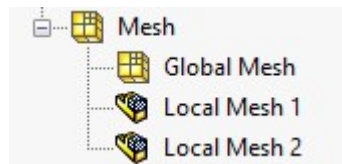

Figure 3-20: Defining the mesh
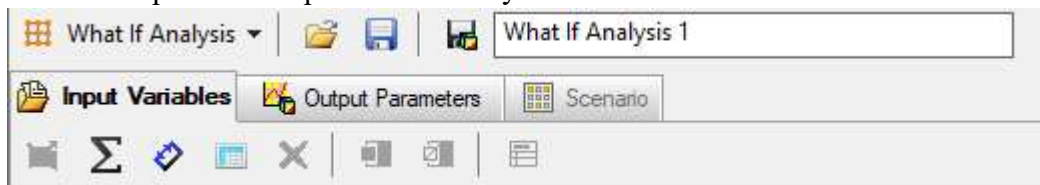
The last step is to set a parametric study:

Figure 3-21: Setting parametric Study

We set the inlet volume flowrate as a variable and we give it the values from 1 to 10 m^3/s:
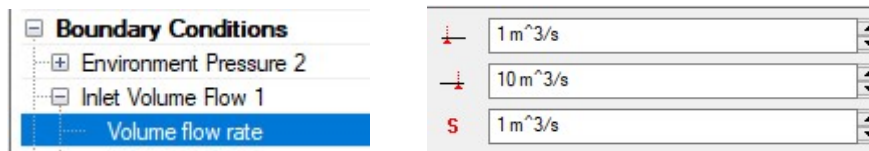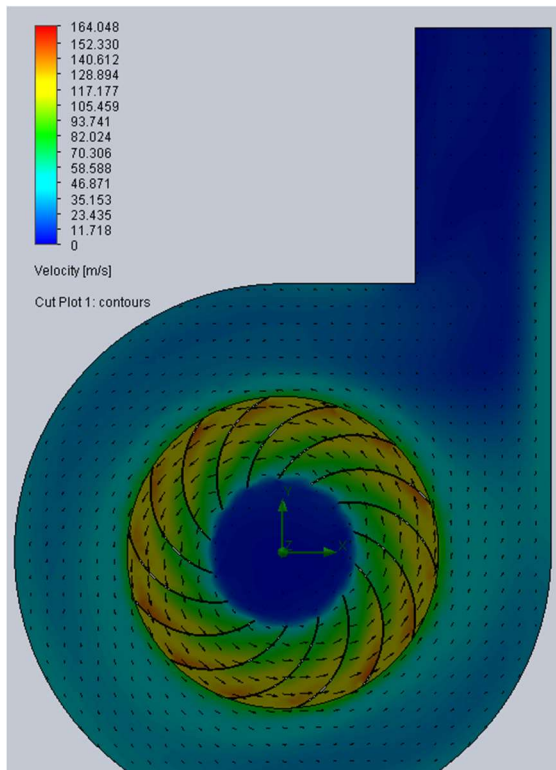

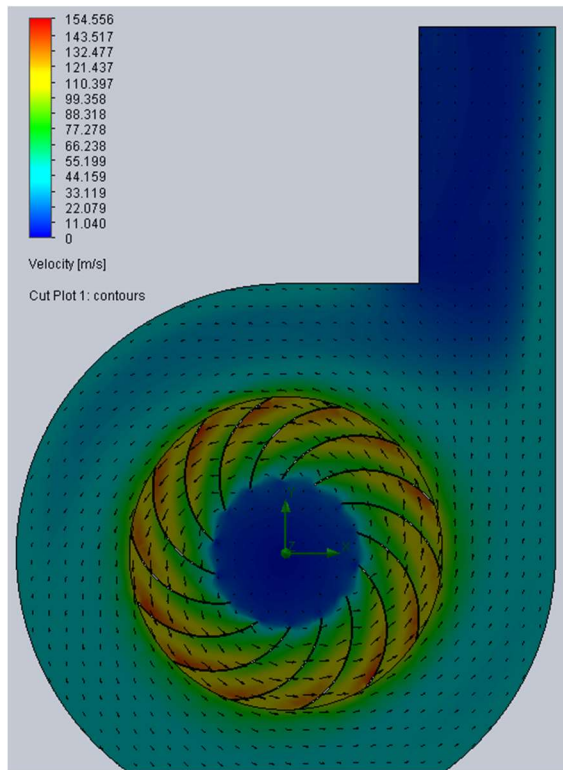***Figure 3-22:*** *setting the inlet volume flowrate*

And we select all the previous goals and cut plots.

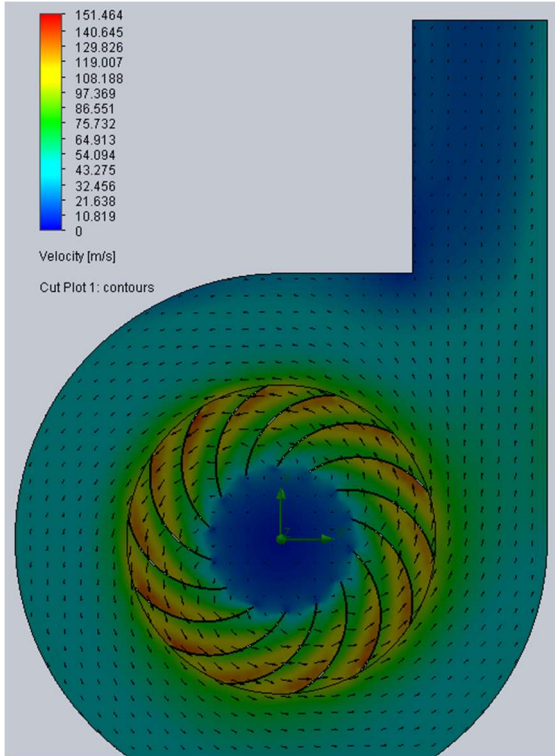Running the parametric study gave us the following results:
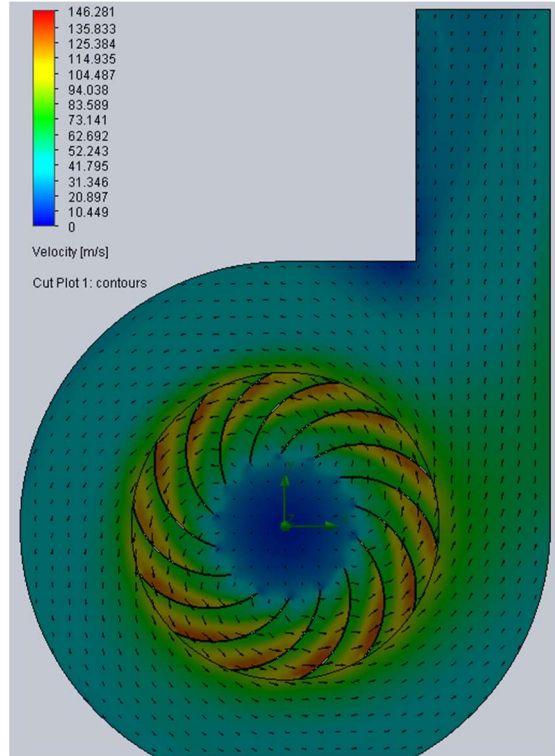
3.5.2.2.1 Velocity cut plots

$1 \text{ m}^3/s$ $2 \text{ m}^3/s$

3 m³/s

4 m³/s

5 m³/s

6 m³/s

28
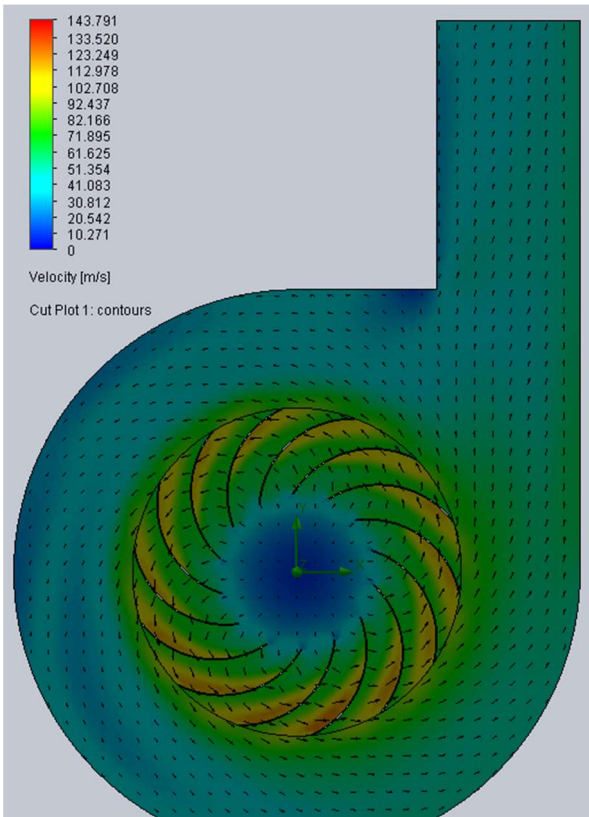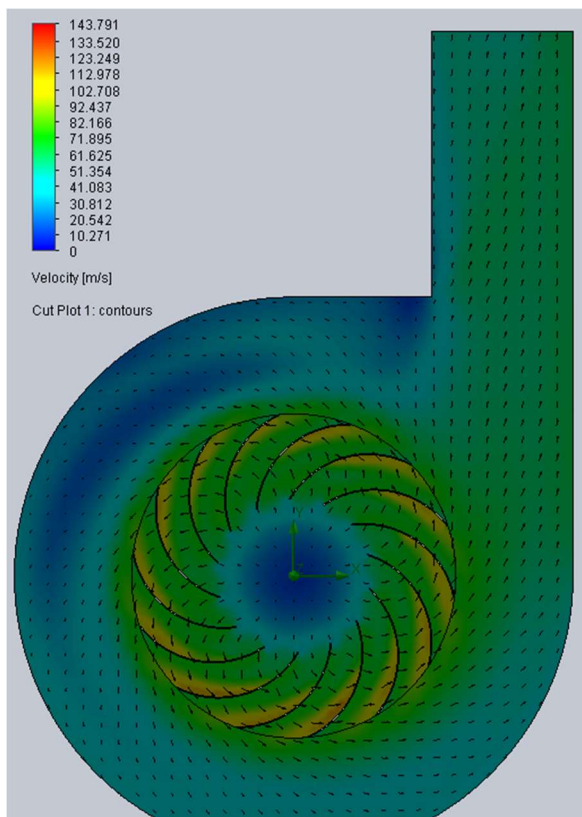
7 m³/s   8 m³/s
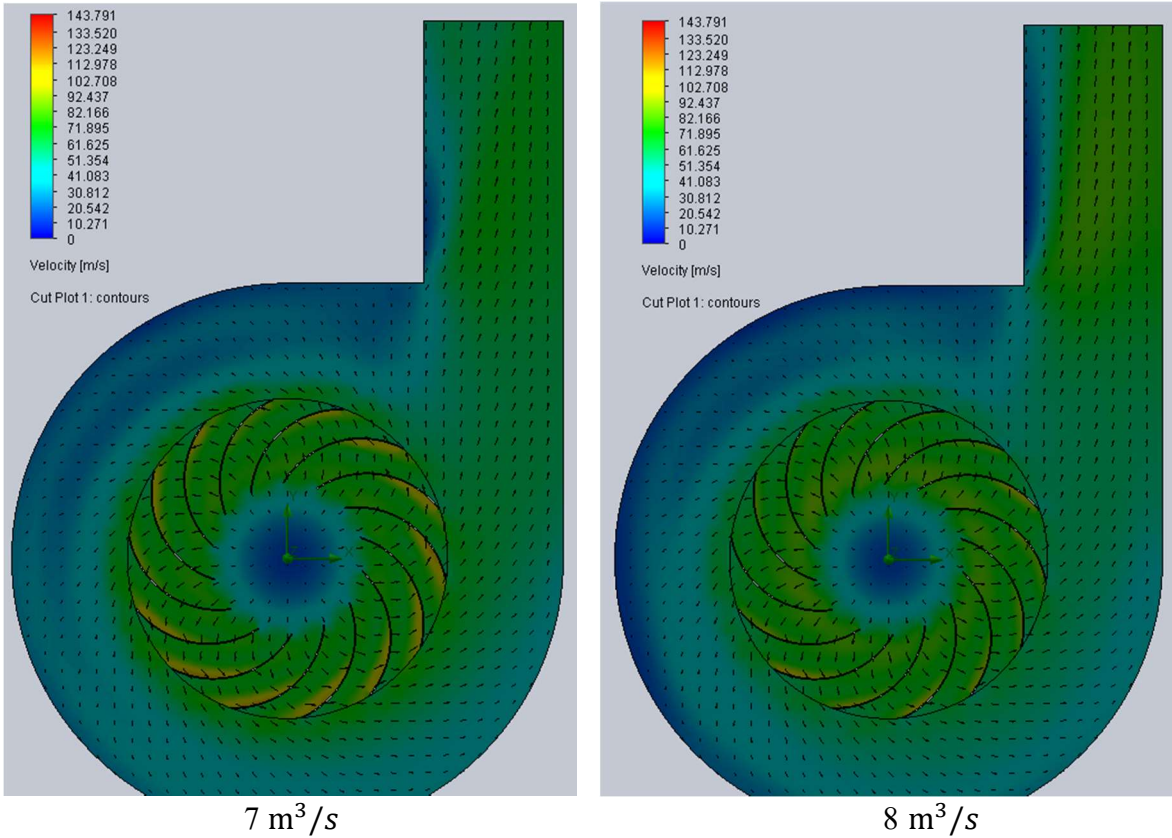
Figure 3.23: *Velocity cut plots*

The cut plots show the velocity contours across the fan, we can see in general that the air enters the impeller eye with the defined velocities in the boundary conditions (v =Q/eye area), the air kinetic energy increases due to the centrifugal force acting on it by the impeller, it follows the blade passage and reaches its maximum velocity at the impeller outer edge which is equal to the tangential velocity previously calculated (143 m²/s), then leaves the fan.

We can also see that as the volume flow rate increases, the velocity at the outlet increases and that can be explained by the inverse relationship between the pressure and the velocity, from the theoretical fan curves we concluded that lower flowrate means higher pressure, and higher pressure means lower velocity.

3.5.2.2.2 Fan performance curves
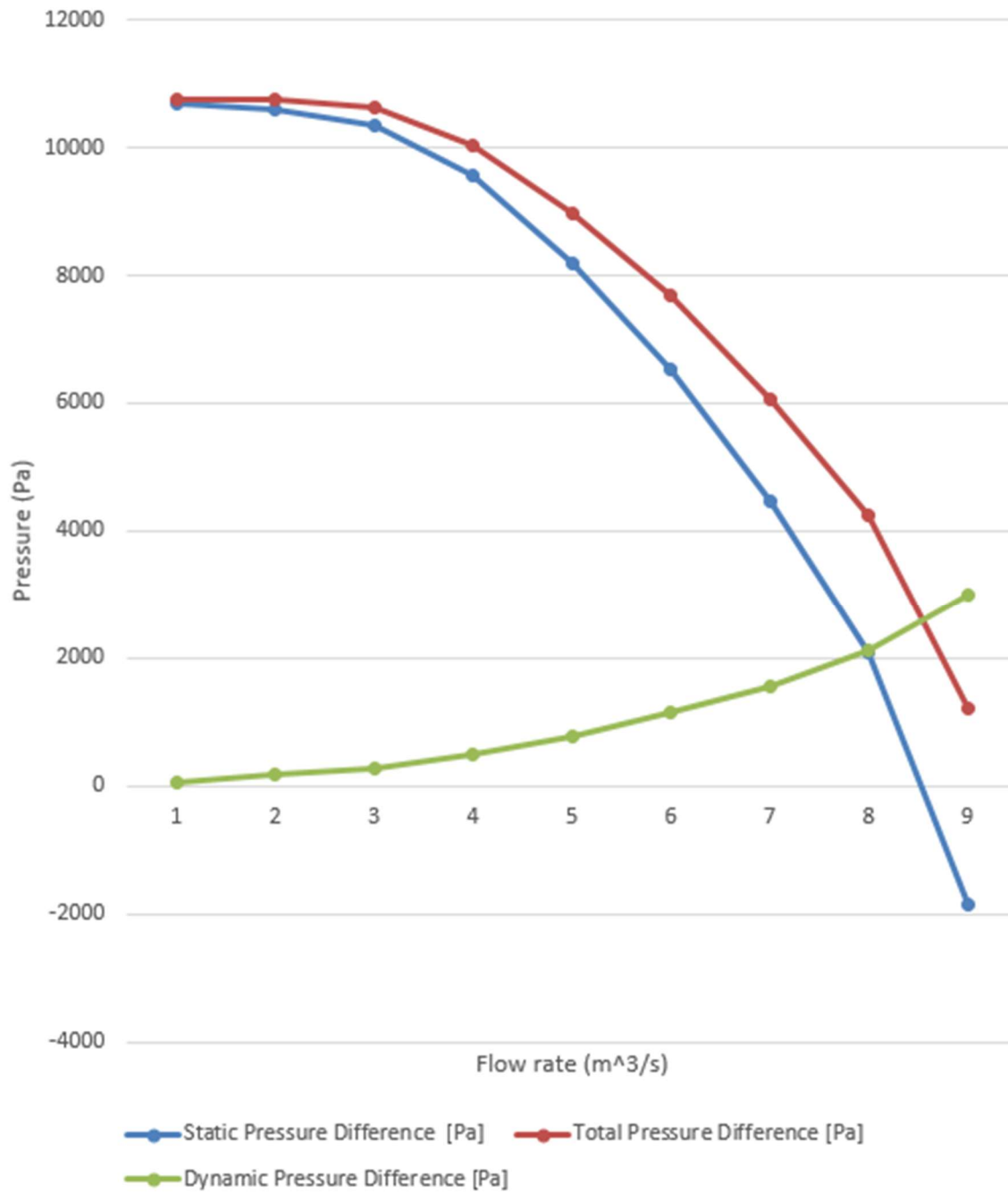
Figure 3.24: Fan pressure curves
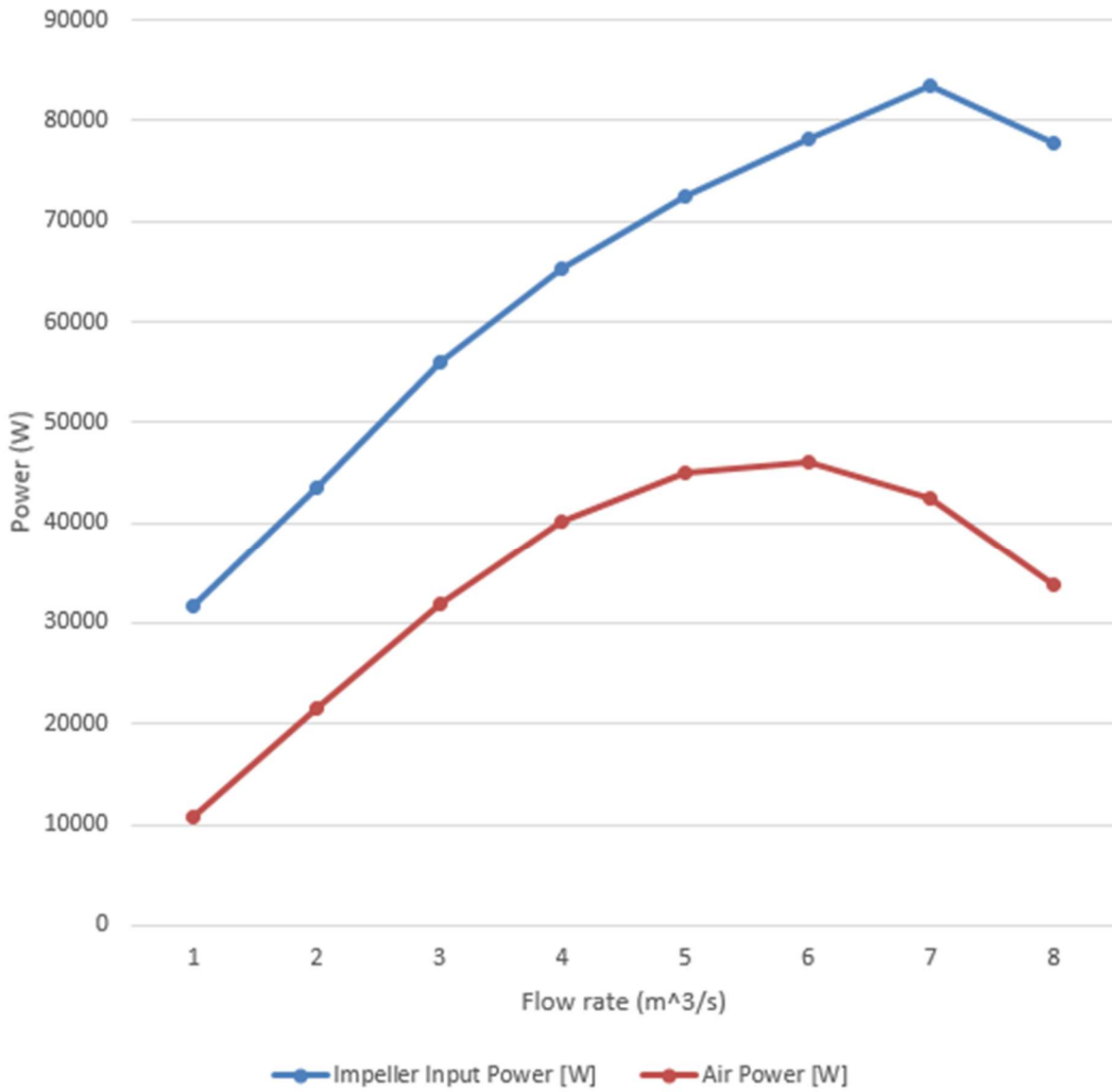
Figure 3.25: *Fan power curves*
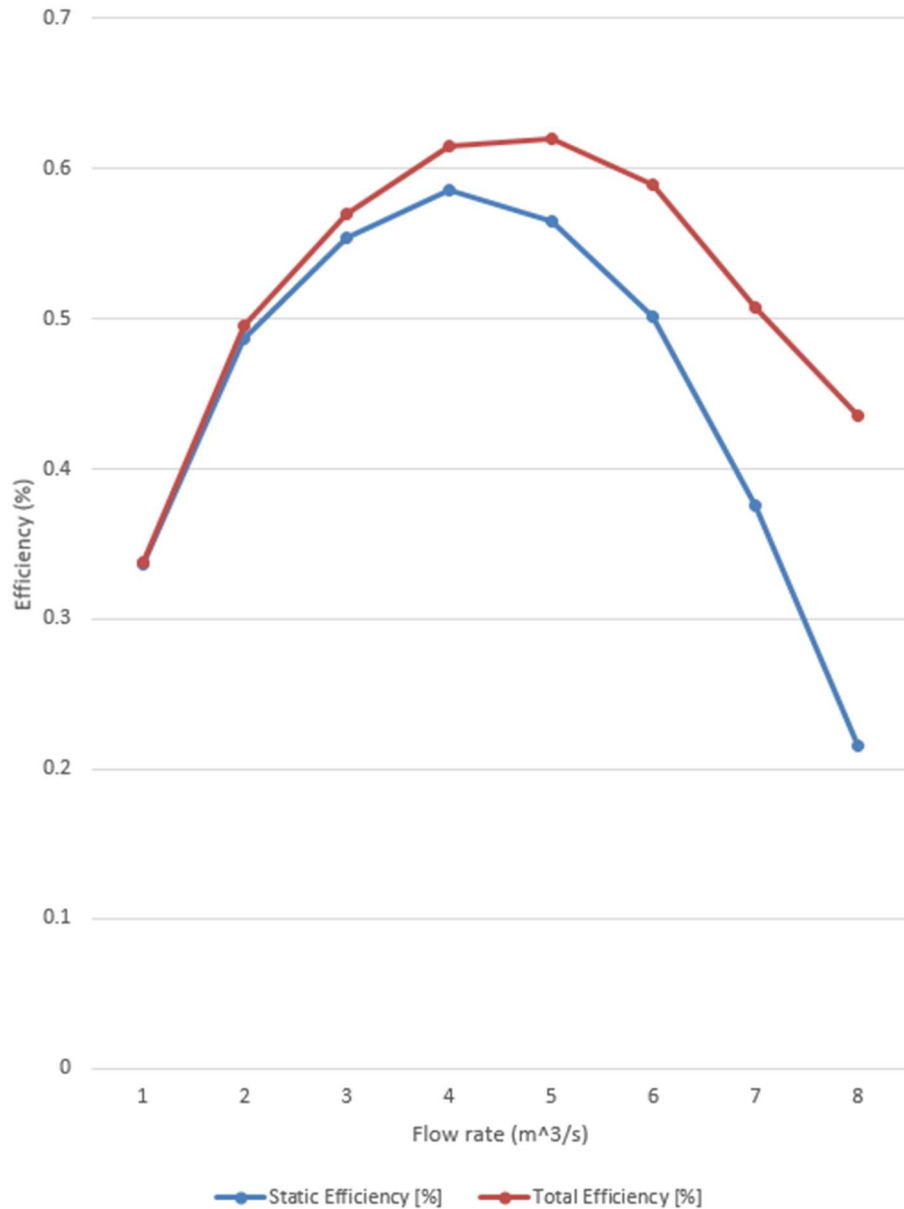
Figure 3.26: *Fan efficiency curves*

Figure 3.24 shows the curves of static pressure difference, total pressure difference, and dynamic pressure difference as a function of flow rate, the first two curves decrease as the flow rate increase while the third curve represents the velocity pressure and it is proportional to the square of the air velocity. The total pressure difference is the sum of the static and dynamic pressure differences.

The curves show that the fan can generate a maximum pressure of 10500 pa and can lift a maximum air volume flow rate of $8.5 \ \text{m}^3/s$.

The power curve (Figure 3.25) shows the relationship between the fan's air volume flow rate and the power required from the motor to run the fan and the power absorbed by the air, it is clear from the curve that more air needs more power to be lifted.

The power absorbed by the air is lower than the required power to rotate the impeller, the area between the two power curves represents the losses in the system, where the two curves will be identical for an ideal fan.

The required power to rotate the impeller is always lower than 85 kW, which means that the 110 kW motor is always capable of running the fan.

The efficiency curve (Figure 3.26) shows the relationship between the air volume flow rate and the fan efficiency, which is the ratio of the air power to the shaft power, the highest point refers to the best efficiency point which is 62%.

3.6 Dust collector system design and simulation

A dust collector is a system used to enhance the quality of air released from industrial and commercial processes by collecting dust and other impurities from air or gas.

Photo 3.27: *Dust collector*

3.6.1 System design
3.6.1.1 Bag filter

The bag filter is made of polyester.
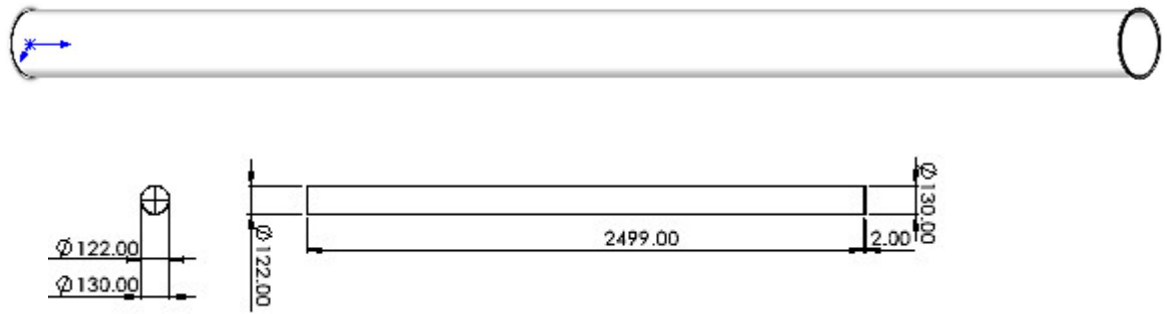
Figure 3.28: Bag filter

3.6.1.2 Bag cage (steel):
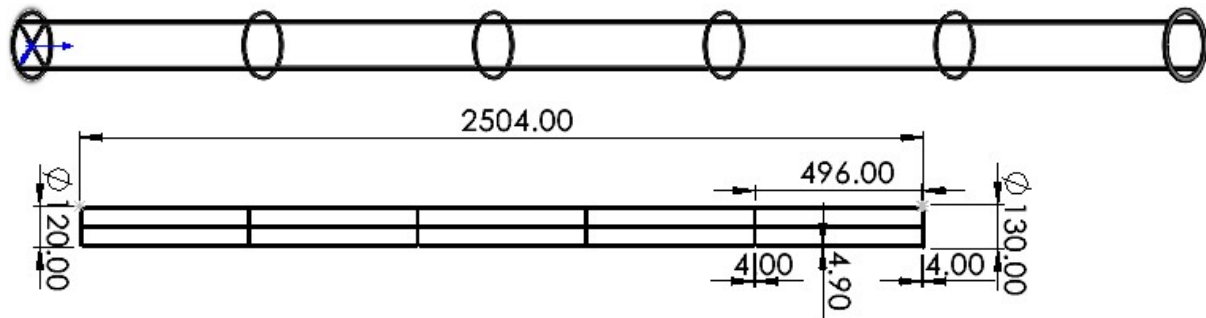
Figure 3.29: Bag cage

System assembly:
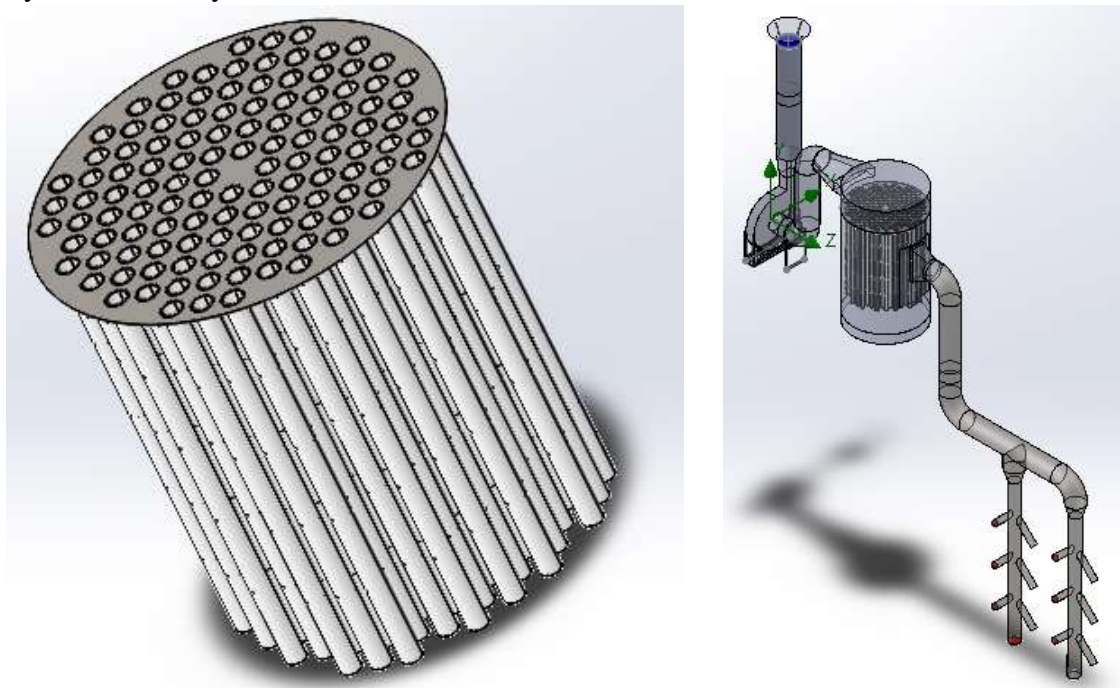
Figure 3.30: System assembly

3.6.2 CFD simulation

For the simulation, the boundary conditions are similar to the condition we applied to the fan except for rotating region and equation goals, since we just need the pressure drop between the outlet and the inlet of the system, also the air had to pass through the filter bags, therefore we need to define it as porous medium material and we did choose the UFM-100 white polyester for this case.
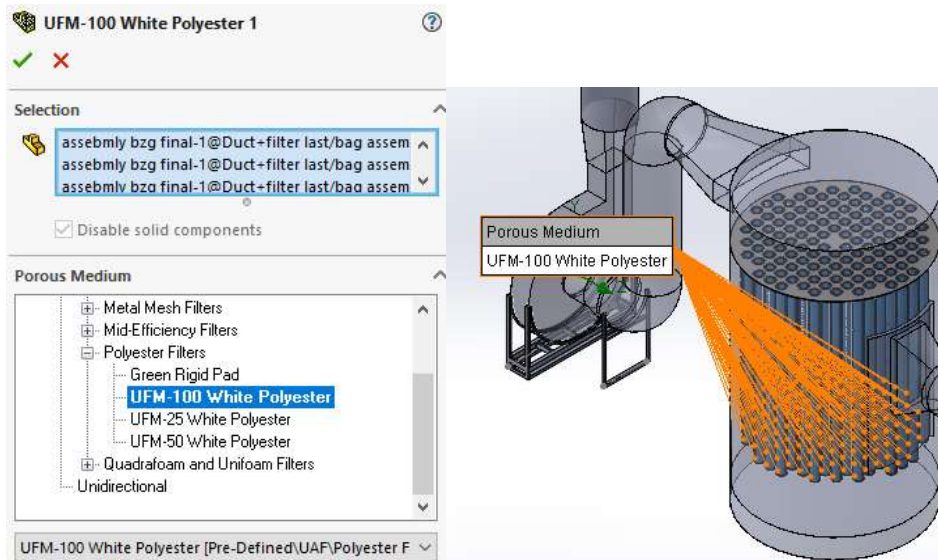
Figure 3-31: *Setting Porous Medium*

Running the parametric study gave the following plot:

Total Pression Diffrence [Pa]
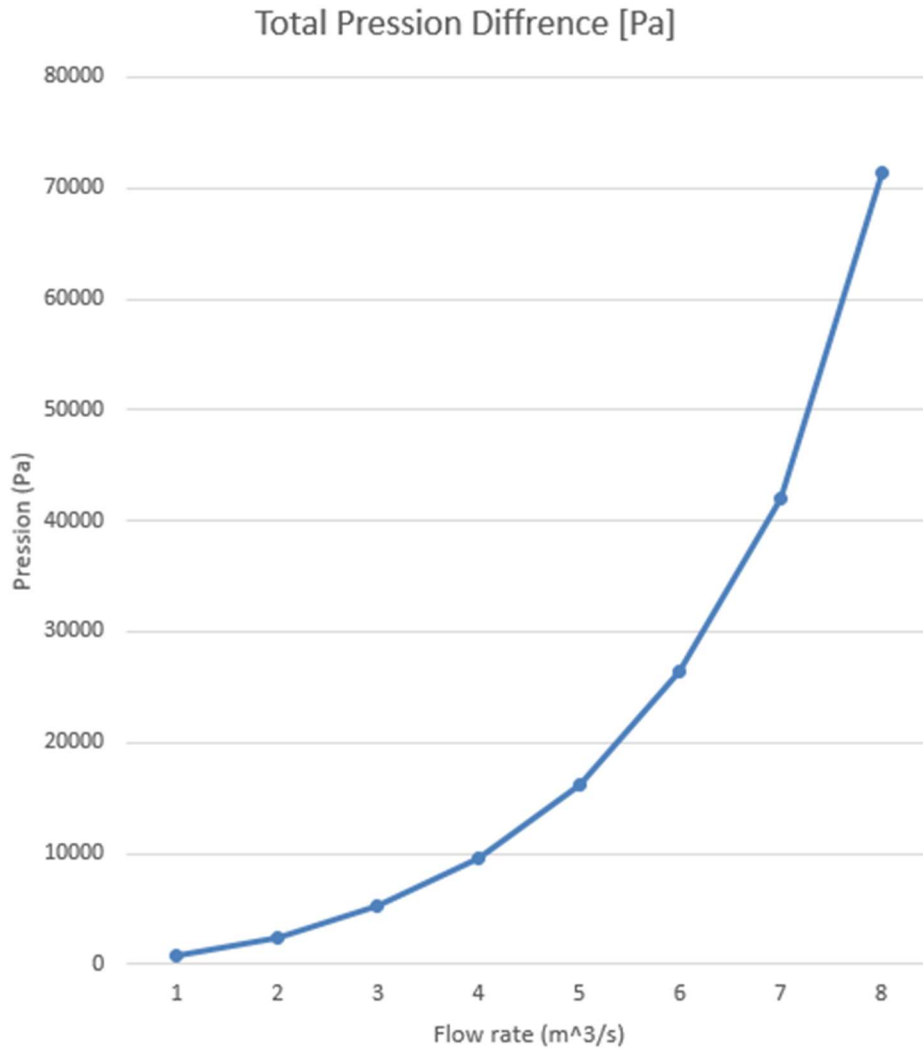
Figure 3-32: System curve

Figure 3.32 shows the relationship between the system curve and the volume flow rate.
We can see that the pressure loss is proportional to the square of the flow rate.
As more volume passes through the duct-filter system, more pressure will be lost.
These results are accurate for a new clean dust collector filter, a working filter will increase the system resistance due to the dirty filter bags, this improvement in the system resistance will cause a steeper pressure drop curve, and that will shift the intersection point to the left, which that the fan will operate at lower flowrate than the one corresponding to the intersection point.

3.7 Fan operational point

The fan operational point is the intersection point between the fan performance curve and the system pressure drop curve.
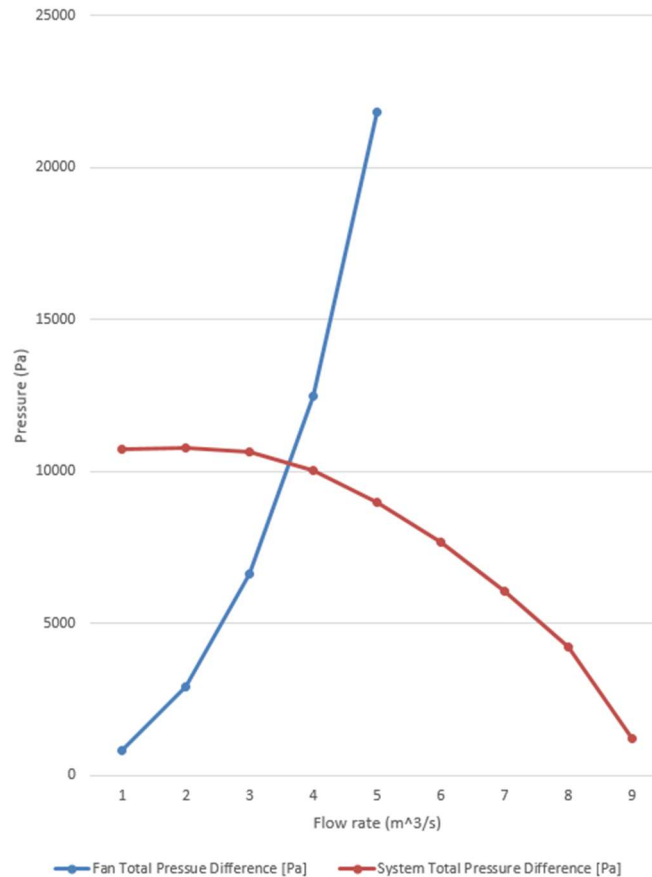
Figure 3-33: *Fan Operational point*

Figure 3.10 shows that the two curves intersect at 3.5 m³/s which is approximately 16 tons/hour. This means that the fan is capable of lifting the required air volume.

From the efficiency curve (figure 3.26) we can see that the fan will operate near its best efficiency point.

Conclusion

The fan performance and the duct-filter system can be described by a set of characteristic curves which can be derived from both theatrical study and CFD simulation.

The fan operational point is the intersection of the fan pressure curve and the system resistance curve.

The CFD results are more accurate than the theatrical results, and that is due to the number of ignored losses in the theatrical study and the limitation of the laws that describe these losses.

Both theatrical study and CFD simulation show that the fan can fulfill the required conditions.

The fan's actual operational volume flow rate is lower than the one corresponding to the intersection point, and that is because the dirty bag filter of an operating dust collector adds extra resistance to the system, which will shift the intersection point to the left.

Chapter 04: Static study & Bearings performance

4-1 Introduction

  Just because a fan curve and the fan laws say that the fan can lift the required flowrate does not mean that it can. Many factors can affect the fan performance like the shaft resistance to bending and torsion and bearings performance.

In this chapter we will first verify the resistance of the shaft to the bending and torsion using both classical strengths of material laws and finite element, then we will perform an FEA simulation using Solidworks to validate the previous results, then and to predict the bearing performance we simulate the rotor-bearing system using an SKF-Simpro software.

4.2 System modeling

  The system consists of an impeller attached directly to the electric motor shaft of 65 mm diameter and 1293 mm length, the shaft is supported at both ends with bearings situated at a distance of 140 mm from the shaft edges. Therefore it is modelized as follows:
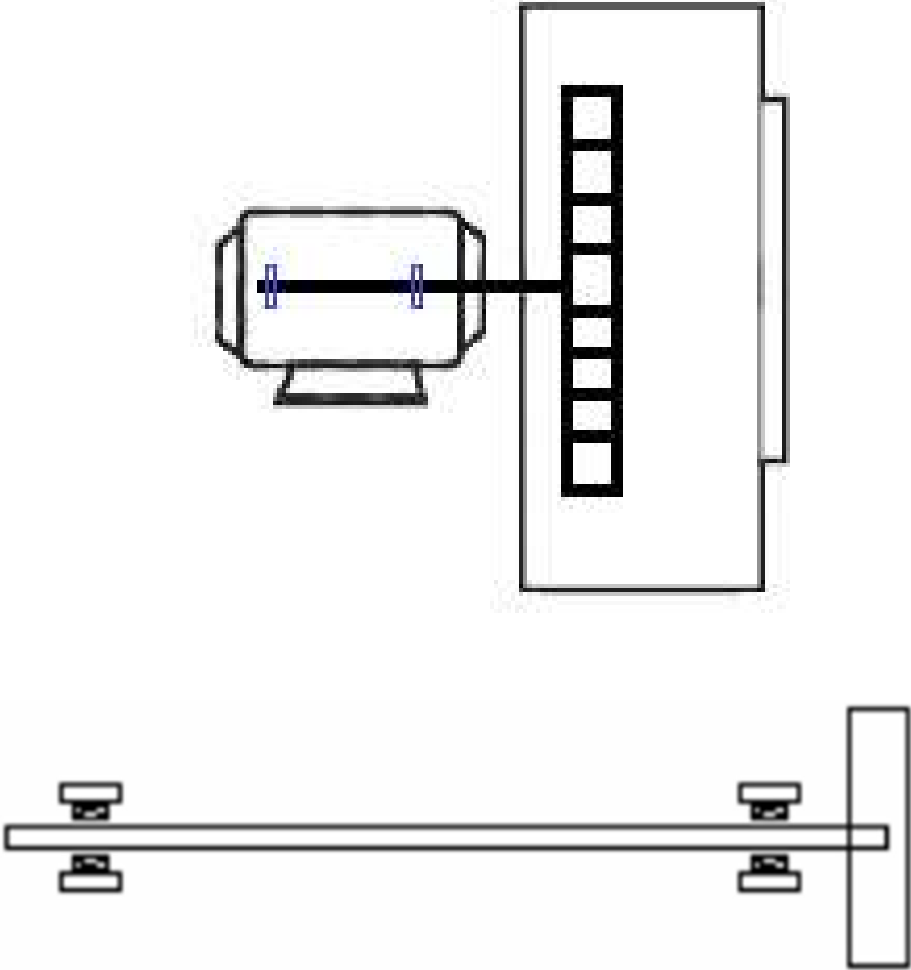
Figure 4.1: *Kinetic diagram and approximate model of the rotor*

4.3 Shaft internal torsion resistance

Condition of resistance: $\dfrac{\tau}{r} = \dfrac{M_t}{I_0}$ (4-1)

$$\tau = \dfrac{M_t}{I_0/r} \leqslant \dfrac{\sigma_y}{s}$$ (4-2)

τ = Shear stress (N/m^2)

I_0 = Polar moment of inertia

For a cylindrical shaft (our case): $I_0 = \dfrac{\pi d^4}{32} \ (m^4)$ (4-3)

$$I_0 = \dfrac{\pi d^4}{32} = \pi \dfrac{2^4 R^4}{32} = \pi \dfrac{16 R^4}{32} = \pi \dfrac{R^4}{2} = 1.7524 * 10^{-6} \ m^4$$ (4-4)

r = Shaft radius equal to 32.5 mm

M_t = Torsional moment

The torsional moment can be written as: $M_t = \dfrac{P}{\omega}$

P: Motor power equal to 110 kW.

ω: Angular velocity equal to 312.588 (rad/s) (4-5)

s: Factor of safety

Calculating the torsional moment:

$$M_t = \dfrac{P}{\omega}$$ (4-6)

$$M_t = \dfrac{110 * 10^3}{312.588} = 351.90 \ N.m$$ (4-7)

4.3.1 Calculating shear stress

$$\tau = \dfrac{M_t}{I_0/r} = \dfrac{351.90 * 0.0325}{1.7524 * 10^{-6}} = 6.526 \ 10^6 \ (N.m^2)$$ (4-8)
$$\tau = 6.525 \ Mpa$$

For 1020 cold-rolled steel (the material of the shaft), the yield strength is:

$$\sigma_y = 350 \ mpa$$ (4-9)

$$\tau \leqslant \dfrac{\sigma_y}{s}$$ (4-10)

$$\tau \, s \leqslant \sigma_y$$ (4-11)

For electric motor shafts the safety factor s is around 1.2 to 2.25:

$$\tau = \dfrac{\sigma y}{s} = \tau = \dfrac{\sigma y}{2.25} = \tau = \dfrac{350}{2.25} = 155.55 \ Mpa$$ (4-12)

$\tau \leqslant \frac{\sigma y}{s}$, Which means that the condition is verified.

4.4 Shaft resistance to bending

The first thing to do is the determination of the reactions R_A and R_B:
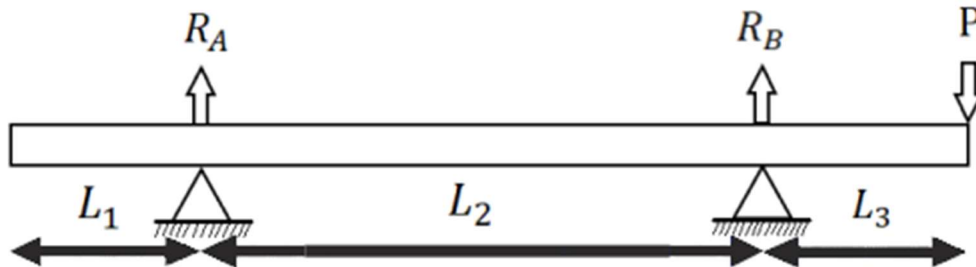
Figure 4.2 Forces applied on the shaft

Data:

P: weight if the turbine

R_A: Reaction at point A

R_B: Reaction at point B

The data	L = 1293 mm, L1 = 140 mm, L2 = 1013 mm, L3 = 140 mm $M_{impeller}$ = 70.56885 kg (Calculated by Solidworks) P= $M_{impeller}$ g P =70,56885 x 9.81 P =692.28 N		
Determination of the reactions **R_A and R_b**	$R_A = -\frac{PL_3}{L_2}$ $R_B = P\frac{(L_2+L_3)}{L_2}$	(4.13) (4.14)	**Numerical application :** $R_A = -95{,}675N$ (4.15) $R_B = 787{,}956N$ (4.16)

considered section	section drawing	Numerical application
first section $0 \leqslant x < L_1$		$\Sigma F_{/y} = 0$ $T = 0$ (4.17) $\quad \Sigma M/G1 = 0$ $Mf = 0$
Second section $L_1 \leqslant x < L_1 + L_2$		$T = R_A = -\dfrac{PL_3}{L_2} =$ -95.675 N (4.18) $M_f = -\dfrac{pL_3}{L_2}x + \dfrac{PL_1L_3}{L_2}$ (4.19) for $x = L_1 \Rightarrow Mf = 0$ (4.20) For $x = L_1 + L_2$ (4.21) $Mf = -\dfrac{pL_2L_3}{L_2} = -PL_3$ $Mf = -96,919 N \cdot m$ (4.22)
Third section $L_1 + L_2 \leqslant x \leqslant L$		$T = R_A + R_B = P$ For x = L1 + L $M_f = -PL_3$ $M_f = -96,919 N \cdot m$ For $x = L$ $M_f = 0$
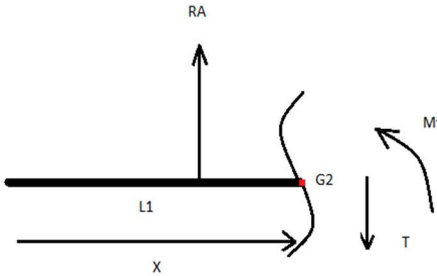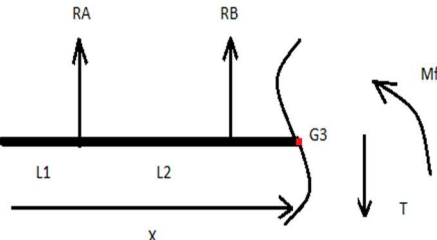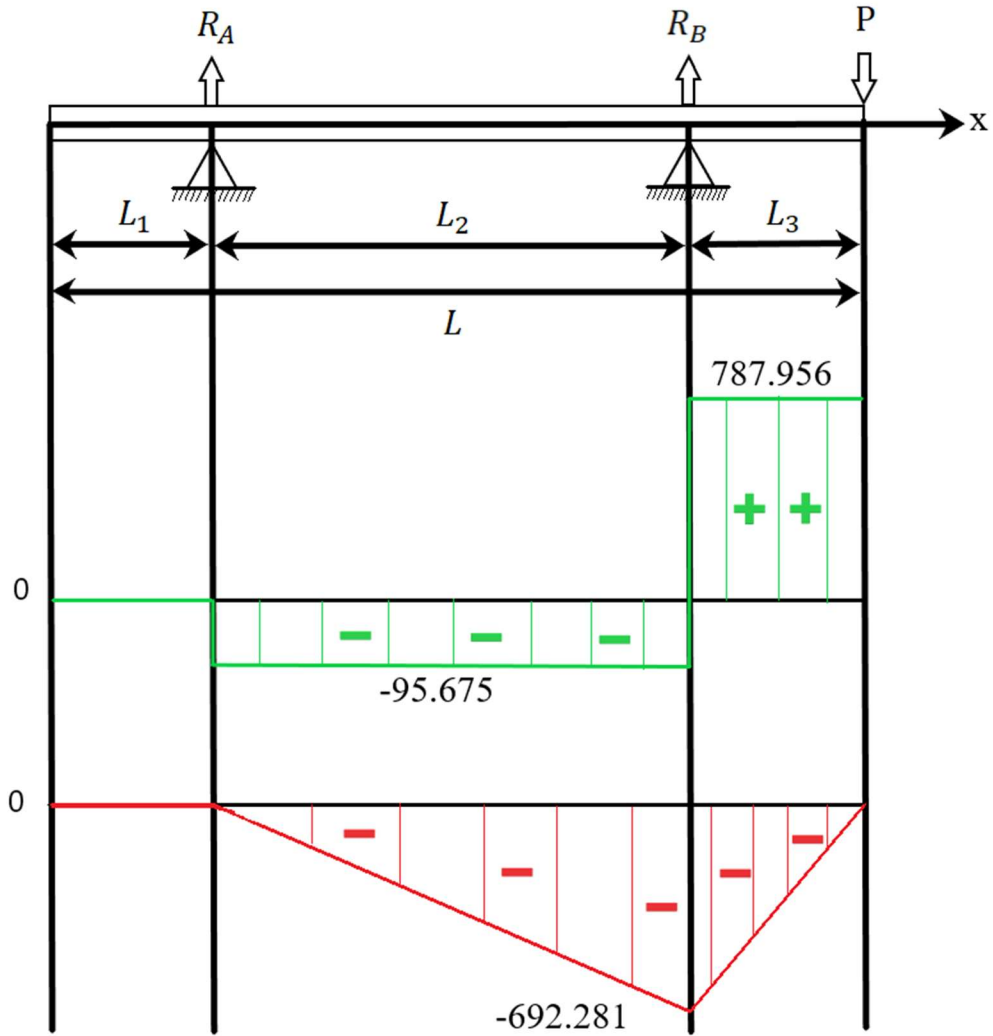
Figure 4-3 Shear force and bending moment diagrams

4.4.1 Verifying the resistance to the bending

Condition of resistance:
$$\sigma = \frac{M_{max}}{I_y} \cdot y \leqslant \frac{\sigma_y}{s} \qquad (4\text{-}25)$$

M_{max}: Maximum bending moment equal to 96.91 N.m.

I_x: Second moment of inertia of the neutral axis.

$$I_x = \frac{\pi d^4}{64} = 8.7624 \cdot 10^{-7} \quad m^4 \qquad (4\text{-}26)$$

y: The distance between the neutral axis and the furthest fiber and it is equal to r.

$$\sigma = \frac{M_{max}}{I_x} = \frac{96.91}{8.7624*10^{-7}} * 0.0325 = 3.56 \; Mpa \;\; (N.m^2) \tag{4-27}$$

$$\frac{\sigma_y}{s} = \frac{350}{2.25} = 155.55 \; Mpa \tag{4-28}$$

$\frac{M_{max}}{I_y} \cdot x \leqslant \frac{\sigma_y}{s}$, The condition is verified.

4.5 Calculating the shaft deflection using singularity functions

Singularity functions:

$$\langle x - a \rangle^n = \begin{cases} 0 \text{ for } x < a \\ (x-a)^n \text{ for} (x > a) \end{cases} \tag{4-29}$$

The relation between the bending moment and deflection is:

$$EI \frac{d^2 v(x)}{dx^2} = M(x) \tag{4-30}$$

$$EI \frac{d^2 v(x)}{dx^2} = [R_A \langle x - L_1 \rangle^1 + R_B \langle x - (L_1 + L_2) \rangle^1 + P \langle x - L \rangle^1] \tag{4-31}$$

We have $P(x - L)^1 = 0$ because x is always less than L

And by putting: $L_4 = L_1 + L_2$ and integrating one time:

$$EI \frac{dv(x)}{dx} = \frac{R_A}{2} \langle x - L_1 \rangle^2 + \frac{R_B}{2} \langle x - L_4 \rangle^2 + C_1 \tag{4-32}$$

After integrating a second time:

$$EIv(x) = \frac{R_A}{6} \langle x - L_1 \rangle^3 + \frac{R_B}{6} \langle x - L_4 \rangle^3 + C1x + C_2 \tag{4-33}$$

Boundary conditions:

$$\begin{aligned} x &= L_1 \quad y = 0 \\ x &= \; L_4 \; y = 0 \end{aligned} \tag{4-34}$$

$for \; x = L_1 \; y = 0$

$$\frac{RA}{6} \langle L1 - L1 \rangle^3 + \frac{R_\beta}{6} \langle L_1 - L_4 \rangle + C_1 L_1 + C_2 = 0$$
$$(L_1 - L_4) < 0 \tag{4-35}$$
$$So$$
$$C_1 L_1 + C_2 = 0$$

$for \; x = L_4 \; y = 0$

$$\frac{RA}{6} \langle L_4 - L_1 \rangle^3 + \frac{R_B}{6} \langle L_4 - L_4 \rangle^3 + c_1 L_4 + C_2 = 0 \tag{4-36}$$

$$(L_4 - L_1)^3 = L_2^3 \tag{4-37}$$

$$\frac{R_A}{6} L_2^3 + C_1 (L_1 + L_2) + C_2 = 0 \tag{4-38}$$

$$\begin{cases} C_1 L_1 + C_2 = 0 \quad \dots . 1 \\ \frac{RA}{6} L_2^3 + C_1 L_2 + C_1 L_1 + C_2 = 0 \dots .2 \end{cases}$$
(4-39)

$$\frac{R_A}{6} L_2^3 + C_1 L_2 = 0 \Rightarrow$$
(4-40)

$$C_1 = -\frac{R_A L_2^2}{6}$$
(4-41)

From (1) we have:

$$C_2 = \frac{R_A}{6} L_2^2 L_1$$
(4-42)

$$EIv(x) = \frac{R_A}{6} \langle x - L_1 \rangle^3 + \frac{R_B}{6} \langle x - L_4 \rangle^3 + C1x + C_2$$
(4-43)

$$v(x) = \frac{1}{EI} \left[\frac{R_A}{6} \langle x - L_1 \rangle^3 + \frac{R_B}{6} \langle x - L_4 \rangle^3 - \frac{R_A L_2^2}{6} x + \frac{R_A}{6} L_2^2 L_1 \right]$$
(4-44)

The deflection where the impeller is attached to the shaft is

$$v(L) = \frac{P L_1^2 (L_1 + L_2)}{3EI}$$
(4-45)

$$v(L) = 2.9031 \times 10^{-5} \text{ m}$$

4.6 Unbalance mass

$$M e = m_u r$$
(4-47)

$$m_u = \frac{Me}{r}$$
(4-48)

$$M = M_{impeller} + M_{Shaft}$$

m_u = Unbalance mass.

$M_{impeller}$ =70568.85 g (Calculated by Solidworks).

M_{Shaft} =33766.80 g (Calculated by Solidworks).

e= $v(L) = 2.9031 \times 10^{-5}$ m

$r = \frac{920}{2} = 460$ mm (assuming that the unbalance mass is situated at the edge of the impeller).

m_u = ((70568.85+33766.80) x2.9031 $\times 10^{-5}$)/0.460

m_u = 6,5849 g = 0,00658 kg

The unbalance mass is 6.58 g.

4.7 Shaft analysis using finite element method

We divided the shaft into four elements, two at the ends of the shaft, two at reactions (bearings), and one between the reactions.
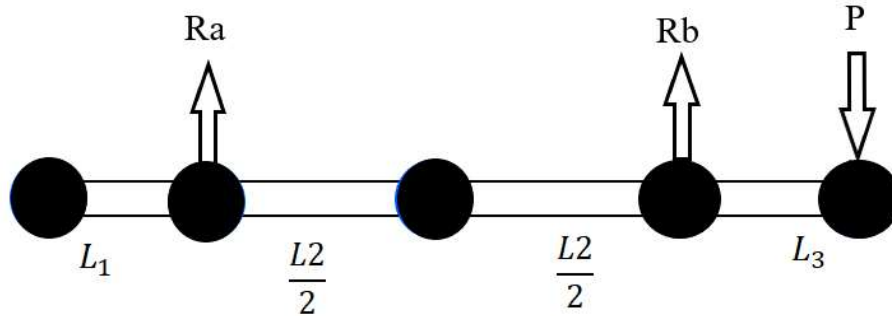
Figure 4-4 *Shaft model for FEM*

4.7.1 Elements stiffness matrixes

Boundary conditions: $V1 = 0$; $B1 = 0$ (no vertical displacement at the reactions).

Stiffness matrix first element K1:

$$k1 = EI \begin{bmatrix} \frac{12}{L_1^3} & \frac{6}{L_1^2} & \frac{-12}{L_1^3} & \frac{6}{L_1^2} \\ \frac{6}{L_1^2} & \frac{4}{L_1} & \frac{-6}{L_1^2} & \frac{2}{L_1} \\ \frac{-12}{L_1^3} & \frac{-6}{L_1^2} & \frac{12}{L_1^3} & \frac{-6}{L_1^2} \\ \frac{6}{L_1^2} & \frac{2}{L_1} & \frac{-6}{L_1^2} & \frac{4}{L_1} \end{bmatrix} \begin{Bmatrix} V1 \\ B1 \\ V2 \\ B2 \end{Bmatrix} = \begin{Bmatrix} 0 \\ 0 \\ R1 \\ 0 \end{Bmatrix} \qquad (4.49)$$

Stiffness matrix of second element K2:

$$K2 = EI \begin{bmatrix} \frac{96}{L_2^3} & \frac{24}{L_2^2} & \frac{-96}{L_2^3} & \frac{24}{L_2^2} \\ \frac{24}{L_2^2} & \frac{8}{L_2} & \frac{-24}{L_2^2} & \frac{4}{L_2} \\ \frac{-96}{L_2^3} & \frac{-24}{L_2^2} & \frac{96}{L_2^3} & \frac{-24}{L_2^2} \\ \frac{24}{L_2^2} & \frac{4}{L_2} & \frac{-2}{L_2^2} & \frac{8}{L_2} \end{bmatrix} \begin{Bmatrix} V2 \\ B2 \\ V3 \\ B3 \end{Bmatrix} = \begin{Bmatrix} R1 \\ 0 \\ 0 \\ 0 \end{Bmatrix} \qquad (4.50)$$

Stiffness matrix of the third element K3:

$$
K3 = EI \begin{bmatrix}
\frac{96}{L_2^3} & \frac{24}{L_2^2} & \frac{-96}{L_2^3} & \frac{24}{L_2^2} \\
\frac{24}{L_2^2} & \frac{8}{L_2} & \frac{-2}{L_2^2} & \frac{4}{L_2} \\
\frac{-9}{L_2^3} & \frac{-12}{L_2^2} & \frac{96}{L_2^3} & \frac{-2}{L_2^2} \\
\frac{24}{L_2^2} & \frac{4}{L_2} & \frac{-24}{L_2^2} & \frac{8}{L_2}
\end{bmatrix}
\times \begin{Bmatrix} V3 \\ B3 \\ V4 \\ B4 \end{Bmatrix}
= \begin{Bmatrix} 0 \\ 0 \\ R2 \\ 0 \end{Bmatrix}
\qquad (4.51)
$$

Stiffness matrix fourth element K4:

$$
K4 = EI \begin{bmatrix}
\frac{12}{L_3^3} & \frac{6}{L_3^2} & \frac{-12}{L_3^3} & \frac{6}{L_3^2} \\
\frac{6}{L_3^2} & \frac{4}{L_3} & \frac{-6}{L_3^2} & \frac{2}{L_3} \\
\frac{-12}{L_3^3} & \frac{-6}{L_3^2} & \frac{12}{L_3^3} & \frac{-6}{L_3^2} \\
\frac{6}{L_3^2} & \frac{2}{L_3} & \frac{-6}{L_3^2} & \frac{4}{L_3}
\end{bmatrix}
\times \begin{Bmatrix} V4 \\ B4 \\ V5 \\ B5 \end{Bmatrix}
= \begin{Bmatrix} R2 \\ 0 \\ -P \\ 0 \end{Bmatrix}
\qquad (4.52)
$$

4.7.2 Global stiffness matrix

After assembly A= K1+K2+K3+K4

We have: A * displacement vector = force vector

$$
\begin{bmatrix}
\frac{12}{L_1^3} & \frac{6}{L_1^2} & \frac{-12}{L_1^3} & \frac{6}{L_1^2} & 0 & 0 & 0 & 0 & 0 & 0 \\[6pt]
\frac{6}{L_1^2} & \frac{4}{L_1} & \frac{-6}{L_1^2} & \frac{4}{L_1} & 0 & 0 & 0 & 0 & 0 & 0 \\[6pt]
\frac{-12}{L_1^3} & \frac{-6}{L_1^2} & \left(\frac{12}{L_1^3}+\frac{96}{L_2^3}\right) & \left(\frac{-6}{L_1^2}+\frac{24}{L_2^2}\right) & \frac{-96}{L_2^3} & \frac{24}{L_2^2} & 0 & 0 & 0 & 0 \\[6pt]
\frac{6}{L_1^2} & \frac{2}{L_1} & \left(\frac{-6}{L_1^2}+\frac{24}{L_2^2}\right) & \left(\frac{4}{L_1}+\frac{8}{L_2}\right) & \frac{-24}{L_2^2} & \frac{4}{L_2} & 0 & 0 & 0 & 0 \\[6pt]
0 & 0 & \frac{-96}{L_2^3} & \frac{-24}{L_2^2} & \left(\frac{96}{L_2^3}+\frac{96}{L_2^3}\right) & \left(\frac{-24}{L_2^2}+\frac{24}{L_2^2}\right) & \frac{-96}{L_2^3} & \frac{24}{L_2^2} & 0 & 0 \\[6pt]
0 & 0 & \frac{24}{L_2^2} & \frac{4}{L_2} & \left(\frac{-24}{L_2^2}+\frac{24}{L_2^2}\right) & \left(\frac{8}{L_2}+\frac{8}{L_2}\right) & \frac{-24}{L_2^2} & \frac{4}{L_2} & 0 & 0 \\[6pt]
0 & 0 & 0 & 0 & \frac{-96}{L_2^3} & \frac{-24}{L_2^2} & \left(\frac{96}{L_2^3}+\frac{12}{L_3^3}\right) & \left(\frac{-24}{L_2^2}+\frac{6}{L_3^2}\right) & \frac{-12}{L_3^3} & \frac{6}{L_3^2} \\[6pt]
0 & 0 & 0 & 0 & \frac{24}{L_2^2} & \frac{4}{L_2} & \left(\frac{-24}{L_2^2}+\frac{6}{L_3^2}\right) & \left(\frac{8}{L_2}+\frac{4}{L_3}\right) & \frac{-6}{L_3^2} & \frac{2}{L_3} \\[6pt]
0 & 0 & 0 & 0 & 0 & 0 & \frac{-12}{L_3^3} & \frac{-6}{L_3^2} & \frac{12}{L_3^3} & \frac{-6}{L_3^2} \\[6pt]
0 & 0 & 0 & 0 & 0 & 0 & \frac{6}{L_3^2} & \frac{2}{L_3} & \frac{-6}{L_3^2} & \frac{4}{L_3}
\end{bmatrix}
$$

$$* \begin{Bmatrix} V1 \\ B1 \\ V2 \\ B2 \\ V3 \\ B3 \\ V4 \\ B4 \\ V5 \\ B5 \end{Bmatrix} = \begin{Bmatrix} 0 \\ 0 \\ R1 \\ 0 \\ 0 \\ 0 \\ R2 \\ 0 \\ -P \\ 0 \end{Bmatrix} + \begin{Bmatrix} F1 \\ M1 \\ 0 \\ M2 \\ F3 \\ M3 \\ 0 \\ M4 \\ 0 \\ M5 \end{Bmatrix} \qquad (4.53)$$

Using Matlab, we got these results:

$$\text{Displacement vector} = \begin{Bmatrix} V1 \\ B1 \\ V2 \\ B2 \\ V3 \\ B3 \\ V4 \\ B4 \\ V5 \\ B5 \end{Bmatrix} = \begin{Bmatrix} -0.013072047240034 \\ 0.000093371766016 \\ 0 \\ 0.000093371765992 \\ 0.035469599599822 \\ 0.000023342941495 \\ 0 \\ -0.000186743531964 \\ -0.029757296081394 \\ -0.000225456406344 \end{Bmatrix} \qquad (4.54)$$

$$\text{Force vector} = \begin{Bmatrix} F1 \\ M1 \\ R1 \\ M2 \\ F3 \\ M3 \\ R2 \\ M4 \\ 0 \\ M5 \end{Bmatrix} = \begin{Bmatrix} 0 \\ 0 \\ -95.6755581191584 \\ 0 \\ 0 \\ 0 \\ 787.956556981282 \\ 0 \\ -692.280999140417 \\ 0 \end{Bmatrix} \qquad (4.55)$$

The results are very close to the previous results, we can see that the more nodes we use more precise results we get.

4.8 FEA simulation using Solidworks

4.8.1 Study properties

The properties of the study are shown in **Table 4.1**, also the material used and its specifications are shown in **Table 4.2**, same as the boundary conditions and the fixations are in **Figure 4.3** and **4.4**

Study name	Static 1
Analysis type	Static
Mesh type	Beam Mesh
Solver type	Direct sparse solver
Inplane Effect:	Off
Soft Spring:	Off

Inertial Relief:	Off
Incompatible bonding options	Automatic
Large displacement	Off
Compute free body forces	On
Result folder	SOLIDWORKS document (C:\Users\Basset\Desktop)

Table 4.1 *Study properties*

Model Reference	Properties	
	Name:	AISI 1020 Steel, Cold Rolled
	Model type:	Linear Elastic Isotropic
	Default failure criterion:	Max von Mises Stress
	Yield strength:	3.5e+08 N/m^2
	Tensile strength:	4.2e+08 N/m^2
	Elastic modulus:	2.05e+11 N/m^2
	Poisson's ratio:	0.29
	Mass density:	7,870 kg/m^3
	Shear modulus:	8e+10 N/m^2
	Thermal expansion coefficient:	1.17e-05 /Kelvin

Table 4.2 *Material properties*

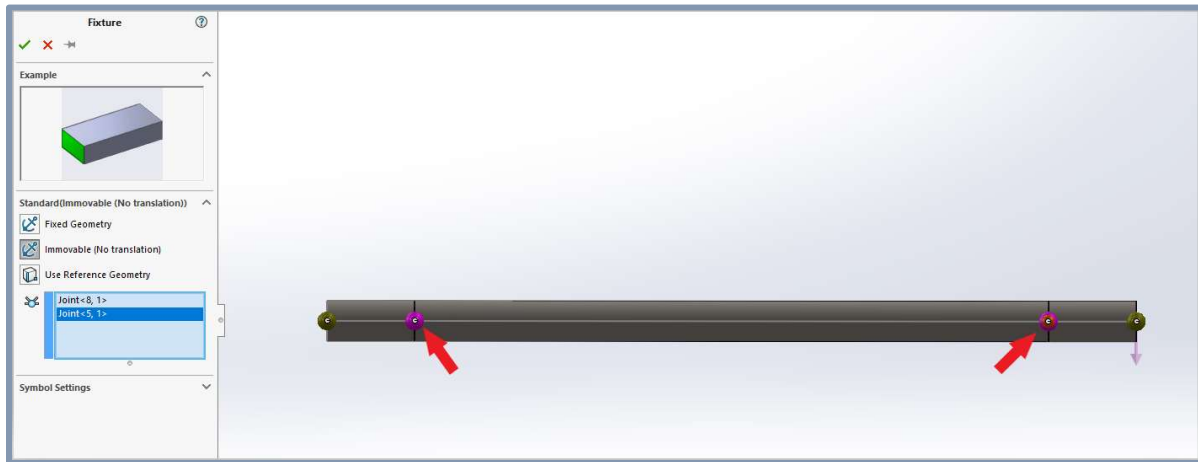***Figure 4.5:*** *The applied fixtures on the shaft*

Figure 4.6: *The applied force on the shaft*

4.8.2 Meshing information

Table 4.3 contains the mesh used for the shaft and all the details about the mesh used in this study.

Mesh type	Beam Mesh
Total Nodes	84
Total Elements	80
Time to complete mesh(hh;mm;ss):	00:00:00

Table 4.3: *Meshing details*

4.8.3 Study Results

The results obtained from the study are shown in the tables and figures below:

Name	Type	Min	Max
Stress1	Upper bound axial and bending	3.373e-08N/m^2 Element: 80	3.610e+06N/m^2 Element: 10

Table 4.4: *Stress results*

Name	Type	Min	Max
Displacement1	URES: Resultant Displacement	0.000e+00mm Node: 10	3.563e-02mm Node: 36
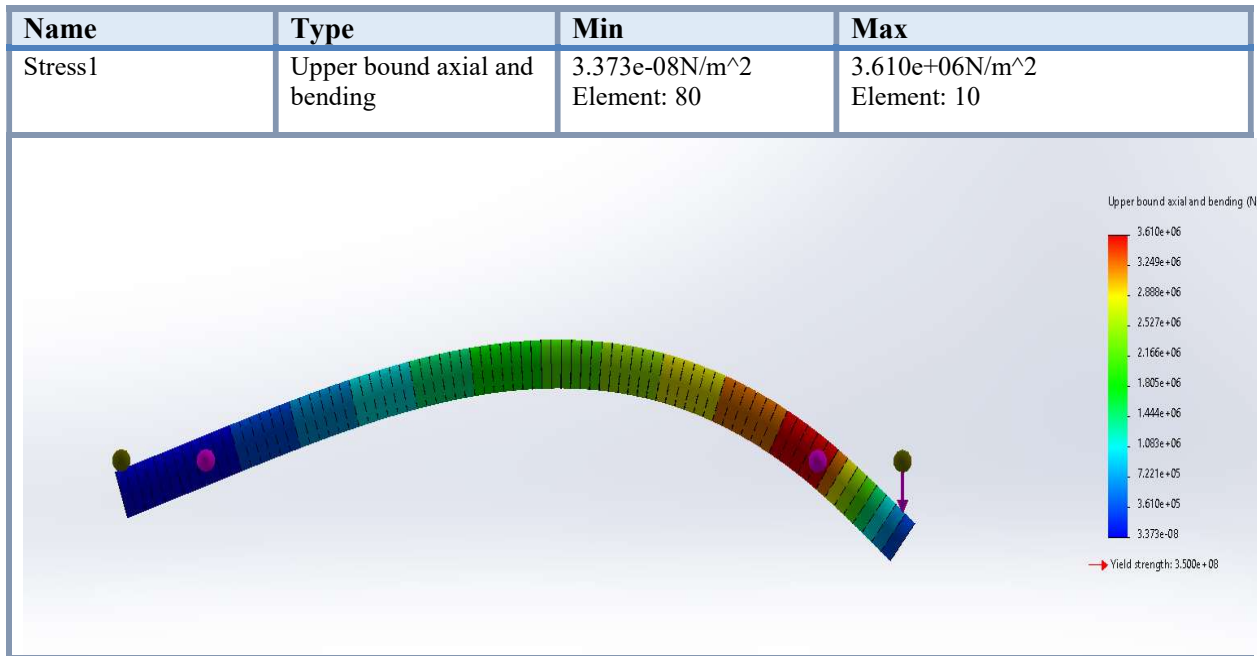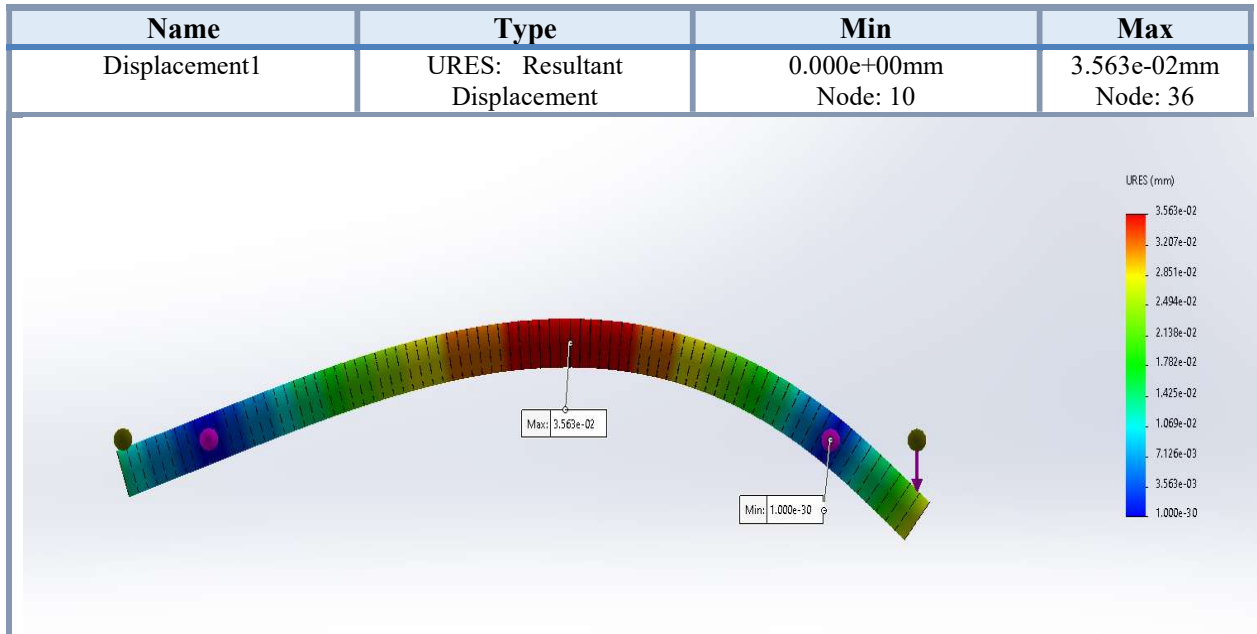
Table 4.5: *Displacement results*
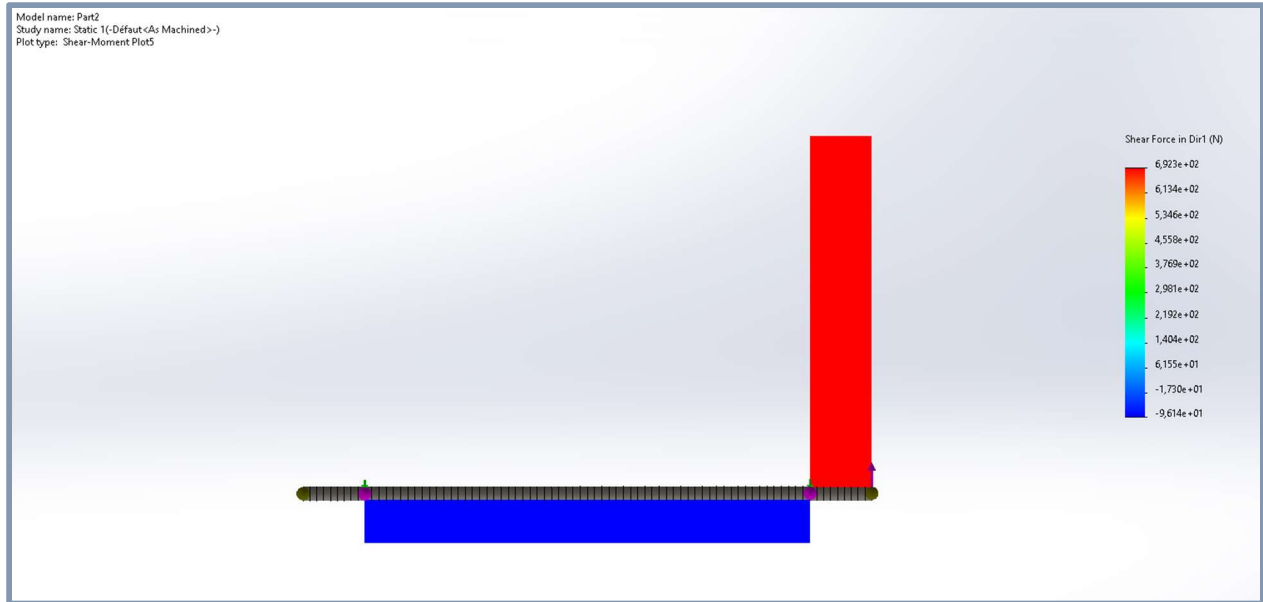
Figure 4.7: *Shear force diagram*
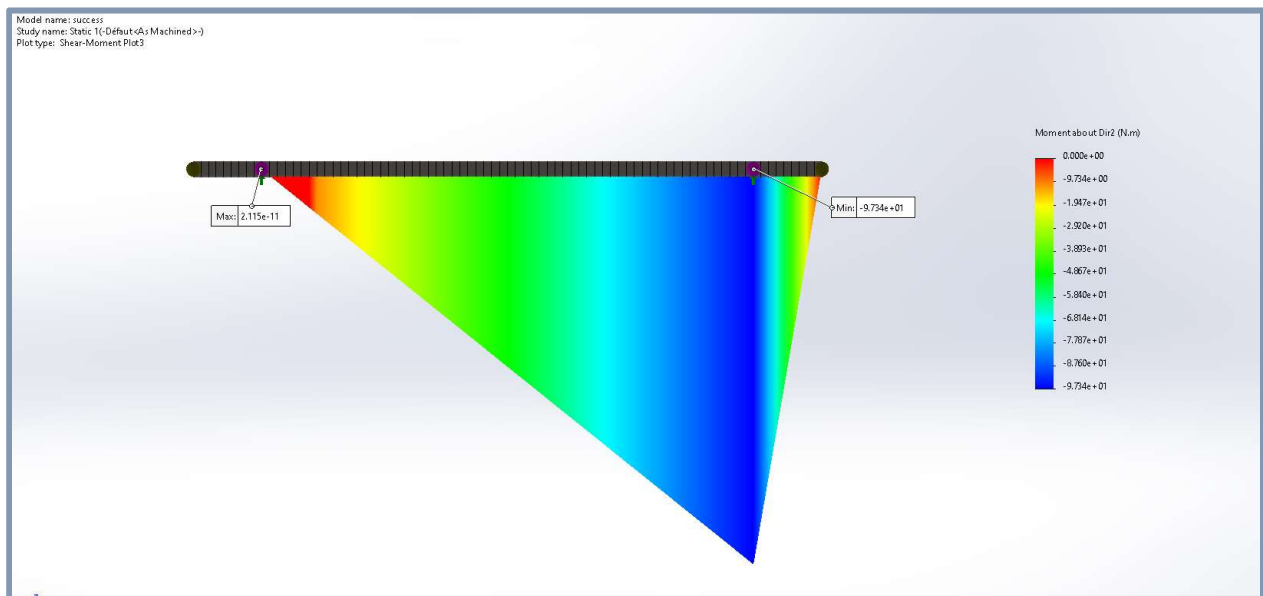
Figure 4.8: *Bending moment diagram*

We can see that the displacement and the diagrams are similar to the theoretical results.

4.9 Bearings simulation using SKF-Simpro

Bearings are one of the most critical components in rotating machinery. Their influence on the rotor dynamic performance, life, and reliability of the machine cannot be ignored. To evaluate that influence we did contact SKF Company and we request a version of SKF-Simpro software,

which is used to simulate bearings and shafts. The company considered our request and provided us with a version of this software.

4.9.1 Preparing the simulation

Shaft dimensions and boundary conditions:

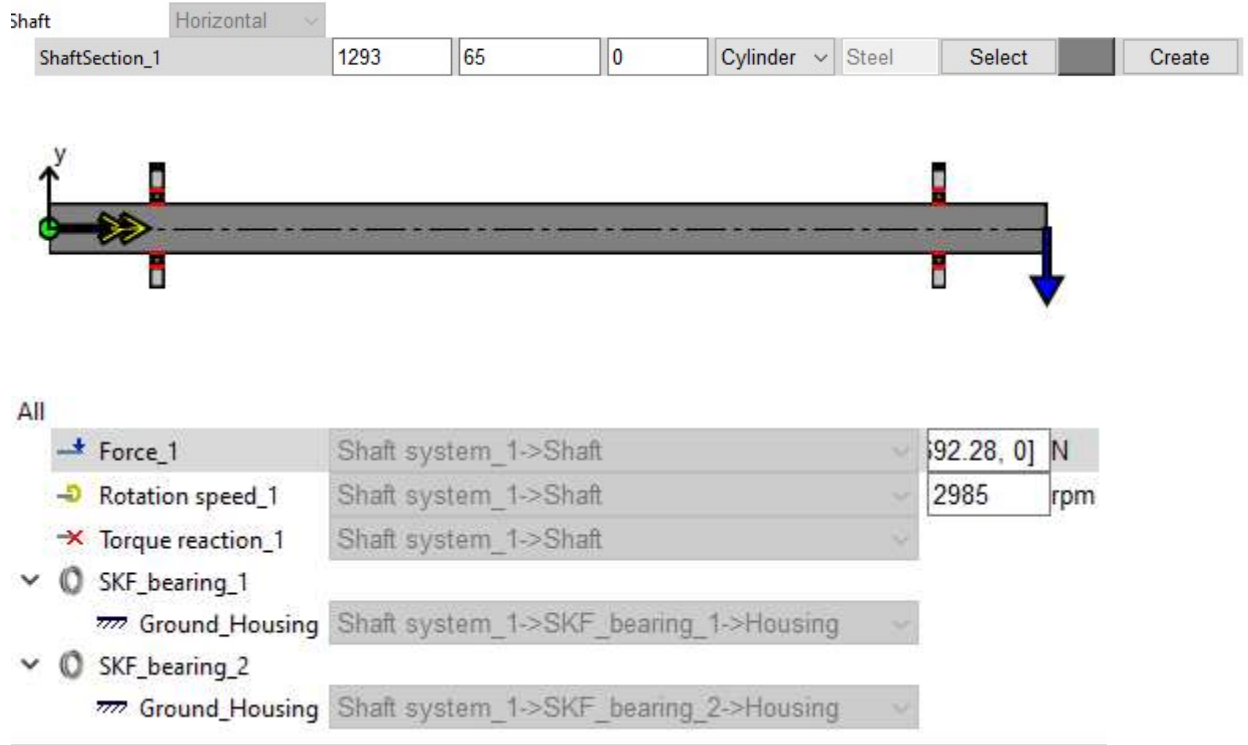| Force	Force [N]				Relative position [mm]			
	X	Y	Z	magnitude	X	Y	Z	magnitude
Force_1	0	-692	0	692	0.00	0.00	0.00	0.00

Boundary	Rotation speed [rpm]
Rotation speed_1	2985

Figure 4.9 *simulation preparing*
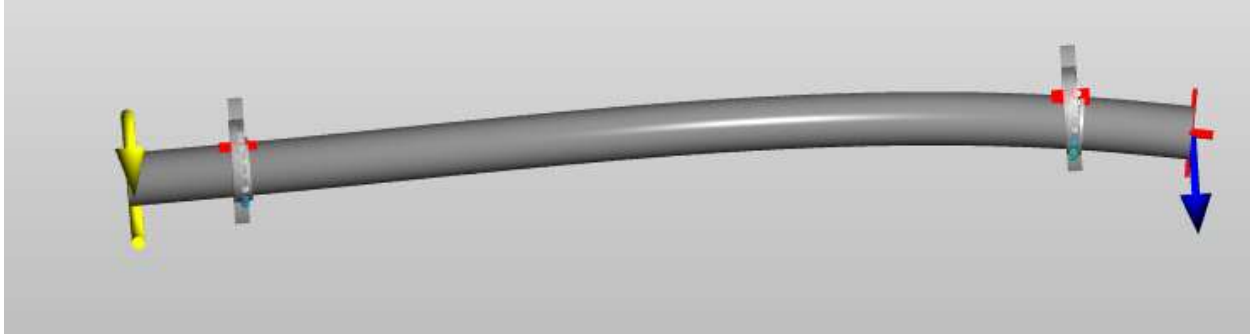
Defining the bearings:

Bearing	Bearing designation	Bearing type	Bearing execution	Bore diameter (d) [mm]	Outer diameter (D) [mm]	Bearing width (B) [mm]
SKF_bearing_1	6013-2Z	DGBB	SKF EXPLORER	65.000	100.000	18.000
SKF_bearing_2	6013-2Z	DGBB	SKF EXPLORER	65.000	100.000	18.000

Table 4.6 *Defining the bearings*

Simulation Results

Bearing	Bearing radial load [N]	Bearing axial load [N]	Forces [N]			Moments [Nm]		
			X	Y	Z	YZ	ZX	XY
SKF_bearing_1	70	1	0	-70	1	0	0	0
SKF_bearing_2	954	-1	0	-954	-1	0	0	0

Bearing	Equivalent static bearing load (P0) [N]	Static safety factor s0	Equivalent dynamic bearing load (P) [N]	C/P
SKF_bearing_1	70	> 100	70	> 100
SKF_bearing_2	954	26.2	954	33.5

Bearing	Basic rating life (ISO 281) (L10h) [h]	SKF load based method (SKF rating life, GBLM) [h]	Modified reference rating life (ISO/TS 16281) (L10mrh) [h]	Static safety s0
SKF_bearing_1	N/A	N/A	N/A	357.13
SKF_bearing_2	> 200000	> 200000	> 200000	26.22

SKF load based life: SKF rating life (L10m) for steel-steel bearings; GBLM load based life (L10GM) for hybrid bearings

Bearing	Internal radial clearance before mounting [um]	Operating radial clearance [um]	Internal axial clearance before mounting [um]	Operating axial clearance [um]
SKF_bearing_1	18	18	174	174
SKF_bearing_2	18	18	174	174

Bearing	Rotational frequency IR [hertz]	Rotational frequency OR [hertz]	Rotational frequency of RE set and cage [hertz]	Rolling element about its axis [hertz]	Over-rolling frequency of point on IR [hertz]	Over-rolling frequency of point on OR [hertz]	Over-rolling frequency of point on RE [hertz]
SKF_bearing_1	49.75	0	21.76	195.76	419.79	326.46	391.53
SKF_bearing_2	49.75	0	21.76	195.76	419.80	326.45	391.53

Table 4.7 Simulation results
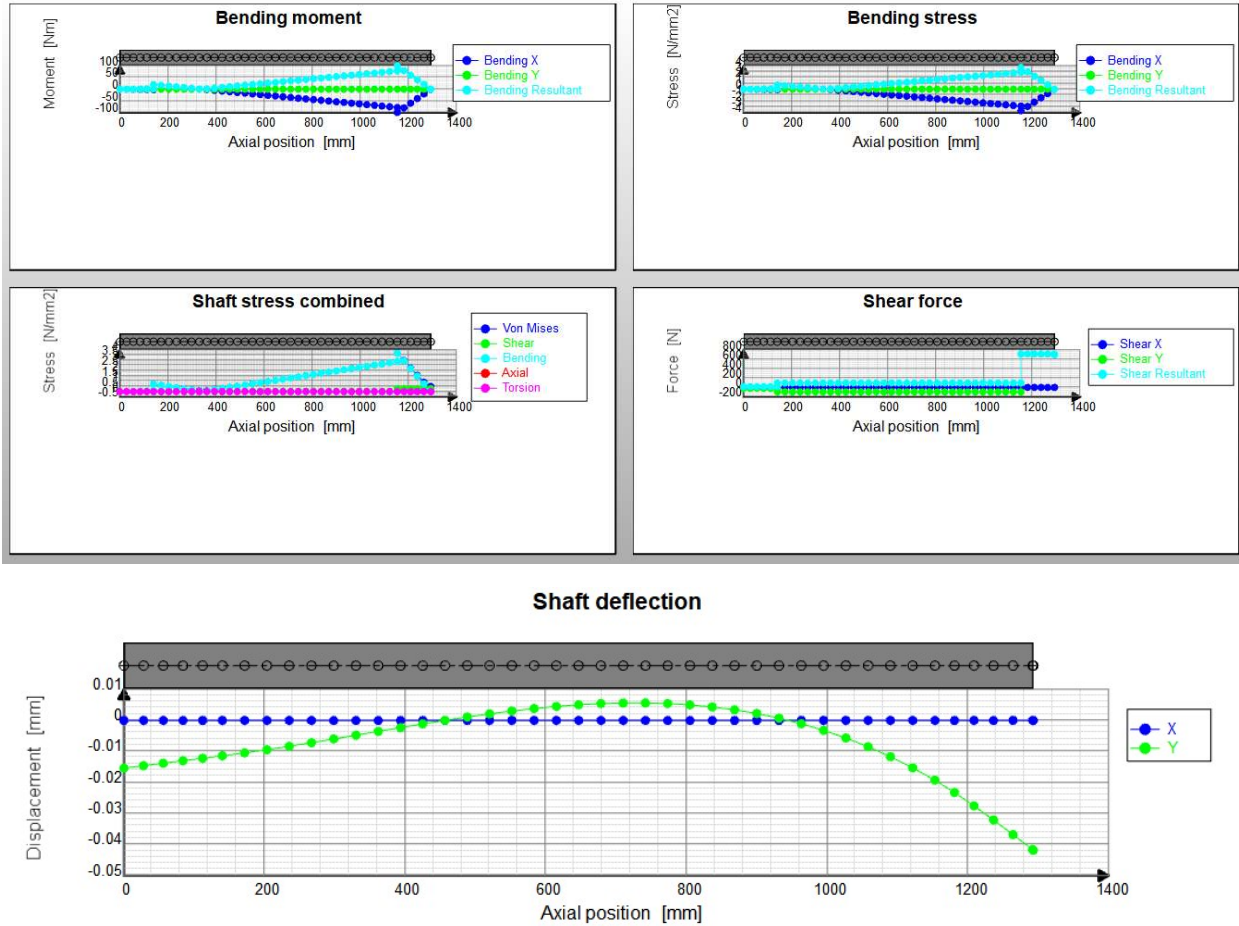
Figure 4.10 *Results diagrams*

The results show bearings life, loads, safety factors, frequencies, and clearance, it also shows the bending stress, the bending moment, the shear stress, and the deflection of the shaft.

Conclusion

 In this chapter we verified the shaft resistance to bending and torsion, we determined the deflection of the shaft at the disk and we calculated the unbalance mass due to this deflection which we will study its influence on the rotor dynamic in the next chapter.
We also calculate these reactions and deflections using the finite element method, and the results were very close to the previous results.
We validate these results by performing an FEA simulation.
Finally, we simulate the bearings and we determined all their specifications.

Chapter 05: Rotor Dynamic Study

5.1 Theoretical Study

5.1.1 Introduction

   Industrial fans are a necessity in milling plants that run around the clock. Unexpected downtime due to a fan's mechanical issues can cost a company hundreds of thousands of dollars in lost time and throughput. Accurate predictions of rotor system dynamic characteristics are very important and essential for reliable long-term fan operation.

   During its operation, several forces act on the centrifugal forces; like fluid-induced forces but also forces with a mechanical background. These forces originate due to imperfect balance (like a slight bend in the shaft or a mass eccentricity), design faults, and bearings. These forces may grow to an unacceptable level when the rotor is operational near its natural frequency.

In part 1, rotor vibration was studied analytically and numerically using Solidworks frequency analysis, in part 2 an experimental test is performed to validate the results obtained in part 1.

A solution to the founded problem was proposed at the end.

Machine description:

The rotor consists of an impeller with a diameter of 0.92 m attached to the end of the electric motor shaft.

The power of the motor is 110 kW and it is operating at constant rotation speed Ω =2985 (rpm) and a frequency of 49.75 Hz.

Photo 5.1: *Impeller attached to the electric motor*   **Figure 5.1**: *Motor shaft*

5.1.2 System Modeling

   The rotor of a centrifugal fan photo 5.1 is approximated by a simple model as shown in Figure 5.2. The model is composed of a shaft of length L and is supported by two bearings located at L1 and L4 along the shaft.

   The shaft is modeled as an Euler-Bernoulli beam. In this model, rotary inertia and gyroscopic effect have been considered considering the improvement of Rayleigh (1877) and the shear deformation has been neglected. The shaft rotates at a constant speed Ω around its longitudinal axis. In addition, it has a uniform constant circular cross-section. [12]
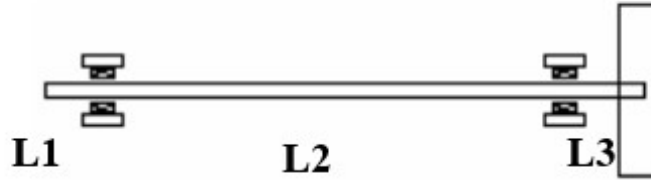
Figure 5.2: Rotor model

We assume that the disk is symmetric and rigid and has been fixed at the end of the shaft. The motion of the disk can be defined as two superimposed rotations ψ, θ, and two translational deflections u, w in directions X and Z where $R_0(XYZ)$ is an inertial frame and $R(x, y, z)$ is fixed to the disk (Figure 5.3). To achieve the orientation of the disk we first rotate it by an amount ψ around the Z-axis; then by an amount θ around the new x-axis, denoted by x_1; and lastly by an amount ϕ around the final y_2 axis. [12] [13] [14]

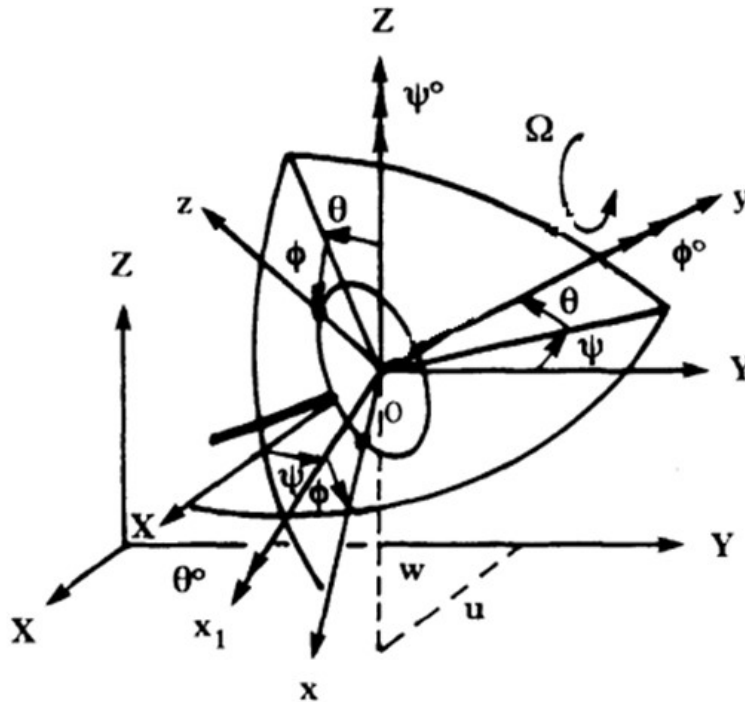*Figure 5.3: Reference frames for a disk on a rotating flexible shaft*

The instantaneous angular velocity vector of the xyz frame is about XYZ frame is:

$$w_{R/R_0} = \dot{\psi}Z + \dot{\theta}x_1 + \dot{\phi}y_2 \qquad (5.1)$$

Equivalent to:

$$w_{R/R_0} = \begin{bmatrix} \dot{\psi} \\ \dot{\theta} \\ \dot{\phi} \end{bmatrix} \cdot \begin{bmatrix} Z \\ x_1 \\ y_2 \end{bmatrix} \qquad (5.2)$$

56

The Rotation matrix about the Z-axis:

$$\begin{bmatrix} x_1 \\ y_1 \\ z_1 \end{bmatrix}_{R_Z} (\psi) = \begin{bmatrix} c\psi & s\psi & 0 \\ -s\psi & c\psi & 0 \\ 0 & 0 & 1 \end{bmatrix} \begin{bmatrix} X \\ Y \\ Z \end{bmatrix} \tag{5.3}$$

The Rotation matrix about the new x-axis noted x_1 :

$$\begin{bmatrix} x_2 \\ y_2 \\ z_2 \end{bmatrix}_{R_{x_1}} (\theta) = \begin{bmatrix} 1 & 0 & 0 \\ 0 & c\theta & s\theta \\ 0 & -s\theta & c\theta \end{bmatrix} \begin{bmatrix} x_1 \\ y_1 \\ z_1 \end{bmatrix} \tag{5.4}$$

The Rotation matrix about the final axis y_2 :

$$\begin{bmatrix} x_3 \\ y_3 \\ z_3 \end{bmatrix}_{R_{y_2}} (\phi) = \begin{bmatrix} c\phi & 0 & -s\phi \\ 0 & 1 & 0 \\ s\phi & 0 & c\phi \end{bmatrix} \begin{bmatrix} x_2 \\ y_2 \\ z_2 \end{bmatrix} \tag{5.5}$$

The expression of the instantaneous angular velocity vector of the xyz frame about XYZ frame in xyz frame is:

$$\omega^R_{R/R_0} = \begin{bmatrix} \omega_x \\ \omega_y \\ \omega_z \end{bmatrix} = R_{y_2} R_{x_1} \begin{bmatrix} 0 \\ 0 \\ \dot{\psi} \end{bmatrix} + R_{y_2} \begin{bmatrix} \dot{\theta} \\ 0 \\ 0 \end{bmatrix} + \begin{bmatrix} 0 \\ \dot{\phi} \\ 0 \end{bmatrix} \tag{5.6}$$

$$= \begin{bmatrix} c\phi & 0 & -s\phi \\ 0 & 1 & 0 \\ s\phi & 0 & c\phi \end{bmatrix} \begin{bmatrix} 1 & 0 & 0 \\ 0 & c\theta & S\theta \\ 0 & -S\theta & c\theta \end{bmatrix} \begin{bmatrix} 0 \\ 0 \\ \dot{\psi} \end{bmatrix} + \begin{bmatrix} c\phi & 0 & -s\phi \\ 0 & 1 & 0 \\ s\phi & 0 & c\phi \end{bmatrix} \begin{bmatrix} \dot{\theta} \\ 0 \\ 0 \end{bmatrix} + \begin{bmatrix} 0 \\ \dot{\phi} \\ 0 \end{bmatrix}$$

$$= \begin{bmatrix} c\phi & s\phi\, s\theta & -s\phi\, c\theta \\ 0 & c\theta & s\theta \\ s\phi & -c\phi\, s\theta & c\phi\, c\theta \end{bmatrix} \begin{bmatrix} 0 \\ 0 \\ \dot{\psi} \end{bmatrix} + \begin{bmatrix} \dot{\theta}\, c\phi \\ 0 \\ \dot{\theta}\, s\phi \end{bmatrix} + \begin{bmatrix} 0 \\ \dot{\phi} \\ 0 \end{bmatrix} = \begin{bmatrix} -\dot{\psi} & s\phi & c\phi \\ \dot{\phi} & s\theta \\ \dot{\psi} & c\phi & c\theta \end{bmatrix} + \begin{bmatrix} \dot{\theta}\, c\phi \\ 0 \\ \dot{\theta}\, s\phi \end{bmatrix} + \begin{bmatrix} 0 \\ \dot{\phi} \\ 0 \end{bmatrix}$$

And we get:

$$\omega^R_{R/R_0} = \begin{bmatrix} \omega_x \\ \omega_y \\ \omega_z \end{bmatrix} = \begin{bmatrix} -\dot{\psi}\, c\theta\, s\phi + \dot{\theta}\, c\phi \\ \dot{\psi}\, s\theta + \dot{\phi} \\ \dot{\psi}\, c\theta\, c\phi + \dot{\theta}\, s\phi \end{bmatrix} \tag{5.7}$$

The tensor of inertia in the center of the disk O as xyz are principal directions of inertia is defined by:

$$I_{/O} = \begin{bmatrix} I_{D_x} & 0 & 0 \\ 0 & I_{D_y} & 0 \\ 0 & 0 & I_{D_z} \end{bmatrix} \tag{5.8}$$

In this study we will only treat the lateral vibration, therefore the free longitudinal displacement of the rotor will be neglected which means the coordinate along the y axis will be constant. Also, the forces acting on the impeller due to the fluid are unknowns and they will be neglected.

We will also ignore the influence of the bearing on the shaft for simplicity.
The Kinetic energy of the disk T_D is defined by: [13] [14]

$$T_D = \frac{1}{2} M_D (\dot{u}^2 + \dot{w}^2) + \frac{1}{2} \left(I_{D_x} w_x^2 + I_{Dy} w_y^2 + I_{D_z} w_z^2 \right) \tag{5.9}$$

Because the disk symmetric mass distribution: $I_{D_x} = I_{D_y}$

Where:

$I_{D_x} = I_{D_y} = I_{D_d}$ is the diametral mass moment of inertia of the disk.

$I_{D_y} = I_{D_p}$ is the polar mass moment of inertia of the disk.

T_D becomes:

$$T_D = \frac{1}{2} M_D (\dot{u}^2 + \dot{w}^2) + \frac{1}{2} \left(I_{D_d} (w_x^2 + w_z^2) + I_{D_p} w_y^2 \right) \tag{5.10}$$

From (5.7) we have:

$$w_x^2 = [-\dot{\psi} \cos\theta \sin\phi + \dot{\theta}\cos\phi]^2$$
$$= \dot{\psi}^2 \cos^2\theta \sin^2\phi + \dot{\theta}^2 \cos^2\phi - 2\dot{\psi}\dot{\theta} \cos\theta \sin\phi \cos\phi \tag{5.11}$$

$$w_z^2 = [\dot{\psi} \cos\theta \cos\phi + \dot{\theta} \sin\phi]^2$$
$$= \dot{\psi}^2 \cos^2\theta \cos^2\phi + \dot{\theta}^2 \sin^2\phi + 2\dot{\psi}\dot{\theta} \cos\theta \cos\phi \sin\phi \tag{5.12}$$

$$w_x^2 + w_z^2 = \dot{\psi}^2 \cos^2\theta \sin^2\phi + \dot{\theta}^2 \cos^2\phi - 2\dot{\psi}\dot{\theta} \cos\theta \sin\phi \cos\phi$$
$$+ \dot{\psi}^2 \cos^2\theta \cos^2\phi + \dot{\theta}^2 \sin^2\phi + 2\dot{\psi}\dot{\theta} \cos\theta \cos\phi \sin\phi$$
$$= \dot{\psi}^2 \cos^2\theta (\cos^2\phi + \sin^2\phi) + \dot{\theta}^2 (\cos^2\phi + \sin^2\phi)$$
$$= \dot{\psi}^2 \cos^2\theta + \dot{\theta}^2 \tag{5.13}$$

Since ψ is too small (5.13) becomes:

$$w_x^2 + w_z^2 = \dot{\psi}^2 + \dot{\theta}^2 \tag{5.14}$$

Then we have:

$$w_y^2 = [\dot{\psi} \sin\theta + \dot{\phi}]^2$$
$$= \dot{\phi}^2 + \dot{\psi}^2 \sin^2\theta + 2\dot{\phi}\dot{\psi} \sin\theta \tag{5.15}$$

Since θ is also too small we have: $(\sin\theta \simeq \theta; \sin^2\theta \simeq 0)$, therefore (5.15) becomes:

$$w_y^2 = \dot{\phi}^2 + 2\dot{\phi}\dot{\psi}\theta \tag{5.16}$$

And since $\dot{\phi} = \Omega$ is the rotor angular velocity we get:

$$w_y^2 = \Omega^2 + 2\Omega\dot{\psi}\theta \tag{5.17}$$

Finally, the kinetic energy of the disk becomes:

$$T_D = \frac{1}{2}M_D(\dot{u}^2 + \dot{w}^2) + \frac{1}{2}I_{D_d}(\dot{\theta}^2 + \dot{\psi}^2) + \left[\frac{1}{2}I_{Dp}(\Omega^2 + 2\Omega\dot{\psi}\theta)\right] \tag{5.18}$$

Where the term $I_{Dp}\Omega\dot{\psi}\theta$ represents the gyroscopic effect.

5.1.2.1 Kinetic energy of the shaft

By the same analogy:

$$T_s = \frac{\rho S}{2}\int_0^L (\dot{u}^2 + \dot{w}^2)dy + \frac{\rho}{2}I_{S_d}\int_0^L (\dot{\theta}^2 + \dot{\psi}^2)dy + \frac{\rho}{2}I_{S_p}L\Omega^2 + \rho I_{S_p}\Omega\int_0^L \dot{\psi}\,\theta\,dy \tag{5.19}$$

Where:

ρ: Shaft density.

S: Shaft cross-sectional area.

$I_{S_x} = I_{S_y} = I_{S_d}$: Diametric area moment of inertia of the shaft.

$I_{S_y} = I_{S_p}$:   Polar area moment of inertia of the shaft.

The term $\rho I_{S_p}\Omega\int_0^L \dot{\psi}\,\theta\,dy$ represents the gyroscopic effect.

5.1.2.2 Shaft strain energy

Let C be the center of the shaft cross-sectional area, B an arbitrary, x and z the coordinates of B in the reference attached to the center C, and u* and w* the coordinates of C in xyz frame.[13]
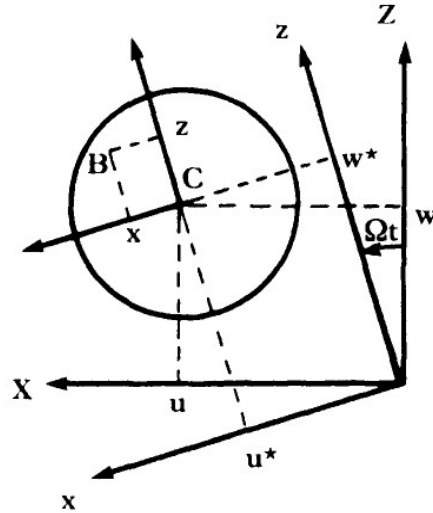

Figure 5.4: *Coordinates of B and C with respect to xyz frame*

The longitudinal displacement of B:

The point B rotates with an angle θ about the x-axis, therefor its displacement in the y axis is equal to (z sinθ) in the negative direction, and since θ is too small, the displacement will be approximated by (z θ) in the negative direction. [15] [16]
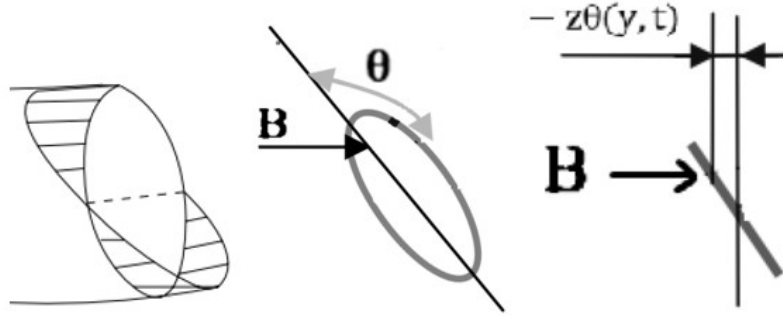

Figure 5.5: *The displacement of point B*

Point B also rotates with an angle ψ about the z-axis, and by the same analogy, we can prove that this displacement is equal to xψ in the positive direction.

The total displacement of point B will be:

$$u(x, y, z, t) = x\psi(y, t) - z\theta(y, t) \tag{5.20}$$

The longitudinal strain of point B:

We have ψ and θ too small

$$\psi = \frac{\partial u^*}{\partial y}, \theta = \frac{dw^*}{dy} \tag{5.21}$$

So:

$$u(y, x, z, t) = -x\frac{\partial u^*}{\partial y} - z\frac{\partial w^*}{\partial y} \tag{5.22}$$

The longitudinal strain is:

$$\varepsilon_{yy} = \frac{\partial u}{\partial y}$$

$$= -x\frac{\partial^2 u^*}{\partial y^2} - z\frac{\partial^2 w^*}{\partial y^2} \tag{5.23}$$

The strain energy is given as:

$$U_s = \frac{1}{2}\int_\tau \varepsilon^T \sigma d\tau \tag{5.24}$$

And since σ= Eε

60

$$U_S = \frac{E}{2} \int_\tau \varepsilon^T \cdot \varepsilon \ d\tau$$

Since ε_{yy} is composed of a single term, $\varepsilon^T \cdot \varepsilon = \varepsilon^2$

$$U_S = \frac{E}{2} \int_\tau \varepsilon^2 \ d\tau$$

$$U_S = \frac{E}{2} \int_0^L \int_S \left(-x \frac{\partial^2 u^*}{\partial y^2} - z \frac{\partial^2 w^*}{\partial y^2} \right)^2 dS dy$$

$$= \frac{E}{2} \int_0^L \int_S \left[x^2 \left(\frac{\partial^2 u^*}{\partial y^2} \right)^2 + z^2 \left(\frac{\partial^2 w^*}{\partial y^2} \right)^2 + 2xy \frac{\partial^2 u^*}{\partial y^2} \frac{\partial^2 w^*}{\partial y^2} \right] dS dy \qquad (5.25)$$

We have:

$$\int_0^L \int_S 2xy \frac{\partial^2 u^*}{\partial y^2} \frac{\partial^2 w^*}{\partial y^2} dS dy = 0 \text{ By symmetry [13]}$$

By introducing the cross-sectional moment of inertia of the shaft:

$$I_{S_x} = \int_S z^2 dS$$
$$I_{S_z} = \int_S x^2 dS \qquad (5.26)$$

We get:

$$U_S = \frac{E}{2} \int_0^l \left[I_{S_x} \left(\frac{\partial^2 u^*}{\partial y^2} \right)^2 + I_{S_z} \left(\frac{\partial^2 w^*}{\partial y^2} \right)^2 \right] dy \qquad (5.27)$$

We have also:

$I_{S_x} = I_{S_z}$ (By the symmetric mass distribution).

$I_{S_x} = I_{S_z} = I_{S_d}$: Diametral area moment of inertia of the shaft.

$$U_S = \frac{E I_{S_d}}{2} \int_0^l \left[\left(\frac{\partial^2 u^*}{\partial y^2} \right)^2 + \left(\frac{\partial^2 w^*}{\partial y^2} \right)^2 \right] dy \qquad (5.28)$$

E: Young modulus of the shaft.

We have from figure 5.4:

$$u^* = u \cos \Omega t - w \sin \Omega t$$

$$w^* = u \sin \Omega t + w \cos \Omega t$$

Therefore, the final expression of the strain energy will be:

$$U_S = \frac{E I_{S_d}}{2} \int_0^L \left[\left(\cos \Omega t \frac{\partial^2 u}{\partial y^2} - \sin \Omega t \frac{\partial^2 w}{\partial y^2} \right)^2 + \left(\sin \Omega t \frac{\partial^2 u}{\partial y^2} + \cos \Omega t \frac{\partial^2 u}{\partial y^2} \right)^2 \right] dy$$

$$U_S = \frac{E I_{S_d}}{2} \int_0^L \left[\left(\frac{\partial^2 u}{\partial y^2} \right)^2 + \left(\frac{\partial w}{\partial y^2} \right)^2 \right] dy \qquad (5.29)$$

5.1.2.3 Mass unbalance kinetic energy

The unbalance is defined by a mass m_u situated at distance d from the center of disk O.

The coordinates of the mass unbalance in XYZ frame is

$$OD = \begin{vmatrix} u + d \sin \Omega t \\ L \\ w + d \cos \Omega t \end{vmatrix} \tag{5.30}$$

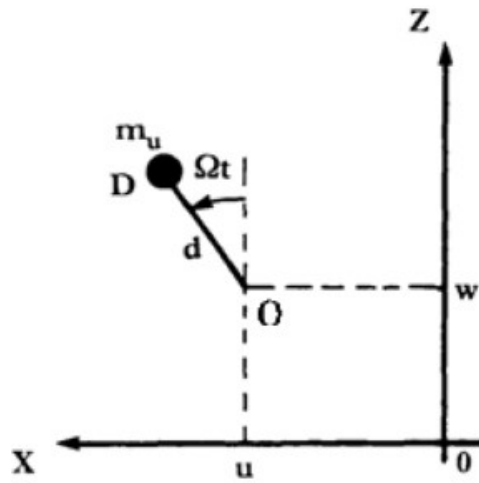The coordinate of the mass unbalance in The Y-axis is assumed to be constant and equal to the length of the shaft L.

Figure 5.6: *Mass unbalance*

The velocity vector is:

$$V = \frac{dOD}{dt} = \begin{vmatrix} \dot{u} + d \,\Omega \cos \Omega t \\ 0 \\ \dot{w} - d \,\Omega \sin \Omega t \end{vmatrix} \tag{5.31}$$

The kinetic energy of the mass unbalance is:

$$T_u = \frac{m_u}{2} (\dot{u}^2 + \dot{w}^2 + \Omega^2 d^2 + 2\Omega d \,\dot{u} \cos\Omega t - 2\Omega d \,\dot{w} \sin\Omega t) \tag{5.32}$$

m_u is too small comparing to disk mass, therefore (5.32) becomes:[13]

$$T_u = m_u \Omega d \,(\dot{u} \cos\Omega t - \dot{w} \sin \Omega t) \tag{5.33}$$

5.1.2.4 Mass unbalance centrifugal force [12]

The centrifugal force due to the mass unbalance is given as:

$$F_{un} = m_u d \,\Omega^2 \tag{5.34}$$

62

The components in the X and Z direction are:

$$F_u = m_u d \, \Omega^2 \sin \Omega t \tag{5.35}$$

$$F_w = m_u d \, \Omega^2 \cos \Omega t$$

It is assumed that the unbalance mass is in the X direction in the initial state. The deflections in the *x* and *y* directions are expressed as:

$$u(y,t) = f(y)q_1(t)$$
$$w(y,t) = f(y)q_2(t) \tag{5.36}$$

Where:

q_1 and q_2 are generalized independent coordinates.

f(y) is the displacement function that satisfies the boundary conditions of the system (the approximated sinusoidal motion of the shaft). As the rotor of the centrifugal fan is simply supported at both ends, f(y) has been selected as: [12] [17]

$$f(y) = \sin\left(\frac{n\pi}{L_4 - L_1} y - L_1\right) \tag{5.37}$$

n: stands for the higher-order vibration modes.
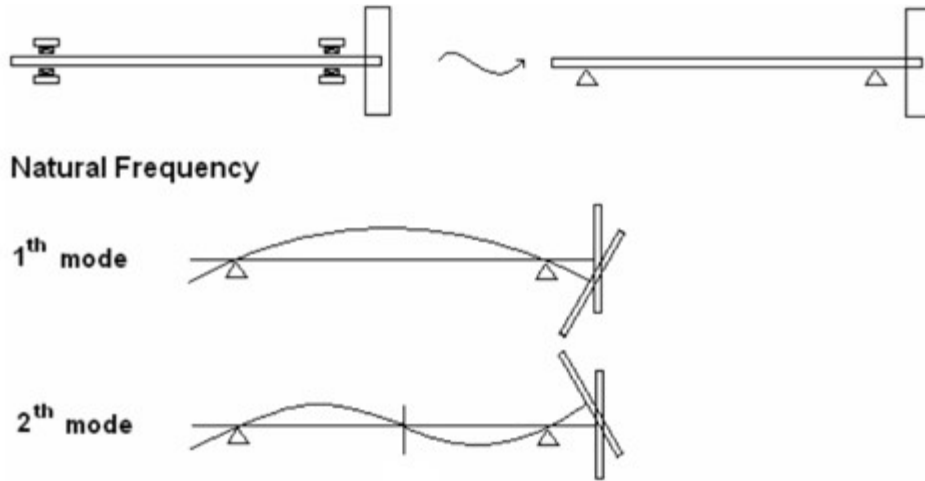
$$L_4 = L_1 + L_2$$

Figure 5.7: Possible mode of a rotor-bearing system

Ψ and θ are too small, therefore they are approximated by the derivatives of u and w respectiely :

$$\psi(y,t) = -\frac{\partial u}{\partial y} = -\frac{df(y)}{dy} q_1 = -g(y)q_1 \tag{5.38}$$

$$\theta(y,t) = \frac{\partial w}{\partial y} = \frac{df(y)}{dy} \cdot q_2 = g(y)q_2 \tag{5.39}$$

The second derivatives are:

$$\frac{\partial^2 u}{\partial y^2} = \frac{d^2 f(y)}{dy^2} q_1 = h(y)q_1 \tag{5.40}$$

$$\frac{\partial^2 w}{\partial y^2} = \frac{d^2 f(y)}{dy^2} q_2 = h(y)q_2 \tag{5.41}$$
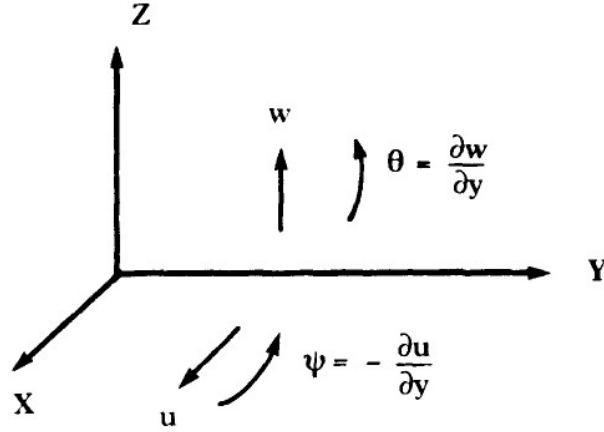

Figure 5.8: *Coordinates*

The kinetic energy of the disk becomes:

$$T_D = \frac{1}{2} M_D f^2(L)(\dot{q}_1^2 + \dot{q}_2^2) + \frac{1}{2} I_{Dd} g^2(L)(\dot{q}_1^2 + \dot{q}_2^2) - I_{D_p} \Omega g^2(L)\dot{q}_1 q_2 \tag{5.42}$$

$$T_D = \frac{1}{2}\big[M_D f^2(L) + I_{D_d} g^2(L)\big](\dot{q}_1^2 + \dot{q}_2^2) - I_{D_p} \Omega g^2(L)\dot{q}_1 q_2 \tag{5.43}$$

The kinetic energy of the shaft becomes:

$$T_s = \frac{\rho S}{2} \int_0^L f^2(y)dy(\dot{q}_1^2 + \dot{q}_2^2) + \frac{\rho}{2} I_{S_d} \int_0^L g^2(y)(\dot{q}_1^2 + \dot{q}_2^2)dy - \rho I_{S_p} \Omega \int_0^L g^2(y)dy\dot{q}_1 q_2$$

$$T_s = \frac{1}{2}\Big[\rho S \int_0^L f^2(y)dy + \rho I_{S_d} \int_0^L g^2(y)dy\Big](\dot{q}_1^2 + \dot{q}_2^2) - \rho I_{S_p} \Omega \int_0^L g^2(y)dy\, \dot{q}_1 q_2 \tag{5.44}$$

The kinetic energy of the unbalance mass becomes:

$$T_u = m_u \Omega d\, (\dot{u}\cos\Omega t - \dot{w}\sin\Omega t)$$

$$\quad = m_u \Omega d\, (f(L)\dot{q}_1 \cos\Omega t - f(L)\dot{q}_2 \sin\Omega t)$$

$$\quad = m_u \Omega d\, f(L)(\dot{q}_1 \cos\Omega t - \dot{q}_2 \sin\Omega t) \tag{5.45}$$

The total kinetic energy is:

$$T = T_D + T_s + T_u$$

$$= \frac{1}{2}\Big[M_D f^2(L) + I_{Dd} g^2(L) + \rho S \int_0^L f^2(y)dy + \rho I_{S_d} \int_0^1 g^2(y)dy\Big](\dot{q}_1^2 + \dot{q}_2^2) - \Omega\Big[I_{D_p} g^2(L) + \rho I_{S_p} \int_0^L g^2(y)dy\Big]\dot{q}_1 q_2 + m_u \Omega d f(L) \cos\Omega t\, \dot{q}_1 - m_u \Omega d f(L)\sin\Omega t\, \dot{q}_2$$

$$T = \frac{\tilde{m}}{2}(\dot{q}_1^2 + \dot{q}_2^2) - a\Omega\dot{q}_1 q_2 + C\dot{q}_1 + D\dot{q}_2 \tag{5.46}$$

Where:

$$\tilde{m} = \left[M_D f^2(L) + I_{Dd} g^2(L) + \rho S \int_0^L f^2(y)d + \rho I_{S_d} \int_0^1 g^2(y)dy \right] \tag{5.47}$$

$$a = \left[I_{D_p} g^2(L) + \rho I_{S_p} \int_0^L g^2(y)dy \right] \tag{5.48}$$

$$C = m_u \Omega df(L) \cos \Omega t \tag{5.49}$$

$$D = -m_u \Omega df(L) \sin \Omega t \tag{5.50}$$

The strain energy of the shaft becomes:

$$U_s = \frac{EI_{S_d}}{2} \int_0^L h^2(y)dy(q_1^2 + q_2^2)$$
$$U_s = \frac{1}{2}\tilde{k}(q_1^2 + q_2^2) \tag{5.51}$$

Where:

$$\tilde{k} = EI_{S_d} \int_0^L h^2(y)dy \tag{5.52}$$

The centrifugal force expression becomes:

$$F_{q1} = m_u d\, \Omega^2 \cos \Omega t \tag{5.53}$$

$$F_{q2} = m_u d\, \Omega^2 \sin \Omega t \tag{5.54}$$

The equations of motion of the system are obtained using the Lagrangian equations as:
$$\frac{d}{dt}\left(\frac{\partial T}{\partial \dot{q}_1}\right) - \frac{\partial T}{\partial q_1} + \frac{\partial u}{\partial q_1} = F_{q_1}$$
$$\frac{d}{dt}\left(\frac{\partial T}{\partial \dot{q}_2}\right) - \frac{\partial T}{\partial q_2} + \frac{\partial u}{\partial q_2} = F_{q2} \tag{5.55}$$

After the derivations we get:

$$\tilde{m}\ddot{q}_1 - a\Omega\dot{q}_2 + \tilde{k}q_1 = m_u d\Omega^2 \sin \Omega t$$
$$\tilde{m}\ddot{q}_2 + a\Omega\dot{q}_1 + \tilde{k}q_2 = m_u d\Omega^2 \cos \Omega t \tag{5.56}$$

The displacement function for the first shape mode is:

$$f(y) = \sin\left(\frac{\pi}{L_2}y - L_1\right) \tag{5.57}$$

Therefore:

$$g(y) = \frac{\partial f(y)}{\partial y} = \frac{\pi}{L_2}\cos\left(\frac{\pi}{L_2}y - L_1\right) \tag{5.58}$$

$$h(y) = \frac{\partial^2 f(y)}{\partial y^2} = -\left(\frac{\pi}{L_2}\right)^2 \sin\left(\frac{\pi}{L_2}y - L_1\right) \tag{5.59}$$

5.1.3 Numerical application

The coordinate of the disk in Y direction is L, therefor:

$$f(y) = \sin\left(\frac{\pi}{L_2}y - L_2\right) = \sin(3,10y - 0,14)$$

$$f(L) = \sin\left(\frac{\pi}{L_2}L - L_1\right) = \sin\left(\frac{\pi\,1,293}{1,013} - 0,14\right) = \sin(3,869) = -0.6656$$

$$f^2(y) = \sin^2(3,10y - 0,4)$$

$$f^2(L) = 0,443$$

$$g(y) = \frac{\pi}{L_2}\cos\left(\frac{\pi}{L_2}y - \frac{\pi}{2}\right) = 3,10\cos(3,10y - 0,14)$$

$$g(L) = 3,10\cos(3,10 \cdot 1,293 - 0,14) = -2,3168$$

$$g^2(y) = 9,618\cos^2(3,10y - 0,14)$$

$$g^2(L) = 5,367$$

$$h(y) = -\left(\frac{\pi}{L_2}\right)^2\sin\left(\frac{\pi}{L_2}y - L_2\right) = -9,618\sin(3,10y - 0,14)$$

$$h^2(y) = 92,506\sin^2(3,10y - 0,14)$$

$$\int_0^L f^2(y)dy = \int_0^L \sin^2(3,10y - 0,14)\,dy = 0.5441$$

$$\int_0^L g^2(y)dy = \int_0^1 9,618\cos^2(3,10y - 0,14)\,dy = 7.20$$

$$\int_0^2 h^2(y)dy = \int_0^1 92,506\ \sin^2(3,10y - 0,14)\,dy = 50.33$$

And we know from that:

$$M_{unbalance} = 6,5849\ g = 0,00658\ kg$$

$$d = 0,46\ m$$

$$R_{Shaft} = 0.0325\ mm$$

And we know from Solidworks that:

$$M_{Disk} = 70.56\ kg$$

$$M_{shaft} = 33,76\ kg$$

$$\rho_{Shaft} = 7870\ kg/m^3$$

$S_{Shaft} = 0,003318 \ m^2$

$I_{D_p} = 8,1784 kg \cdot m^2$

$I_{D_d} = 4,2736 \cdot kg \cdot m^2$

$I_{S_p} = \dfrac{\pi}{2} R_S^4 = 1,7524 . 10^{-6} \ m^4$

$I_{S_d} = \dfrac{\pi}{4} R_S^4 = 8,7624 . 10^{-7} m^4$

E= $2.05 . 10^{11}$ N/m²

By substituting all the previous values in (5.47), (5.48) and (5.52) we get:

$\tilde{m} = 68.45$

$a = 43,99$

$\tilde{k} = 9.02 . 10^6$ N/m

5.1.4 Natural frequencies

We start by studying the free motion:

The equation of motion becomes:

$$\begin{aligned} \tilde{m}\ddot{q}_1 - a\Omega\dot{q}_2 + \tilde{k}q_1 = 0 \\ \tilde{m}\ddot{q}_2 + a\Omega\dot{q}_1 + \tilde{k}q_2 = 0 \end{aligned} \qquad (5.60)$$

It can be written in matrix form as:

$$\begin{bmatrix} \tilde{m} & 0 \\ 0 & \tilde{m} \end{bmatrix}\begin{bmatrix} \ddot{q}_1 \\ \ddot{q}_2 \end{bmatrix} + \Omega\begin{bmatrix} 0 & -a \\ a & 0 \end{bmatrix}\begin{bmatrix} \dot{q}_1 \\ \dot{q}_2 \end{bmatrix} + \begin{bmatrix} \tilde{k} & 0 \\ 0 & \tilde{k} \end{bmatrix}\begin{bmatrix} q_1 \\ q_2 \end{bmatrix} = 0 \qquad (5.61)$$

$$\begin{bmatrix} 68.45 & 0 \\ 0 & 68.45 \end{bmatrix}\begin{bmatrix} \ddot{q}_1 \\ \ddot{q}_2 \end{bmatrix} + \Omega\begin{bmatrix} 0 & -43.99 \\ 43.99 & 0 \end{bmatrix}\begin{bmatrix} \dot{q}_1 \\ \dot{q}_2 \end{bmatrix} + 10^6\begin{bmatrix} 9.02 & 0 \\ 0 & 9.02 \end{bmatrix}\begin{bmatrix} q_1 \\ q_2 \end{bmatrix} = 0 \qquad (5.62)$$

The solution is of the form:

$$\begin{aligned} q_1 = Q_1 e^{rt} \\ q_2 = Q_2 e^{rt} \end{aligned} \qquad (5.63)$$

Substituting (5.63) in (5.61) gives the homogeneous set of equations:

$$\begin{bmatrix} \tilde{k} + \tilde{m}r^2 & -a\Omega r \\ a\Omega r & \tilde{k} + \tilde{m}r^2 \end{bmatrix}\begin{bmatrix} Q_1 \\ Q_2 \end{bmatrix} = 0 \qquad (5.64)$$

The characteristic equation is:

$$\left(\tilde{k} + \tilde{m}r^2\right)^2 + a^2\Omega^2 r^2 = 0 \qquad (5.65)$$

Which can be written as:

$$\tilde{m}^2 r^4 + \left(2\tilde{k}\tilde{m} + a^2\Omega^2\right)r^2 + \tilde{k}^2 = 0 \tag{5.66}$$

at rest ($\Omega = 0$) the roots of (5.66) are :

$$r_{10}^2 = r_{20}^2 = j^2\omega_{10}^2 = j^2\omega_{20}^2 = -\frac{\tilde{k}}{\tilde{m}} \tag{5.67}$$

And the natural pulsations at rest are:

$$\omega_{10} = \omega_{20} = \sqrt{\frac{\tilde{k}}{\tilde{m}}} = 363.0126 \text{ rad/s} \tag{5.68}$$

The natural frequency at rest is:

$$f_{10} = \frac{\omega_{10}}{2\pi} = 57.77 \text{ Hz} \tag{5.69}$$

When the rotor is operating ($\Omega \neq 0$), the expression of the first root is:

$$r_1^2 = -\left[\omega_{10}^2 + \frac{a^2\Omega^2}{2\tilde{m}^2}\left(1 - \sqrt{1 + \frac{4\tilde{m}^2\omega_{10}^2}{a^2\Omega^2}}\right)\right] \tag{5.70}$$

Hence:

$$r_1 = \pm j\omega_1 \tag{5.71}$$

Then:

$$\omega_1 = \sqrt{\omega_{10}^2 + \frac{a^2\Omega^2}{2\tilde{m}^2}\left(1 - \sqrt{1 + \frac{4\tilde{m}^2\omega_{10}^2}{a^2\Omega^2}}\right)} \tag{5.72}$$

For our case (Ω=2985 rpm):

ω_1=276.60 rad/s

And the first natural frequency is:

$$f_1 = \frac{\omega_1}{2\pi} = 44.02 \text{ Hz}$$

The expression of the second root is:

$$r_2^2 = -\left[\omega_{10}^2 + \frac{a^2\Omega^2}{2\tilde{m}^2}\left(1 + \sqrt{1 + \frac{4\tilde{m}^2\omega_{10}^2}{a^2\Omega^2}}\right)\right] \tag{5.73}$$

Hence:

$$r_2 = \pm j\omega_2 \tag{5.74}$$

Then:

$$\omega_2 = \sqrt{\omega_{10}^2 + \frac{a^2\Omega^2}{2\tilde{m}^2}\left(1 + \sqrt{1 + \frac{4\tilde{m}^2\omega_{10}^2}{a^2\Omega^2}}\right)} \tag{5.75}$$

For our case (Ω=2985 rpm):

ω_2= 477.485 rad/s

The second natural frequency is:
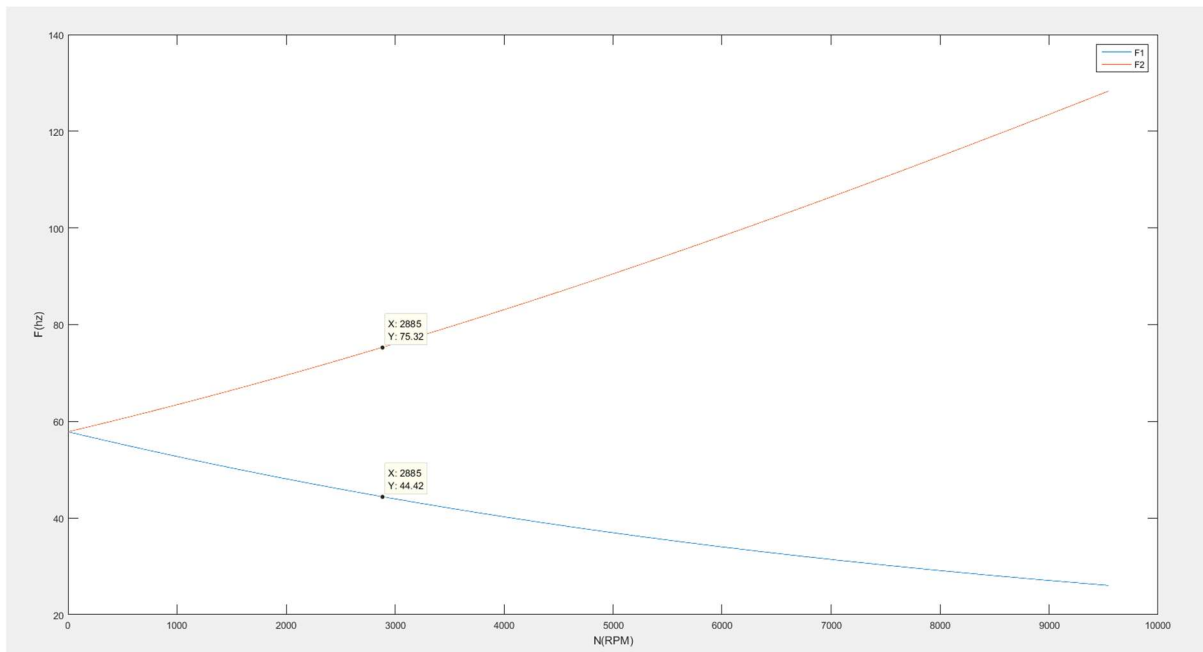
$$f_2 = \frac{\omega_2}{2\pi} = 75.99 \text{ Hz}$$

Figure 5.9: *Natural frequencies (Hz) vs shaft speed (RPM)*

Figure (5.9) shows the system's natural frequencies as a function of the shaft rotation speed.

We can get the natural frequency of any rotation speed from this plot (known as the Campbell diagram).

We can see that the natural frequencies corresponding to our shaft rotation speed are 44.42 Hz and 75.32 Hz.

5.1.5 Response to the forces of excitation

The equation of motion is:

$$\begin{aligned}\tilde{m}\ddot{q}_1 - a\Omega\dot{q}_2 + \tilde{k}q_1 &= m_u d\,\Omega^2 \sin\Omega t \\ \tilde{m}\ddot{q}_2 + a\Omega\dot{q}_1 + \tilde{k}q_2 &= m_u d\,\Omega^2 \cos\Omega t\end{aligned} \tag{5.76}$$

And because we neglected the dumping, the solution can be found as: [13]

$$q_1 = Q_1 \sin \Omega t$$
$$q_2 = Q_2 \cos \Omega t$$

(5.77)

Substituting (5.76) in (5.77) gives:

$$-\tilde{m}\Omega^2 Q_1 + a\Omega^2 Q_2 + \tilde{k}Q_1 = m_u d\Omega^2$$
$$-\tilde{m}\Omega^2 Q_2 + a\Omega^2 Q_1 + \tilde{k}Q_2 = m_u d\Omega^2$$

(5.78)

Solving (4.77) gives:

$$Q_1 = Q_2 = \frac{m_u d\Omega^2}{\tilde{k}+(a-\tilde{m})\Omega^2}$$

(5.79)

The amplitude corresponding to our system rotation speed (2985 RPM) is:

$$Q_1 = Q_2 = 2.9710 \cdot 10^{-5} \text{ m}$$

The critical speed is the speed at which the rotor becomes resonant, and when natural vibration increases, and causes the fan to function incorrectly. It corresponds to the value where the displacement becomes infinite and that happens when the denominator of (5.79) is null.

$$\Omega_c = \sqrt{\frac{k}{m-a}} = 607.89398 \text{ rad/s} \Omega_c = 5804.95 \text{ rpm}$$

The frequency that corresponds to critical speed is:
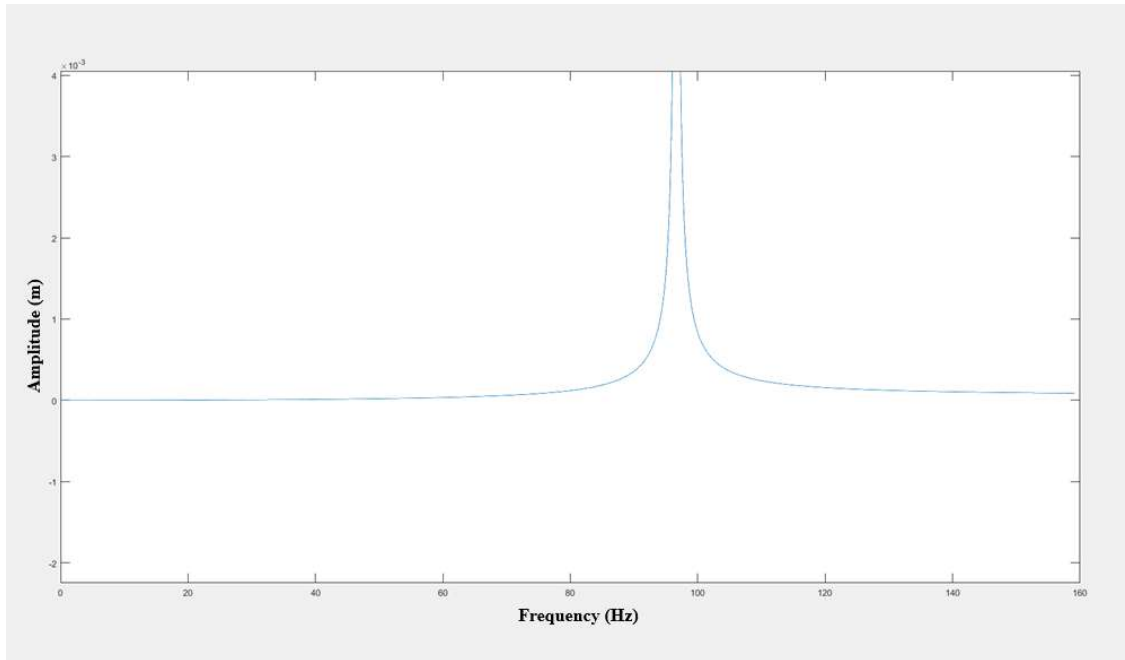
$$\frac{\Omega_c}{2\pi} = 96.7493 \text{ Hz}$$

Figure 5.10: *Amplitude (m) as a function of natural frequency (Hz)*

Figure (5.10) show the variation of the amplitude of the system as a function of frequency, the fan is operating at a safe zone since most fans operate at less than 75% of their critical speed.

5-2 Solidworks frequency analysis

Every structure has the tendency to vibrate at certain frequencies, called natural or resonant frequencies. Each natural frequency is associated with a certain shape, called mode shape that the model tends to assume when vibrating at that frequency. When a structure is properly excited by a dynamic load with a frequency that coincides with one of its natural frequencies, the structure undergoes large displacements and stresses. This phenomenon is known as resonance. For undamped systems, resonance theoretically causes infinite motion. Damping, however, puts a limit on the response of the structures due to resonant loads. [18]

To get more accurate results we will introduce the effect of the flowing air on the impeller in this study, this effect is called "fluid-structure interaction".

To do that we first run a CFD simulation for the fan-impeller-shaft system, we set the inlet volume flowrate to the value of the fan operational point we found in chapter 3 which is 3.5 m^3/s, when the CFD simulation is finished, we export the results to Solidworks simulation.

5-2-1 System Modeling

The system on which we will perform a frequency analysis consists of the impeller, the shaft, and two rings to represent the stator.

71

Figure 5.11: system modeling

Boundary conditions:
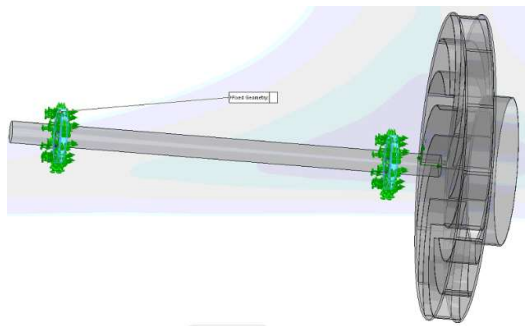
We start by fixing the stator (the two rings)

Figure 5.12: Fixing

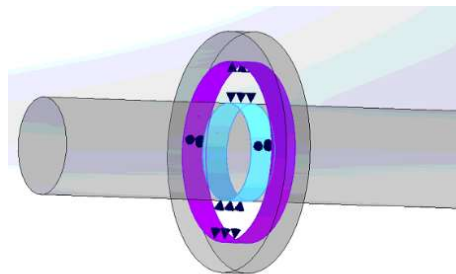Then we define a bearing connector between the shaft and the rings:

Figure 5.13: Defining Bearing Connector
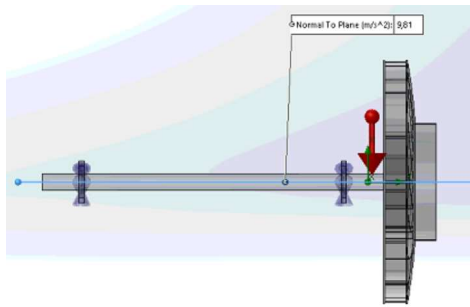
After that we define the gravity:

Figure 5.14 Defining gravity force

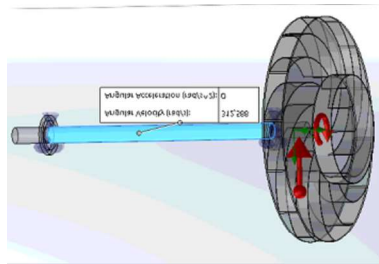We define a centrifugal force of 312.588 (rad/s) on the shaft:

Figure 5.15: Defining centrifugal force

Finally, we import the effect of the fluid on the impeller that we exported to simulation earlier:
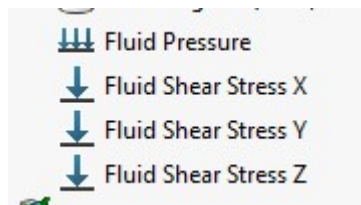
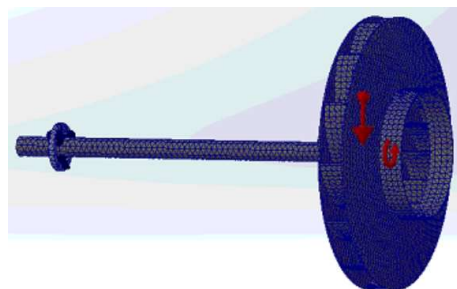*Figure 5.16: Importing the fluid effects*

Meshing the model:

Figure 5.17: Model's mesh

5-2-2 Study Results

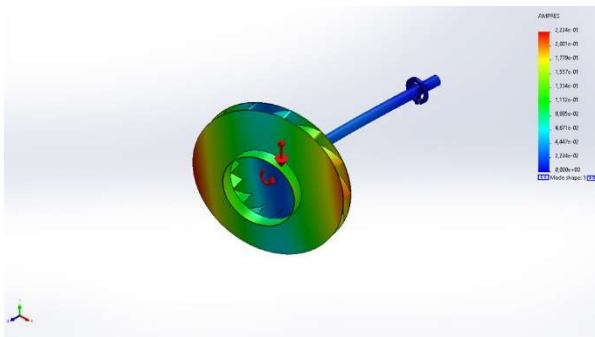Running the simulation gives the following results:
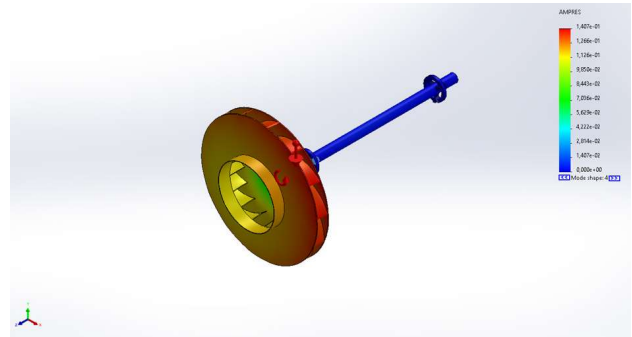

Figure 5.18 *1ˢᵗ frequency mode shape*

at 48.67 Hz

Figure 5.19: *2ⁿᵈ frequency mode shape*

at 53.14 Hz
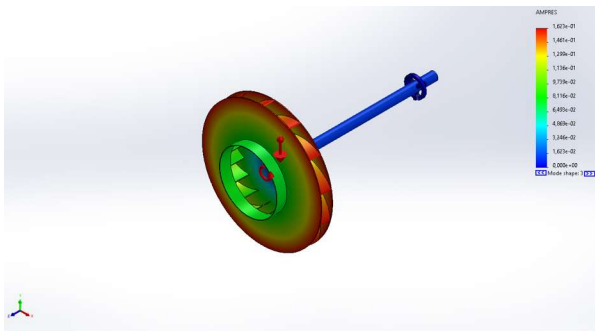

Figure 5.20: 3ʳᵈ frequency mode shape
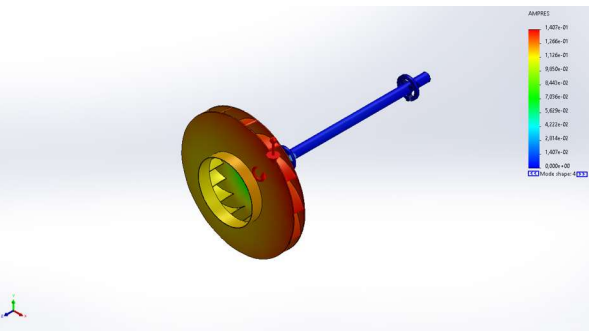
at 52.085 Hz

Figure 5.21: 4ᵗʰ frequency mode shape

at 69.253 Hz

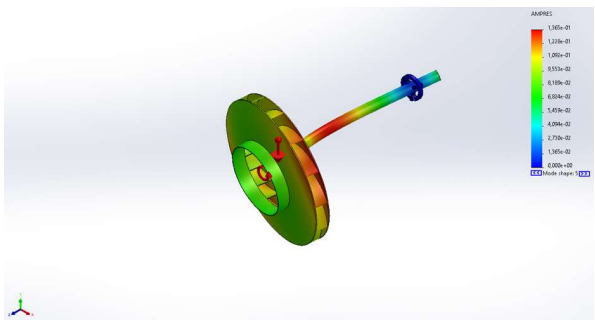***Figure 5.22:*** 5ᵗʰ frequency mode shape

at 82.74 Hz

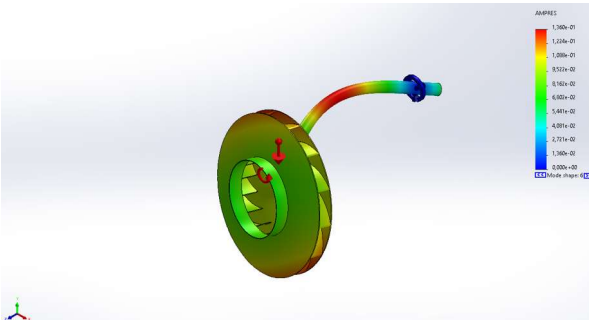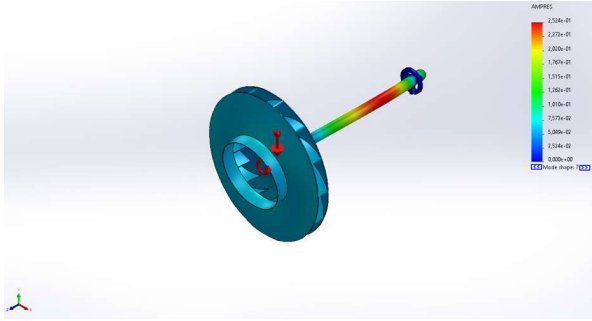***Figure 5.23***:6ᵗʰ frequency mode shape

at 83.40 Hz

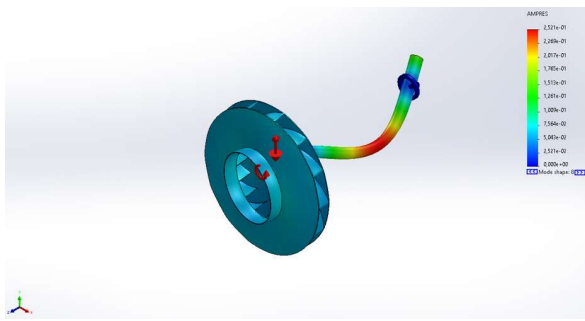**Figure 5.24**: 7th frequency mode shape at 203.56 Hz

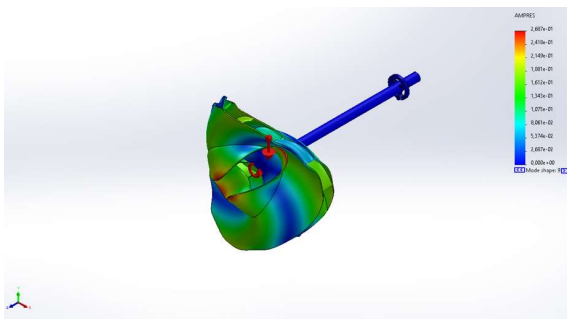**Figure 5.25**: 8th frequency mode shape at 203.71 Hz
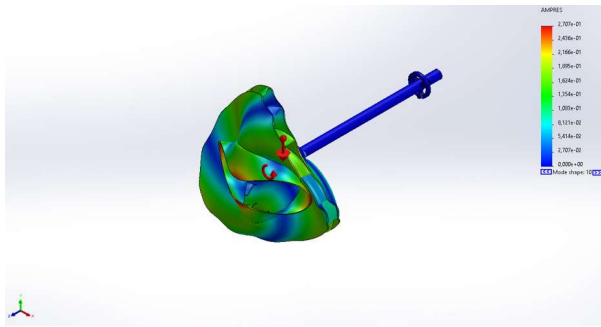

Figure 5.26: 9th frequency mode shape at 280.97 Hz

Figure 5.27:10th frequency mode shape at 283.88 Hz

Mode List

Frequency Number	Rad/sec	Hertz	Seconds
1	305,82	48,673	0,020545
2	306,26	48,743	0,020516
3	308,74	49,138	0,020351
4	333,89	53,14	0,018818
5	519,87	82,74	0,012086
6	524,06	83,407	0,011989
7	1 279	203,57	0,0049124
8	1 280	203,71	0,0049089
9	1 765,4	280,98	0,003559
10	1 783,7	283,88	0,0035226

Table 5.1: *Mode list*

The frequency analysis results are resumed in Table 5.1, the first mode shape represents a bending in the xy plane, the second, the third and the fourth modes represents a torsion, these first four modes are close to the frequency of the motor and that may be explained by a problem in the motor starting. The fifth and the seventh modes represent a bending in xz plane, the sixth

75

and the eighth modes represent a bending in yz plane, while the ninth and the tenth modes shapes represent a torsion.

5.3 Experimental results

Production line characteristics:

Production line	Fan FN 301 (figure 1-1)	Fan FN 501 (figure 1-3)
Motor	90 kW	110 kW.
Rotation speed	2985 RPM	2985 RPM
Turbine	Diameter 800 mm and 12 blades	Diameter 920 mm, 14 blades, width 200 mm
Dust collector linked to fan inlet with filter FL 301. (figure 1-2)/ the filter FL 501	Diameter 525 mm with a Width of 1260 mm	Diameter 640 mm with a Width of 4550 mm
Discharge system which represents the exit path	Diameter 650 mm with a Width of 2100 mm	Diameter 800 mm with a Width of 2000 mm
Filter FL 301	Diameter 1750 mm including 120 filters bag, with a height of 3160 mm. (figure 1-2).	Diameter 2300 mm and a height of 4130 mm. (figure 1-4).
Production capacity	06,5 tones/hour	19 tones/hour

Table 5.2 : Production line characteristics

Photo 5-1   **Photo 5-2**

Photo 5-3

Photo 5-4

1- Realized work

Performing a study and realization proposition of an identical fan 501 and replace it in the production line of semolina 301. The realization consists of:

- Making of an impeller with 920 mm of diameter
- Making of an identical volute to FN 501 (figure 2-1)
- Making of a flow rate regulator with the same capacity as FN 501. (figure 2-2)
- Making of a suction duct and discharge duct with a 640 mm et 800 mm of diameter respectively (figure 2-3) and (figure 2-4) with different lengths from FN 501.
- We get a new fan FN 301 semolina with identical characteristics to FN 501 flour. We replace the old FN 301 with the new FN 301. (Figure 2-5 & 2-6), while we keep the same filter FL 301.

Photo 5-5

Photo 5-6

Photo 5-7	**Photo 5-8**

2- Vibration measurements on the new fan FN 301

- Initially, the results were of the order of 02.66 mm/s, indexed GOOD according to VDI 2056 standards.
- A 09 tones/hours, introduced jamming within the suction line on two ramps with large sections the other ramps (10) normally function.
- The two blocked ramps presented a designing anomaly on the tilting and suction angles at the manifold just before reaching the FL 301 filter in suction mode.

Measurements of vibration levels are taken with spectra. There is an imbalance anomaly.

3- Analysis of vibration measurements

History:

a) The vibration monitoring of the old ventilator began on: July the 3rd 2014, the overall vibration level recorded in RMS was 01,37 mm/s horizontally and 02,12 mm/s vertically, from trend lines respectively Photo 5-1 & 5-2 respectively. These are GOOD levels according to VDI 2056 international standards.

b) b) This fan has operated within a range of Acceptable RMS vibration levels until the 5th of January 2021. The levels were 02,39 mm/s horizontally and 02,48 mm/s vertically same as (figure 5-28 & 5-29).

   c) April the 14th 2021: the tests were carried out with the new fan FN 301. We record an RMS overall vibration levels on :
   - Horizontally: 09,48 mm/s which are Alarming according to the standers (figure 5-30).
   - Vertically: 15, 04 mm/s, which is Dangerous according to the standers (figure 5-31).
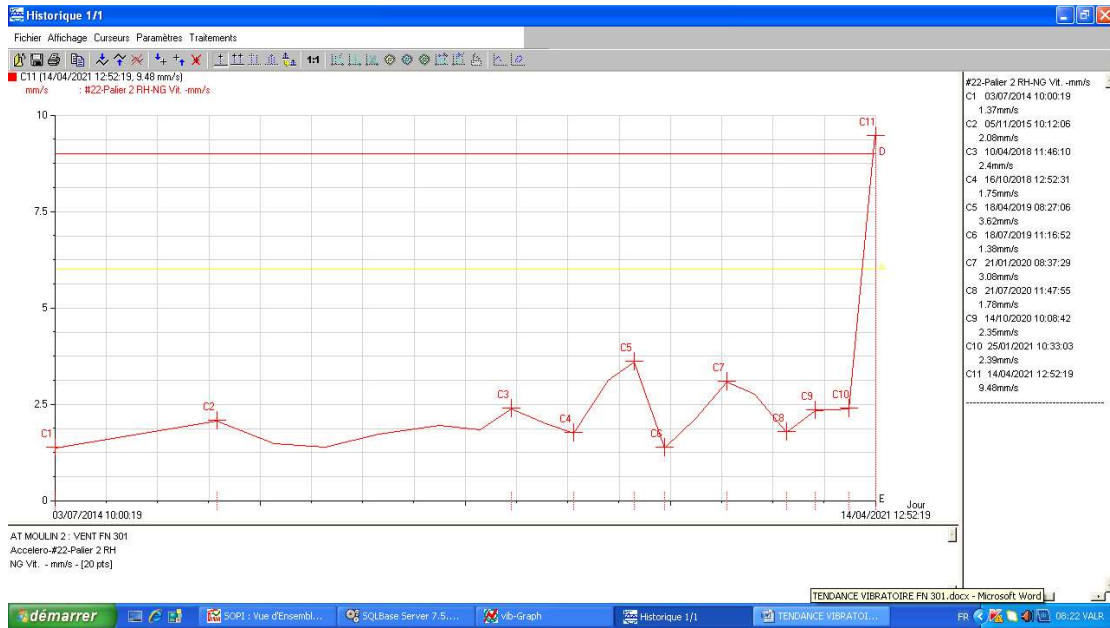
Figure 5-28: FN 301 Fan vibration tendency. Measurements were taken on the motor bearing on the turbine side in the horizontal direction.
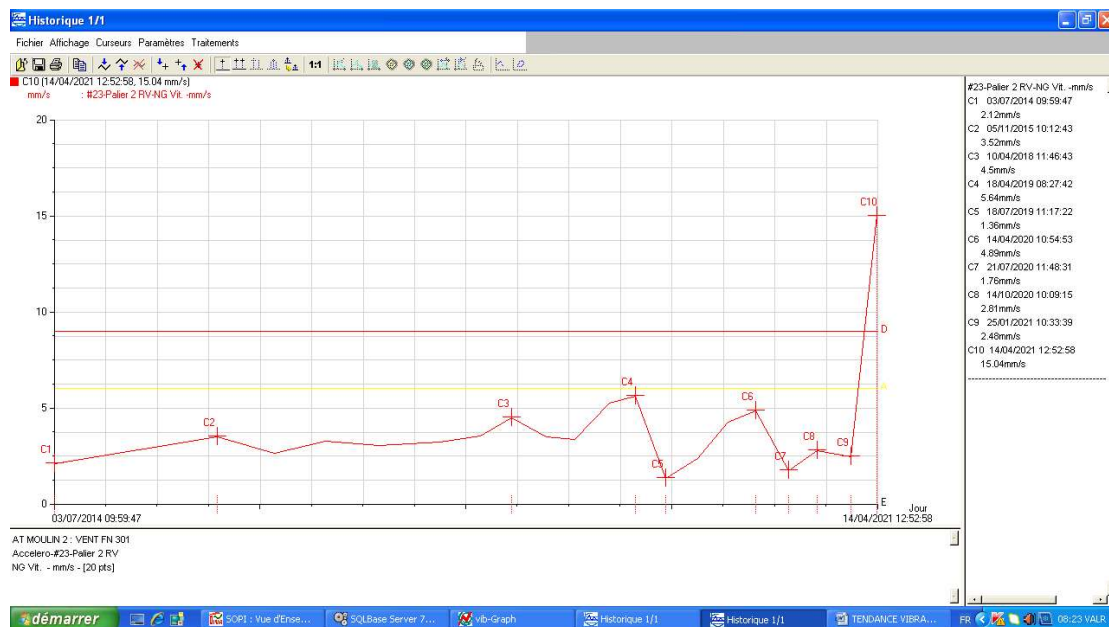

Figure 5-29: FN 301 Fan vibration tendency. Measurements were taken on the motor bearing on the turbine side in the vertical direction.

April the 14th, 2021 analyzes, and comments:

The spectral interpretation of the measurements taken, on the new fan FN 301, reveals the presence of the following anomaly:

- - An unbalance on the turbine, generating vibrations with a peak level of 09,04 mm/s horizontally, is the predominant component linked to the frequency of rotation of 50 Hz shown in the vibration spectrum in figure 14. This peak level is considered Alarming.
- Vertically, This unbalance provokes vibrations with a peak level of 14,40 mm/s, as indicated by the base frequency of 50 Hz. This peak level is considered Danger by standards.
- - The appearance of the unbalance defect is caused by the clogging of the material on the blades of the turbine. This is a blockage on the suction lines at a production rate of 09 tones/hour.
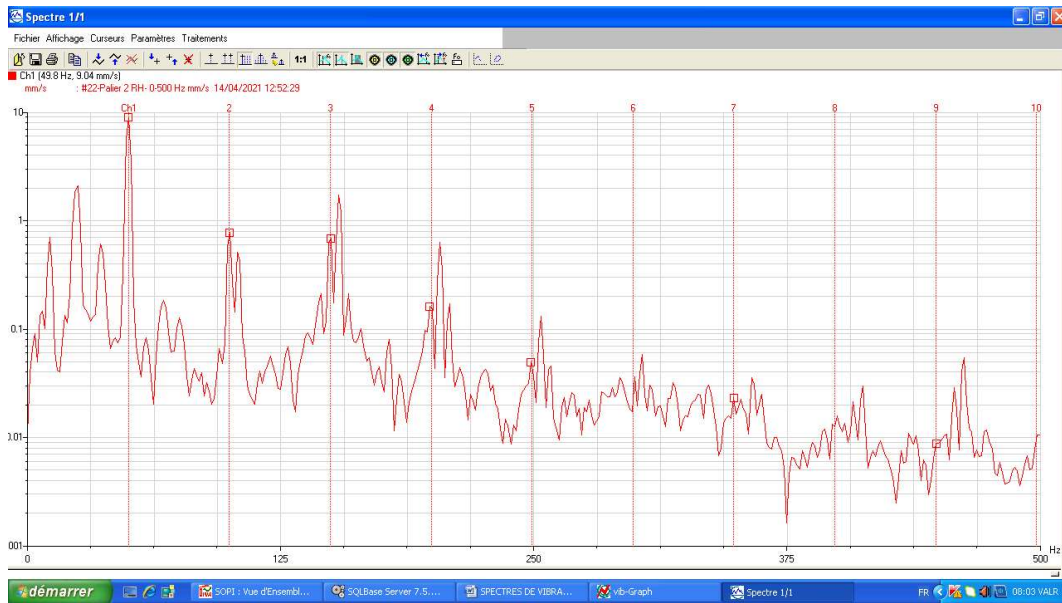

Figure 5-30: Vibration spectrum was taken on April 14, 2021, on the motor bearing on the turbine side in the horizontal direction of the new FN 301 fan. Unbalance of 09,04 mm/s at 50 Hz.
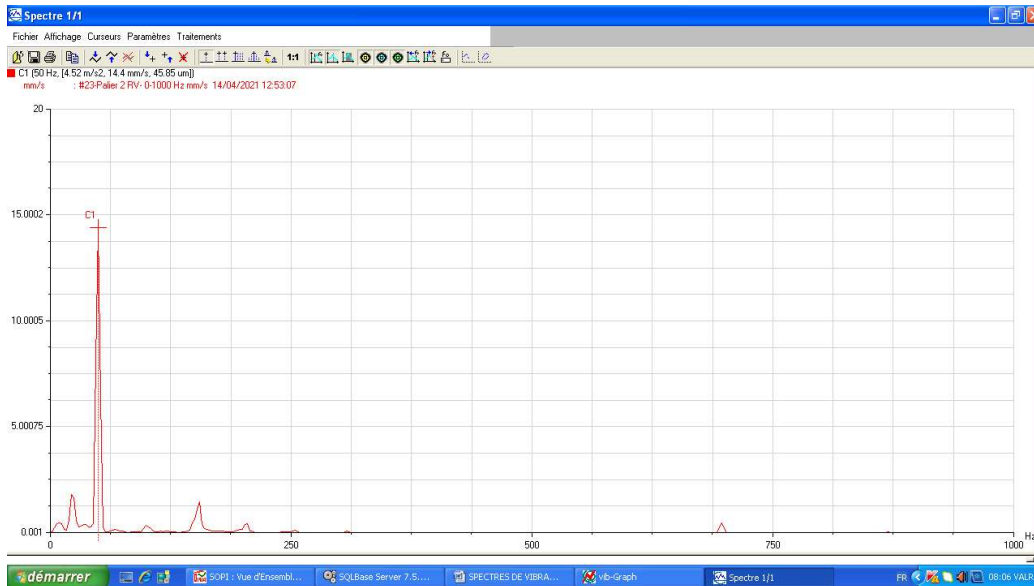
Figure 5-31: Vibration spectrum was taken on April 14, 2021, on the motor bearing on the turbine side in the vertical direction of the new FN 301 fan. Unbalance of 14,40 mm/s at 50 Hz.

5.4 Proposed solution

Balancing rotor

Unbalances are caused by the effective displacement of the mass center of the unit from its true axis. In this study we are willing to propose a balancing solution:

The aim of balancing a rotor such as a fan is to add weight that will counteract the unbalance forces, we first have to determine the location of the heavy spot. To do that we add a trial weight or calibration weight to figure out how much weight to add and to see how it influences the vibration.

In this explanation schematically the unbalance is presented as an orange mass assuming it is 6g the summation of all those unbalance forces because of dirt or erosion etc… and that concentration of weight is in a particular place we can vectorially represent that (blue vector) and we can imagine if we run this machine in this unbalance state creating all these forces that we want to eliminate.
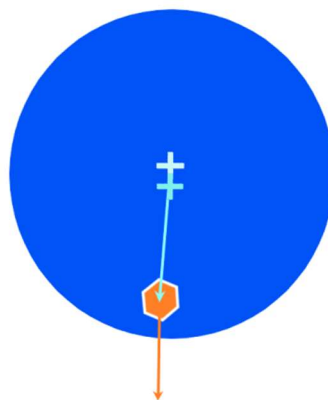

Figure 5.32 Unbalanced system

81

The first thing to do is to locate where the concentration of unbalance forces is by taking the right measurements, starting to add your first trial mass 2g opposite to the unbalance mass and we will try to estimate what that trial weight would be to minimize the vibration and then we can imagine if we run this machine the vibration will be reduced a little bit, we hypothesize that the unbalance vector has changed a little bit in direction and length. This experience has led us to a location where the unbalance forces are located Approximately.
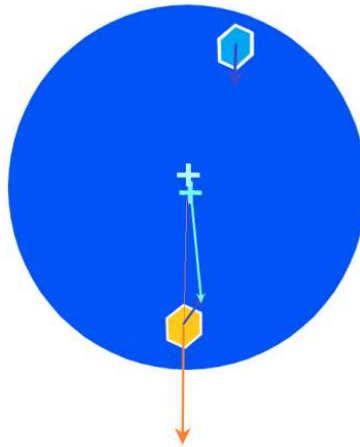

Figure 5.32 *balanced system*

After figuring out where the unbalance forces are located, we are going to add another yellow mass 4g opposite direction to the direction where the unbalance vector (blue vector) is, and then we can imagine if we run the machine the vibrations are significantly low now and we hypothesize schematically that the unbalance vector is significantly small and that led us to estimate that the vibrations levels are much lower after applying this method we can presuppose that the rotor is balanced.

Conclusion

In this chapter we studied the response of the rotor to the unbalance mass that we found in chapter 4, we expressed both system natural frequencies and system amplitude as a function of rotation speed, then we performed a frequency analysis to determine the mode shapes.
These results were validated with the experimental test, where the variation of the results is due to the neglected factors in the analytical study like a motor magnetic field, bearings effects, and air force on the impeller.
A solution for the problem is proposed at the end of this chapter.

General conclusion

In this thesis, we started the work by describing the centrifugal fans and their utilities in the industrial fields.
After diagnosing the problem we proposed a replacement for the old fan (FN 301) with a new one
(FN 501), then we conducted a theoretical study and CFD simulation to predict the performance of the new fan with the old filter (FL 301), we have also extracted the duct filter pressure drop curve to determine the fan operational point, the results show the fan is capable of evacuating the required air flowrate from the flour milling machines.
Despite the fact of the fan curves say that the fan is capable of evacuating the required flowrate does not mean it can, there are other factors that can affect its performance.

Therefore in chapter four we verified the shaft resistance to bending and torsion, we determined the deflection of the shaft at the disk and we calculated the unbalance mass due to this deflection. We also performed a simulation on the bearings to evaluate their performance.

In chapter five we studied the response of the rotor to the unbalance mass that we found in chapter four, we expressed both system's natural frequencies and the system's amplitude as a function of rotation speed, then we performed a frequency analysis to determine the mode shapes.
These results were validated with the experimental test, where the variation of the results is due to the neglected factors in the analytical study like a motor magnetic field, bearings effects, and air force on the impeller.
A solution for the problem is proposed at the end of this chapter.

References

[1] Abraham Engeda, June 1998, Early Historical Development of the Centrifugal Impeller.

[2] Karadzhi Sergey, Brodach Marianna, and Karadzhi Viacheslav, February 2018, Modern developments of high-performance industrial fans Rehva Journal

[3] David J.gingery, 1987, How to design and build centrifugal fans.

[4] David J.gingery, 1987, How to design and build centrifugal fans.

[5] Raymond S. Beebe, April 16, 2004, Predictive Maintenance of Pumps Using Condition Monitoring.

[6] The International authority on-air system components, 2012, Balance Quality and Vibration Levels for Fans by Air Movement.

[7] John tuzson, 2000, Centrifugal pump design.

[8] Johann Friedrich Gülich, 2008, Centrifugal Pumps

[9] Malcolm J. McPherson, 1993, Subsurface Ventilation Engineering

[10] G. W. Fischer,Jean-Marc Chapallaz and Peter Eichenberger, 1992, Manual on Pumps Used as Turbines volume 11.

[11] John Stephen Hunter, December 1996, A design philosophy for centrifugal fans.

[12] Alireza Shooshtari, Mahdi Karimi, Mehrdad Shemshadi and Sarah Seraj, 9 February 2021, Effect of Impeller Diameter on Dynamic Response of a Centrifugal Pump Rotor.

[13] Michel Lalanne and Guy Ferraris, July 23, 1990, Rotordynamics Prediction in Engineering.

[14] Arthur W. Lees, Michael Friswell, Seamus D. Garvey, John E. T. Penny, March 31, 2010, Dynamics of Rotating Machines.

 [15] BOUKHALFA Abdelkrim,May 2009, Doctorat thesis on Comportement vibratoire des arbres tournants en matériaux composites.

[16] Marco Ambali, October 2018, Classical Nonlinear Theories of Elasticity of Plates and Shells.

[17] B.P.M. van Esch, February 2006, Rotor Dynamics of a Centrifugal Pump.

[18] Solidworks Simulation Fundamentals.